2019

An investigation of solar panel thermal images collected from an unmanned aerial vehicle

Ginger Ivy Jo L'Heureux
University of Northern Iowa

AN INVESTIGATION OF SOLAR PANEL THERMAL IMAGES COLLECTED FROM AN UNMANNED AERIAL VEHICLE

An Abstract of a Thesis

Submitted

in Partial Fulfillment

of the Requirements for the Degree

Master of Arts

Ginger Ivy Jo L'Heureux

University of Northern Iowa

July 2019

ABSTRACT

As the population of the world continues to increase, so does energy consumption. At the same time, available fossil fuels continue to be depleted. Knowing these two facts, there is a need to find additional sources of energy. Photovoltaic panels (solar panels) are front and center of the renewable energy available options.

Exploring the practical use of infrared thermal imaging for data collection and maintenance of photovoltaic panels is the main objective of this study. In this research, three unmanned aerial vehicle (UAV) flights were completed to obtain thermal imaging of the Cedar Falls Utilities Solar Field with various dates and weather.

The images obtained by the UAV show varying temperatures of solar panels. The comparison between the power output of the solar garden and the temperature of the panels themselves, did not show any significant correlation. The research opened up more questions and shows the need for more research on the topic of how to utilize drone and thermography technology to assist utility companies.

AN INVESTIGATION OF SOLAR PANEL THERMAL IMAGES COLLECTED FROM AN UNMANNED AERIAL VEHICLE

A Thesis

Submitted

in Partial Fulfillment

of the Requirements for the Degree

Master of Arts

Ginger Ivy Jo L'Heureux

University of Northern Iowa

July 2019

This Study By: Ginger Ivy Jo L'Heureux

Entitled: An Investigation of Solar Panel Thermal Images Collected from an Unmanned Aerial Vehicle

Has been approved as meeting the thesis requirements for the

Degree of Master of Science in Technology

Date Dr. Ali Kashef, Chair, Thesis Committee

Date Dr. James Dietrich, Thesis Committee Member

Date Dr. Shahram VarzaVand, Thesis Committee Member

Date Dr. Jennifer Waldron, Dean, Graduate College

ACKNOWLEDGMENTS

It is my pleasure to acknowledge and thank those who have supported me throughout my academic journey. I would like to thank my thesis committee members Dr. Ali Kashef, Dr. Shahram VarzaVand, and Dr. James Dietrich for their support and encouragement.

Beside my thesis committee members, I would like to thank the Geography Department at the University of Northern Iowa for providing the tools and equipment I have needed to implement and complete this study. I would also like to thank Bill Skubal and Ken Kagy of Cedar Falls Utilities for taking the time to discuss and share collected data. Denise Love of SWE / Disney and Jim Kelly of the UNI Library were instrumental in obtaining research papers and documents. Marcy Seavey for her encouragement, advice and graduate assistantship opportunity, without which, I would not have pursued this adventure.

Last, but not least, I would like to take the opportunity to thank my family, R. Rush, August and Oliver, and especially my husband, Jeremy, and my sister, Christine for their support and encouragement in my professional development, education, and especially this journey of a Master of Science.

TABLE OF CONTENTS

LIST OF TABLES

LIST OF FIGURES

CHAPTER I

INTRODUCTION

Motivation & Background

Energy demand and consumption is increasing worldwide. Society is demanding energy producers implement renewable energy options due to global warming and increasing emissions from fossil fuels. As more renewable energy systems are built and connected to electrical grids, there is a greater need for efficient methods to monitor and maintain these new systems.

Unmanned Aerial Vehicle (UAV or drone) technology is taking humans where they could not previously do so easily, economically, and safely. Drones have been utilized for over a hundred and fifty years, but the roles of drones have been increasingly used for tasks other than traditional weather monitoring and military operations. Such tasks include obtaining information to assist engineers, surveyors, farmers, utility companies and other businesses so that they can better serve their customers; potentially reducing costs and increasing profits. This research seeks to help further understand the information provided by thermal images collected by an UAV and if there is a relationship between temperature and energy collected by solar panels.

Statement of the Problem

With projections of coal, natural gas, and oil being depleted within the next century, the public worldwide is demanding that energy providers find alternate renewable energy sources. Global energy needs are estimated to continue to increase as development and industrialization continues to rise in developing countries (Sharma & Chandel, 2013). As more alternative energy units are installed, from solar fields to wind turbines, the need is increasing for economic and efficient maintenance. The use of unmanned aerial vehicles and thermography to provide information is on the rise as these tools can assist maintenance workers, planners, and engineers with timely decision making.

Purpose of the Study

Obtaining a better understanding of the relationships between temperatures, energy output, and the accuracy of the thermal images is the purpose of this study. This quasi-experimental research focuses on a solar garden located south of Viking Road in Cedar Falls, Iowa between Highway 58 and Hudson Road as shown in Figure 1. Power obtained in this field is sold to Cedar Falls Utilities (CFU) who in turn, sell the energy to CFU customers. Unmanned aerial vehicles can quickly and easily maneuver over and around solar fields and gather data utilizing various types of cameras. This quasi-experimental research utilizes information obtained by a thermal camera mounted on a fixed wing UAV. The thermal information is compared with data collected by Cedar Falls Utilities. This data is either obtained from one of 41 inverters placed

Figure 1. Location of CFU solar garden

under the solar panels or at the generator for the solar garden. The CFU system downloads its power output at the generator along with weather at a weather collection station located north of the solar garden. This study demonstrates that unmanned aerial vehicles and the images obtained from the flights are accurate, efficient, and useful monitoring tools for researchers and utility companies.

Need & Justification

The public is demanding renewable energy units at a reasonable cost. Thus, the need to effectively monitor any problems or anomalies becomes necessary. As more solar fields are built and utilized, efficient maintenance becomes an important consideration in the overall costs of the energy development and distribution. Analyzing enormous amounts of data, typically within spreadsheets, can be difficult and take a significant amount of time.

Thermal images can assist analysts by showing where maintenance is needed through uneven heat signatures or hot spots. Images showing anomalies may reduce the amount of time necessary to identify problems that may or may not be shown on numerous lines of data in a spreadsheet. The information provided by the inverters is a collection of energy from multiple panels and therefore uneven temperatures on individual panels may not be obvious within a single line of data. Images showing these anomalies can assist with maintenance and repair before panel failures become a large problem. This easily accessible and visible data via drone obtained thermal images may lead to overall reliability and efficiency of the system and/or units. The data may also be utilized for estimating and planning future installments of similar systems.

Research Questions

The research questions for this study are as follows:

1. Does a relationship exist between temperatures on and around the solar panels and the output or efficiency of the panel?
2. How accurate are the thermal images?

Assumptions

The following assumptions made in this study are:

1. The angle of the sun or the time of year data was collected does not play a significant role in the solar panel energy output.
2. The solar panels are stationary and do not follow the sun's path across the sky during the day. This does not affect the solar panel energy output.
3. Weather and atmospheric conditions do not impact the data obtained from the drone and no adjustments will be made.
4. There is no thermal drift of the camera.

Limitations

The study has been conducted with the following limitations:

1. Weather cannot be controlled.
2. Time constraints limit the number of UAV flights, therefore limiting the amount of data obtained.
3. The study focuses on only one type of solar panel.
4. The data obtained is from one location.
5. The data received from CFU is from multiple solar panels and the data is either at the location of the inverters or the generator. Due to this set up, individual solar panels may not be monitored, and the inverter capacity is the limiting factor as to how much energy can be produced. The solar garden was designed this way to get the maximum energy per dollar and not to have sharp peaks in energy production.
6. The solar panels are static; they do not follow the movement of the sun during the day or with the changing of the seasons (they are stationary and at the same angle year-round).
7. Data is not always usable and high-quality.

Definition of Terms

Resolution: The "measure of the sharpness of an image or of the fineness with which a device (such as a video display, printer, or scanner) can produce or record such an image usually expressed as the total number or density of pixels in the image," ("Resolution," n.d.).

Infrared Radiation (IR): "Invisible radiation in the part of the electromagnetic spectrum characterized by wavelengths just longer than those of ordinary visible red light and shorter than those of microwaves or radio waves," ("Infrared radiation," n.d.).

Infrared Thermal Images or Infrared Thermography (IRT): Infrared radiation is emitted by all objects. The amount of radiation emitted increases with temperature. With the utilization of specialized thermal cameras, images may be captured and show temperature differences. *Infrared* means "beyond red" and *Thermography* means "temperature picture" ("Thermography fundamentals," n.d.).

Licensed UAV Pilot: To fly a larger drone or UAV in certain airspaces, particularly near airports, the UAV operator is required to be a licensed pilot per the Federal Aviation Administration (FAA) Small UAS Rule Part 107. A licensed pilot must have a Remote Pilot Certificate which shows

that a pilot can safely fly a drone and has the knowledge and understanding of regulations, operating requirements and procedures (“Certificated remote pilots including commercial operators,” n.d.).

Solar Panel: Also known as photovoltaic (PV) or light-electricity, is a collection of solar cells spread over a large area as shown in Figure 2. When light from the sun reaches a panel, the energy from the sun is collected and converted into usable electricity for the general public and industry (“Power: what are solar panels?,” n.d.).

Figure 2. CFU solar panels

Unmanned Aerial Vehicle (UAV): An aircraft with no human pilot onboard. These crafts are typically of smaller scale and controlled by a remote control or an onboard computer. Commonly known as drones (“Unmanned aerial vehicle,” n.d.).

Yaw, Pitch & Roll: The directions in which an aircraft may rotate while in flight. Figure 3 demonstrates these rotations ("Aircraft principal axes," n.d.).

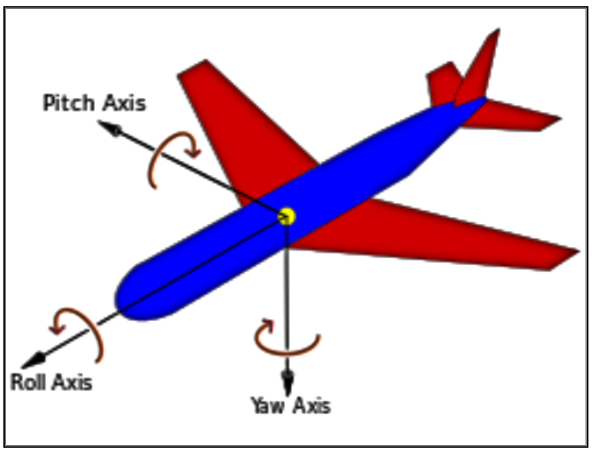

Figure 3. Rotations of an aircraft ("Aircraft principal axes," n.d.)

Electrical Conductivity: A material-specific property of "how well a given material will conduct electricity." Silicon (most solar panels are made from this material) is considered to be a semi-conductor (Donev et al., 2018).

Procedure

In conducting the research, the following procedure was followed to obtain and better understand information collected.

1. Contact Cedar Falls Utilities for cooperation and assistance with
    a. Acquire design information and energy data by inverters and by generator of the solar garden,
    b. Obtain permission to fly over the solar field, and
    c. Provide data collected by the system which will coordinate with the flight times.
2. Coordinate and communicate with the Thesis Committee.
3. Watch the weather and schedule times to the fly the UAV with licensed pilot and committee member Dr. James Dietrich of the University of Northern Iowa Geography Department.
4. Plan four flights at similar times of day but varying
    a. Season,
    b. Temperature,
    c. Weather, and
    d. Ground cover.
5. Obtain ground temperatures with the Fluke 561 Thermometer near the solar garden to compare with temperatures obtained during flights.

6. Download data and thermal images after each flight: process and upload the images utilizing various computer programs.
7. Request power and weather information from CFU after each flight for the power data that coordinates with each flight time.
8. Compare and analyze data.
9. Report findings.

CHAPTER II

REVIEW OF RELATED LITERATURE

Introduction

As the world's population and development continues to grow, so does the demand for energy. Energy for homes and transportation continue to increase and was reported to have increased by 2.1% in 2017 worldwide, with majority of the demand increases being in China, United States, and India ("Global energy and CO2 status report," n.d.). Demand for renewable energy grew worldwide. But demand did not increase as much as it has in previous years due to reduced fossil fuel costs. Regardless of these reduced costs, research is showing that the usage of renewable energy sources continues to rise. Costs are decreasing,

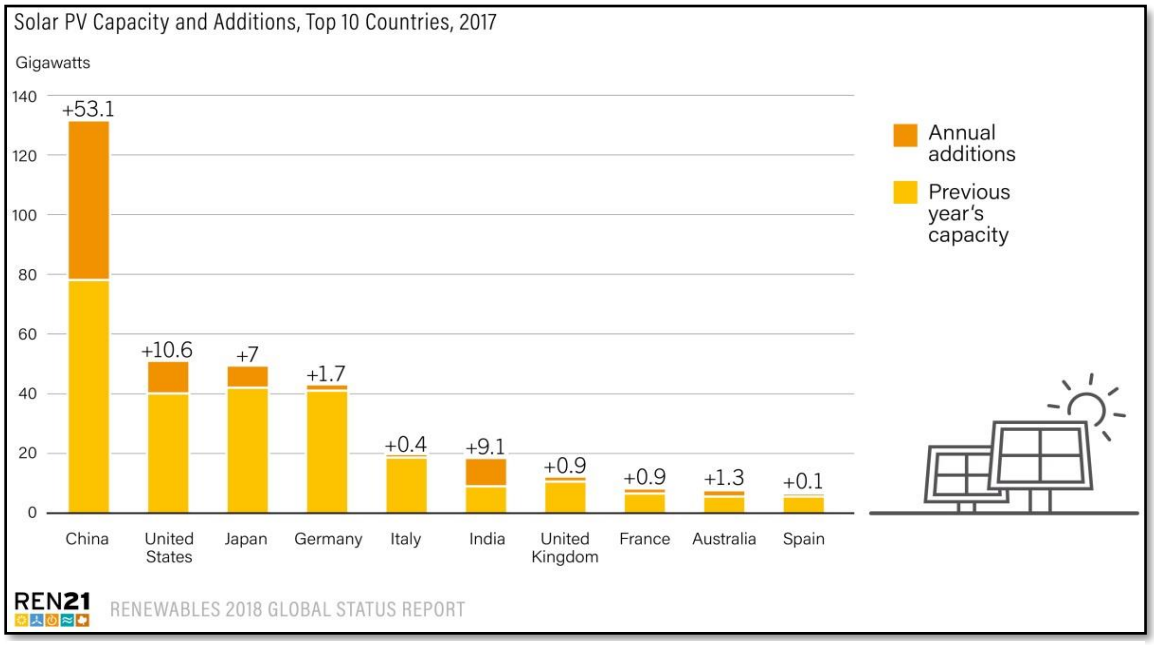

Figure 4. Top 10 countries with solar in 2017, source: ("Renewables 2018: global status report," n.d.)

investments are increasing, and there are numerous advances in the renewable technologies that are leading countries to continue to increase the implementation of these energy sources as shown in Figure 4 ("Renewables 2018: Global status report," n.d.). Building and material costs in addition to operation costs, maintenance, and repair are all significant to the overall expense of building and maintaining an effective solar field (Leva, Aghaei, & Grimaccia, 2015). Wind turbine maintenance is quite expensive and difficult given the size and location of the motor and blades. Infrared thermography via unmanned aerial vehicle is considered a viable and cost-effective way to recognize cracks, failures or other problems before they become problematic (Galleguillos et al., 2015).

The public is pushing for renewable energy options. Some researchers have estimated that coal, natural gas and oil resources will be depleted within the next 50 to 115 years (Ritchie, 2017). Renewable sources of energy, once considered to be niche markets, are becoming mainstream and therefore more competitive in the energy markets (Tsanakas, Ha, & Buerhop, 2016). An increasing number of cities, regions, and countries are joining groups, creating alliances and implementing initiatives with the goal to increase renewable sources of energy. These groups, such as United Nations Climate Change, are setting goals. For example, one goal may be having no or significantly

reduced emissions by 2050 to combat climate change. As seen in Figure 4, according to the Renewables 2018 Global Status Report, China has the largest solar photovoltaic capacity and additions in the world ("Renewables 2018: Global status report," n.d.).

As more renewable sources are researched and developed, the storage of the energy created is becoming a concern. Non-renewable sources, such as a coal power plant, can create energy regardless of the time of day or weather. Because renewable energy is dependent on wind or the sun, the energy production needs to be maximized during production hours and then stored until it can be utilized. Once the energy storage problem is solved, then renewable energy can truly compete in energy production (Hammami, Torretti, Grimaccia, & Grandi, 2017).

Research in the areas of drone technology, uses, and opportunities continue to increase as the technology improves and changes. Not only are researchers striving to answer the question of what unmanned aerial vehicles can do, but also if the data obtained is accurate and usable by the operator and company. Utilizing drones in the area of energy production is still a new concept but is quickly becoming more common.

Photovoltaic Solar Panels

Energy from the sun has been a part of life since creation. But only within the last 200 years have scientists designed and created solar panels that provide energy directed by humankind. In the past half century, the technology for photovoltaic (PV) systems have progressed to be an economical and efficient way for homes and businesses to capture the sun's energy and convert it into electricity on a homestead or for a utility company. Advancements in solar technology have reduced the cost of the panels by over 70% and is expected to continue to decrease with more research and developments (Sharma & Chandel, 2013).

Many materials and designs were created over the years. The first solar cells started collecting energy at an efficiency rate of 1% but have progressed to efficiencies in the range of 20 to 30%. Some of these advances were created for powering satellites orbiting Earth (Baker, n.d.). Current photovoltaic technology utilizes silicon. Silicon is the second most abundant element in the earth's crust and is a semi-conductor with properties allowing it to create electricity from the sun's power.

The cost and payback rates for solar energy is dependent on the life of the solar panels themselves. The solar panel's life is the amount of time at which the panel is capturing energy and providing an optimum, efficient, or expected output. As the cost decreases with the increased number of years a solar panel stays in service, solar energy becomes

more appealing to utility companies and consumers (Tsanakas et al., 2016). If solar energy is considered as being in the early stages of development and implementation there is much more potential. “About 3.8 * 10^24 J of solar energy can be obtained on Earth’s surface which is 6000 times greater than the world consumption,” (Gulkowski & Skomorowska, 2018).

As the need for renewable energy grows, the development of new solar technologies and designs continue to be developed. Testing for the efficiency of solar panels are typically completed on clear days of various seasons. This gives researchers a basepoint but are not true operating conditions (Zaoui, Titaouine, Becherif, Emziane, & Aboubou, 2015).

Rain, snow, wind, clouds, darkness (night), and large temperature ranges are a few of the conditions a solar panel is likely to experience, and much of the time, these environments are experienced in a variety of combinations. These conditions, especially together, may not be fully considered when the manufacturer tests the panels to estimate the life of the panels; laboratory compared to actual conditions. Further research would be helpful in determining the best panel materials under various real-world conditions (Sharma & Chandel, 2013).

Solar Panel Efficiency

As the technology improves and the solar cells become more efficient, researchers start looking more closely at the lifespan of these panels. Many units in place are only expected to last 20 to 25 years. However, there are solar panels still in use that are about 40 years old and they are still operating at an efficient level. Energy efficiency, cost effectiveness, safety and reliability can be prolonged with successful maintenance (Grimaccia, Aghaei, Mussetta, Leva, & Bellezza Quater, 2015).

Photovoltaic cell degradation can occur when the cells are not kept clean. Operators and maintenance personnel must be aware of this to keep the units operating effectively. This is to be sure they are free of dust, smog, dirt, pollen, snow, frost, etc. (Waco, n.d.). When panels are set to almost horizontal angles, chances for the panels to collect dust, snow, etc. increases and therefore increases the chance of failures and loss of power. Horizontal placement of the panels also makes manual visual inspection more difficult as a ladder or some other elevated platform would be needed for the inspector to have an adequate view of the panel from above (Gallardo-Saavedra, Hernandez-Callejo, & Duque-Perez, 2018). Panels placed at an angle to the ground allow for rain and snow to easily slide or run off the panels. Rain also cleans the panels of dust, pollen, bird excrement, etc. Operators could manually dust and

clean the panels, but typically do not as this type of cleaning risks scratching the surface or causing other damage to the panels. In general, the temporary dirt on the panels is preferable to permanent damage.

China's implementation of solar panels, with the goal to reduce CO2 emissions, is increasing at a phenomenal rate. There is a great need for an energy source that does not pollute the air. There is currently severe aerosol pollution (smog) over much of the populated areas of China. This air pollution reduces the effectiveness of the solar panels because the solar radiation is unable to reach the surface of the earth; unable to reach the solar panels ready to collect energy. Weather, such as significant cloud cover, can have the same effect on the efficiency of the photovoltaic cells (Li, Wagner, Peng, Yang, & Mauzerall, 2017). Wind, humidity, and high UV radiation are other types of weather that can impact power generation (Aghaei, Gandelli, Grimaccia, Leva, & Zich, 2015).

There are other possible culprits for photovoltaic cell degradation. Solar cell deterioration may occur due to defects on and in the individual units. This may include sealant problems allowing water penetration, impurities and defects in the crystals, microdefects, and cracks (Kaplani, 2012). Other problems may arise from optical degradation which includes bubbles and discoloration, electrical problems resulting from

poor soldering, snail tracks, shunts and breakage of interconnection ribbons, and non-classified issues such as short-circuited bypass diodes, modules, strings or failures of the junction boxes (Tsanakas, Vannier, Plissonnier, Ha, & Barruel, 2015). These faults are often difficult to identify with visual inspection. When these problems are finally identified, there is a high potential for severe degradation of the panel(s) resulting in significant power loss and safety concerns. Research shows thermal imaging provides details and identifies failures before they become a major problem (Tsanakas et al., 2016).

One would believe that the greater the heat intensity or ambient temperature, the greater the energy created, but the opposite is true. "Efficiency depends strongly on the temperature of the PV modules and an overheating causes a decrease of the produced energy," (Acciani, Simione, & Vergura, 2010). Sharma and Chandel (2013) agreed that the energy output is dependent on the temperature of the solar panels: higher operating temperatures equal a decrease in output power. Temperature affects how electricity flows because a decrease in temperature decreases the resistance in the conductor. "Cooling the PV panels allows them to function at a higher efficiency and produce more power," ("Lesson: The Temperature Effect," 2009).

High ambient temperatures and high solar irradiation have also been shown to increase the degradation of the photovoltaic cells. The

effect of the degradation is significant power loss (Kaplani, 2012). Large temperature variations within a PV module can also cause irreversible damage (Vodermayer et al., 2008). Steps can be taken to reduce the negative temperature effects. Developers may utilize light-colored materials in construction of the panels. Significant airflow under the panels, whether the panels are in freestanding in a field or mounted on a rooftop, is essential. Components not directly attached to the panels should be placed in shaded areas (Fox, n.d.).

Research has been conducted related to the placement of batteries and storing the energy created by the PV panels. It was found that when batteries were stored directly under the panels, even if there was space to allow for airflow, hot spots were created on the panels themselves. These hot spots were found to reduce the voltage and decrease the amount of power created and the efficiency of each of the cells (Hammami et al., 2017). Hot spots are created when a cell has a greater temperature than it is meant to be or is significantly different than those next to it. These spots may show that the cell is defective. It may pass a higher current than it was meant to and therefore takes on power rather than passing it to the inverter and then to the power grid for consumption elsewhere. This higher current in turn creates a higher temperature than the neighboring solar modules which is visible when captured on infrared photos (Tsanakas, Chrysostomou, Botsaris, & Gasteratos, 2013).

The challenge is how operators are able to monitor and diagnose problems in large solar plants, gardens and systems. Most have hundreds or thousands of photovoltaic modules that need to be monitored to ensure that the modules are operating effectively. Some systems, similar to the Cedar Falls Utilities solar garden, are unable to monitor each and every solar cell. The system set up for CFU allows operators to monitor the total garden output in kilowatts by the minute. Operators may also monitor the solar garden at each of the 41 inverters in five-minute increments as shown in Appendix A, though in most cases, studying the data in a spreadsheet is time consuming, does not give exact location of solar panels with problems, and will not provide much assistance to the operators on a day to day basis.

Unmanned Aerial Vehicles

Unmanned Aerial Vehicles (UAV), commonly referred to as drones, for many years, have been used in data collection, military operations, photography, and to provide a source of entertainment for many people. Some histories suggest that the use of UAVs began over 200 years ago.

Drones are taking humans where they could not previously go easily, safely, and economically. According to Goldman Sachs Research, by 2020 the UAV market is forecasted to top $100 billion worldwide with "growing demand from the commercial and civil government sectors," ("Drones reporting for work," n.d.). Drones are being utilized to take photos to record and/or recreate three-dimensional models of historical sites or buildings that are not easily accessed. This could be due to how difficult it is for a person to obtain physical access or possibly because the local government simply does not allow UAVs near its historical buildings or structures of significance (Eisenbeiss, 2004). Drones are also making digital mapping possible, complete with metadata (Grimaccia, Leva, & Niccolai, 2017).

UAV's are able to provide information without risk of human life. Drones can go where humans cannot safely such as in and around tall buildings, under bridges. They can be utilized when inspecting hard to reach areas such as wind-turbines and roof tops. For example, thermal infrared roof inspections have been conducted with workers on rooftops

of homes and other buildings. This task is completed at night which is dangerous for the workers and takes a considerable amount of time. With the help of thermal photographs obtained by a drone, wet and damaged insulation has been located quickly and without risk to human life (Zhang, Jung, Sohn, & Cohen, 2015). Utilizing drones reduces noise on rooftops at night and allows workers to easily assess more rooftops in a given night, than if workers had to continue to physically climb onto the roofs.

Infrared (IR) photography is useful in multiple situations because temperature differences can be seen in a non-destructive manner. Variations in temperature are shown on photos taken by specialized cameras that detect radiation proportional to temperatures and emitted by all objects. Knowledge of objects, what temperature differences should and should not be may help provide useful information to a researcher analyzing the photos. Further observations reveal additional information, useful details and possible abnormalities. It is the abnormalities and gradients that tell the story of the objects in the photos (Tsanakas et al., 2013).

Unmanned aerial vehicles have also been used in disaster responses all over the world. Drones are changing the way researchers, companies and humanitarians operate. UAV's can carry supplies necessary for survival to those in need, assist law, and continue to assist

in military efforts (Thomas, 2018). Drones assisted with relief efforts in 2017 after Hurricane Harvey hit Texas. Public safety was the main concern of officials. Public works and others assisting with relief efforts utilized UAVs to assess damage, speed recovery efforts, and provide citizen support by providing information of the flood status of people's homes, neighborhoods, and businesses. Drones have provided assistance with other rescues as well. They go into places such as caves and above areas struck with natural disasters, with the hope of assisting human responders to save lives and rebuild infrastructure (McCabe, 2018).

The United States Army Corps of Engineers (USACE) needs more than basic surveying after a hurricane makes landfall. With the excessive force of water and wind, not only can dry land be altered but under the water as well; shifting of the shorelines and ocean floor. These changes can impact where ships and boats can maneuver and dock. USACE utilizes Coastal Zone Mapping and Imaging Lidar. Drones with this system can reach affected areas quickly and help assess damage on land, estimate debris quantities and shifting sand and sediment under the water's surface, helping the affected areas to get back to normal (Luccio, 2018).

Thermal imaging is commonplace in identifying flaws within electrical boards and differences in surface temperatures of buildings.

Because of the affordability and timeliness, thermography inspection is becoming one of the more popular methods to identify failures (Aghaei et al., 2015). Thermal images obtained with UAVs is being considered as a tool in Serbia to detect hot water pipelines. These pipelines have been utilized for years to heat apartments in urban areas (Ristic, Bugarinovic, Vrtunski, Govedarica, & Petrovacki, 2017). Identifying these problems is likely not to be done with the naked eye, and therefore thermal imaging is essential in detecting anomalies, according to research. The time of day in which the images are taken do play a part as well. Building inspections should be completed prior to sunrise. PV-systems need to have thermal images taken during daylight hours (Entrop & Vasenev, 2017).

The global push for reduced greenhouse gas emissions has led to the development of the Kyoto Protocol. This is an "international agreement linked to the United Nations Framework Convention on Climate Change, which commits its Parties by setting internationally binding emission reduction targets," ("What is the Kyoto protocol?," n.d.). France, for example, has committed to significantly reduce greenhouse gas emissions. One way the French are doing this is by reducing the energy needed to heat homes which can correspond to making sure that most, if not all buildings, are running efficiently and without excessive heat loss through the roofs. In this scenario, unmanned aerial vehicles

taking thermographic images can help the local governments identify where updates and repair would be helpful in reducing heat loss throughout territories (Molines & Henriot, 2017).

Drones are able to provide accurate survey information with thousands more points than a traditional survey can provide. These points also have more details associated with each point and can be obtained at a rate that cannot be matched by any other method of data collection. As technology continues to evolve, so does accuracy. Some research argues that proper calibration of thermal images is necessary to account for lens distortion for more accurate results (Yahyanejad, Misiorny, & Rinner, 2011). Recent advancements have "made it possible to achieve less than 5 cm in vertical error," (Dixon, 2018). UAVs have been utilized to obtain detailed information about land surface temperatures which was previously done using satellite imagery. The drones are able to fly at low-altitudes. Flying lower will give higher resolution thermal images in which researchers can look at details such as ground temperatures, which is important in many applications and research (Si, Tang, & Li, 2018).

Accuracy of the photos and the temperatures are critical to thermography studies. The quality of the lens and camera are essential in obtaining quality data. The angle in which photos are taken and the focal length can also play an important role in the accuracy of the

information being collected. Operators should try to minimize the distance from the camera to the object/building in order to have accurate and detailed photographs with minimal distortion.

Research on the correlation between flight height and what types of PV panel defects can be seen at various height has been investigated. These range from six to twenty meters with defects including snail trails, white spots, discoloration, and more. The resolution of the image is relevant to the detection of failures and defects. Some research has shown that these images should be within the range of two to ten pixels per centimeter. Gallardo-Saavedra et al. (2018) suggests the resolution of the detector be at least 320 x 240 pixels. This resolution will allow operators to see smaller objects, or failures, more clearly and with more precision.

Obtaining images on clear and cloudless days is not always possible. This is especially true for areas where wind is a common occurrence, such as in the Midwestern states (Aghaei, Dolara, Leva, & Grimaccia, 2016). The UAV pilot needs to be mindful of not flying too close to the objects, solar panels in this case, as shadows could be created and alter the thermographic data collected (Leva et al., 2015).

Unmanned Aerial Vehicles & Solar Energy

Unmanned aerial vehicles are quickly becoming the norm for monitoring utility systems, particularly photovoltaic panels (Grimaccia, Leva, Niccolai, & Cantoro, 2018). Traditional methods, such as manual inspection, are expensive and take a considerable amount of time to complete (Gallardo-Saavedra et al., 2018). One utility company was able to reduce inspection time of transmission poles from one and a half hours to eight minutes (Trojak, 2018). Thermal imagery obtained by an UAV is an economic and efficient tool in solar panel maintenance and data collection; this technology is quickly changing the industry (Thomas, 2018). Companies such as Kespry are making these inspections easy, accurate and safe. Kespry announced in July of 2018 of its new *High-Resolution Thermal Inspection Capabilities* to assist businesses with identifying damage and other potential problems that may not be seen by the naked eye (Kespry, 2018). In some cases, such as solar gardens being installed on the rooftops of tall buildings, the only safe way to inspect the panels is to utilize an unmanned aerial vehicle (Grimaccia et al., 2017).

Problems over large areas may be located quickly and cost effectively with detailed real-time images and without any negative impacts to the solar panels or other utility plants (Leva et al., 2015). One of the goals of utility companies is to collect the maximum amount of

energy and detect problems before they become failures requiring downtime that could impact service and profitability. Research on the infrared analysis has shown that this is possible (Acciani et al., 2010). Grimaccia et al. (2017) found that the two most common defects within a solar field are hot spots and faulty bypass diodes. Both can easily be identified using infrared thermography. Additional research presented the recurring shapes of defects which were different for each type of defect. Hot spots are commonly round on the thermal images whereas faulty diodes present themselves as more rectangular.

With frequent and easily accessible data, companies will be able to reduce energy losses and improve or maintain maximum energy availability. This can be done by reducing or possibly eliminating the time necessary to repair a unit due to the frequent and detailed monitoring of the systems (Baschel, Koubli, Roy, & Gottschalg, 2018). Maximum energy output for the life of the solar garden can be almost guaranteed with good monitoring and locating degraded equipment (Grimaccia et al., 2015).

As solar fields become larger, data in the form of spreadsheets become increasingly difficult to read and detect faults (Tsanakas et al., 2015). Some researchers are investigating and developing possible algorithms to have a computer detect the anomalies by sight. These algorithms are still a work in progress, but once perfected, will reduce

the number of man-hours required to located failures (Gallardo-Saavedra et al., 2018). Infrared thermography is becoming a popular investigative method to inspect and test the solar cells in a nondestructive process as well as without interrupting the operations of the solar field. The infrared images show detailed information on varying surface temperatures allowing operators to quickly identify defects and anomalies. This information can then help managers and operators discuss and create a plan for repairs to keep the cells operating at optimal efficiency (Kaplani, 2012).

The technology and accuracy of thermal images obtained through UAVs will continue to evolve and along with it, tools will continue to be developed for technical analysis. These tools will make it easier, quicker, and cheaper to identify failures and improvements. Researchers continue to prove that thermography inspection is accurate and cost effective with proper tools and analysis programs. Currently, this method requires highly specialized instruments. As development and installation of solar panels and gardens continue to take place throughout the world, research into reliability, improvements, necessary maintenance, and costs will become necessary for consumers and investors (Tsanakas et al., 2016). It has been determined that both quantitative and qualitative data could be obtained from thermal images, identifying faults and diagnosing the reasons for the hot spots using

thermal images as well as “suitable thermal image processing techniques,” (Tsanakas et al., 2013).

Optimizing maintenance activities is essential as larger and more solar fields are installed in various locations throughout the world. Managers, pilots, programmers, and those conducting the analysis will continue to hone their skills. Therefore, the cost per hour for this part of the inspection will continue to decrease. Operators, owners, insurance companies, and others with vested interests in solar gardens will be able to read detailed reports on the performance of the solar fields on a more frequent basis (Grimaccia et al., 2018).

CHAPTER III

METHODOLOGY

Project Location: Cedar Falls Solar Garden at Prairie Lakes

Eight acres of undeveloped land near a recreation area was available to Cedar Falls Utilities (CFU). This small area was limited in use potential due to size and shape of the parcel. It was determined that a solar garden would be a good use of the space and so design and development began. The solar garden was designed to maximize power creation with the limited space. To achieve this design goal, CFU placed as many solar panels in the area and with the largest transformer that was possible. The transformer chosen was similar to that of other CFU transformers currently use throughout the Cedar Falls area and CFU keeps in stock. If an issue with the transformer were to occur, CFU could easily repair and/or replace in a timely manner.

The solar garden design exceeded the number of panels necessary to obtain the desired energy output. The CFU solar garden was built so that a maximum output could be obtained in mornings, evenings, cloudy days and with the knowledge that solar panels degrade over time. The inverters and solar panels were placed so that the maximum output for the longest time possible could be obtained. Thus, economics in getting the most power at the lowest price governed the design. The purpose

was not to obtain peak performance of each solar panel, but to have the most energy production for the longest possible time each day.

Construction for the garden began in November of 2015 and in April of 2016 production began. In the field there are 6516-305 watt panels. Each are about 4 feet by 2 feet and are arranged in groups on top of tables. Three I-beams make up the support structure for each table as shown in Figure 5. The CFU solar garden has 41 inverters like the one shown in Figure 6. The inverters are mounted on the legs of the solar panel tables. The panels are grouped among the 41 inverters as shown in Figure 19 in Appendix A. Each inverter can take up to 36 kW of power. The inverters are the limiting components

Figure 5. Support structure under solar panels

Figure 6. One CFU solar panel inverter

of this system as more power could be created than can pass through to the system. The panels' output is in direct current (DC) but to be useable by the public, the power must be converted to alternating current (AC). This conversion is done at the 480-volt transformer where the power is then fed into the CFU electrical grid.

The system was designed and considered to be a state-of-the-art facility at the time of its creation. 1500 kW of alternating current is considered a full load for the solar garden. The panels have been known to collectively create approximately 2000 kW direct current. There is more energy collected than can be converted to power at peak times. The peak and average power, provided by CFU, can be seen in Appendix A on Figures 20, 22 and 24.

The economics of building and operating the CFU solar garden is not a simple one. CFU did not feel it had the expertise to design, build and maintain the garden, nor could CFU receive any of the federal tax credits being offered as CFU is a non-profit and does not pay income tax. CFU does not own the eight acres of land upon which it is built. The land is leased from the City of Cedar Falls in a 27-year contract. The expert solar company from Pennsylvania, RER Energy, won the bid to build the solar garden. A legal agreement was signed to purchase power from RER Energy for 25 years.

The cost savings of the solar panels are then distributed among the CFU subscribers. The solar field is a community solar garden where people choose to sign up to be subscribers of the solar benefits. In this way, the solar field is revenue neutral and will not impact utility rates for any or all CFU customers. As is the case with most buying opportunities, the more people who sign up, the cost goes down. Because of this, initial cost estimates were difficult to calculate. The solar panels were purchased from an experienced solar panel company – Hanwha. Maintenance of the solar field is mostly directed toward controlling the native grasses that have been planted under and around the panels. The Tallgrass Prairie Center of the University of Northern Iowa assisted with the selection of these prairie plants. The desirable plants were to be a mix of maintenance grasses that would not grow taller than the panels and therefore block the sun.

As can be shown on Figure 21 in Appendix A, the system was at its maximum output during the peak hours of the day; between 11:35 AM and 2:20 PM. The maximum output for any of the inverters during this time was 37.5 kW. The average for the inverters was calculated when power (all 41 inverter values greater than 0.0) was being created at all inverters. 07:25 (7:25 AM) and 18:20 (6:20 PM) The output data is collected at the transformer and is a combination of all the panels; not individual panels.

Figure 23 of Appendix A shows the output variation near the UAV flight time in April. Only the midday data was provided for this day. Because of this limited data, the variation during peak times can be seen in more detail. There is no consistent peak with the output, however the inverters are shown to increase and decrease at approximately the same time and rate. Figure 24 shows the peak and average power in May. The output data in Figure 25 in Appendix A shows inverter power output for the entire day. One can see the plateau, however on this day in May, many of the inverters powered down, likely because the solar cells exceeded their maximum temperature and needed to have some time to cool.

Surveying Tools

The purpose of this study is to investigate and determine if varying temperatures, shown by thermal images taken by Unmanned Aerial Vehicle (UAV), on and around solar panels affect the efficiency and amount of energy captured/created by the solar panels. The tools utilized to obtain information are discussed in the following.

The eBee Ag Fixed Wing Unmanned Aerial Vehicle (eBee), shown in Figure 7, is programmed with eMotion computer software. This gives the drone and camera instructions as to where to take-off, fly, land, how many pictures to take over the specified area and the proximity (overlap) of each of these photos to each other. The operator/pilot chooses where to start, takeoff and programs the cone where the UAV is to land. This needs to be kept fairly narrow so as to ensure that the UAV does not accidently fly into an object and damage itself. These flight components are shown on the eMotion screen shot of a simulated flight in Figure 8. Also seen on this screen is the flight time, ground resolution, and overlap

Figure 7. eBee unmanned aerial vehicle

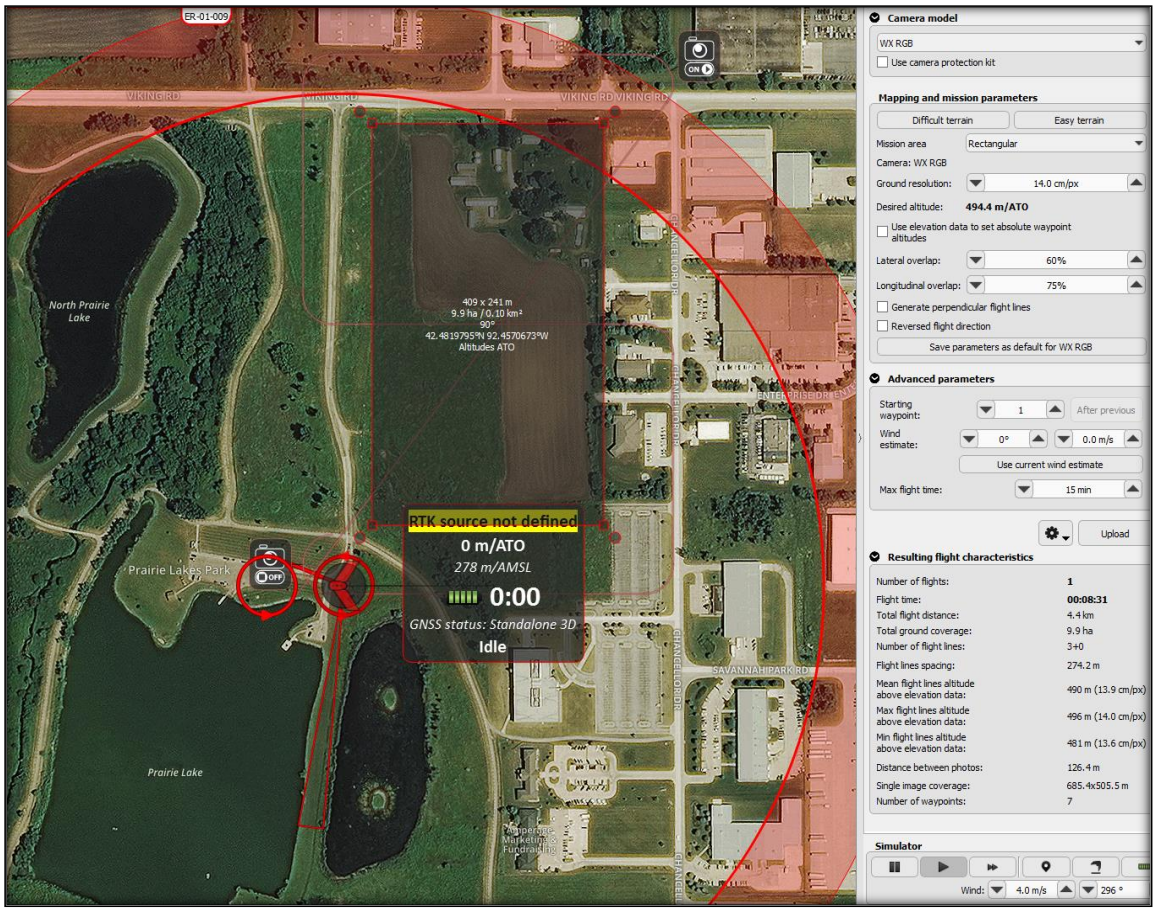

Figure 8. eMotion flight simulation set up

percentages. The flight length must be kept at about 20 minutes before the battery of the eBee will start to become critical.

The direction of the wind needs to be considered during the setup of the flight path. The eBee needs to take off and land into the wind. When in flight and obtaining data, the drone works best flying perpendicular to the wind. If the eBee flies into the wind, there is likely to be a flight with a considerable amount of buckling up and down. This would alter the quality of the photos as well as making it possible for the eBee to lose control and crash on the ground.

When conditions are not perfect, such as a considerable amount of wind, the eBee is programmed to correct its orientation. To do this, the eBee flies across the wind, and "crabs" to obtain a somewhat straight flight path.

A portion of the information available during flight in real-time is shown in Figure 9. This image is taken from the screen of a simulated flight. From this screen the pilot can monitor flight time, battery life, speed, distance, camera information, drone position information such as yaw, pitch and roll, and temperature.

The senseFly thermoMAP camera (Figure 10) is set within the eBee UAV. This camera is a thermal infrared camera designed for the eBee flights. The camera has "radiometric calibration" which means it is created and calibrated especially for obtaining accurate and absolute temperature readings ("The professional mapping drone," n.d.).

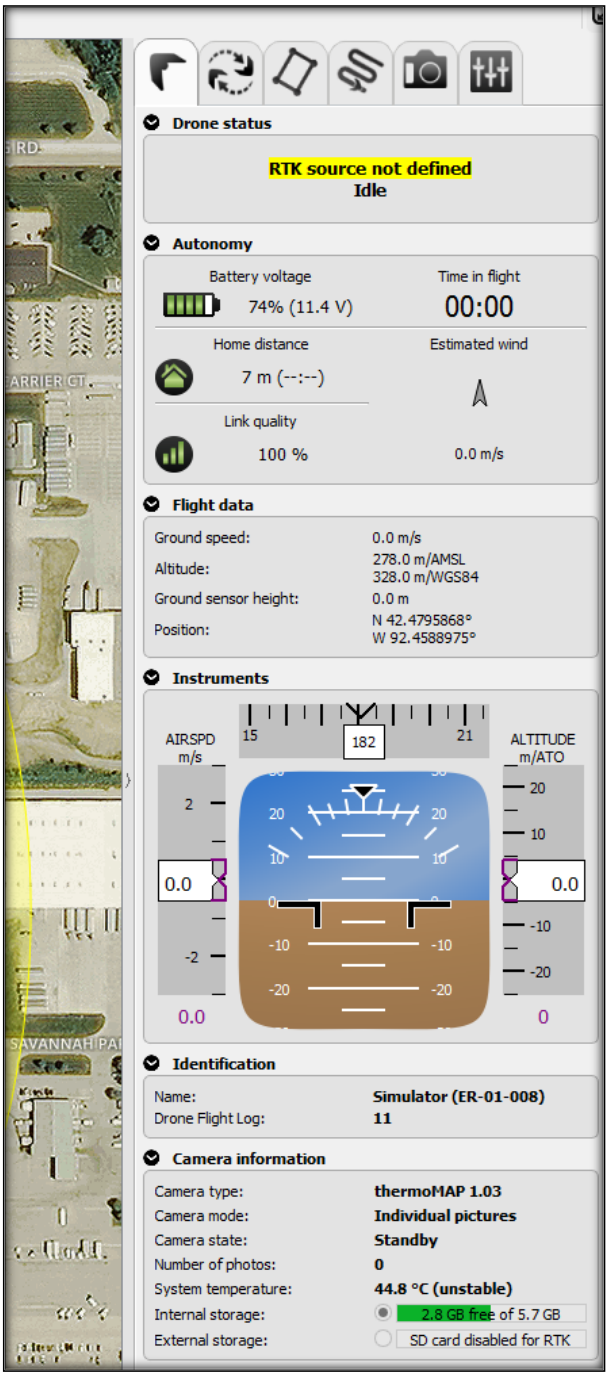

Figure 9. eMotion UAV real-time flight information

Figure 10. senseFly ThermoMAP camera

During the October, April and May flights, ground temperature readings were obtained using a handheld Fluke 561 Infrared Thermometer (Figure 11). Various points within the surveyed area were chosen to get a range of different temperatures due to varying surfaces. Temperatures were taken on asphalt, rock, grass, and prairie grass. This information will verify or show calibration errors of the temperatures obtained by the senseFly camera.

Figure 11. Fluke 561 IR thermometer

Computer Tools

Once returning from the field, photos are downloaded and combined in a process called image mosaicking. Pix4D, a computer program, is utilized to combine photos with overlapping areas. These images are pieced together to create one high resolution image of the area of interest. If only one photo was taken of the entire area, researchers and operators would not have enough resolution and detail to accurately analyze the solar field or any other area of interest. Thus, the need for multiple photos pieced together.

Gallardo-Saavedra et al. (2018) stated detector resolutions of 320 x 240 pixels are the recommended professional minimum pixel resolution. The resolution of the images for this research is 14 centimeters per pixel.

The images with infrared (temperature) information obtained by the UAV are loaded into the ESRI computer program ArcGIS (or ArcMap). ArcMap allows one to visualize, analyze, and compare the temperatures from the images, separately by date. The program also allows researchers to upload an aerial photo and create shapes so that the temperatures can of these shapes can be grouped together and analyzed. The output of the data is in the form of a spreadsheet which can then be combined with other data in a computer program such as Microsoft Excel. Excel was also utilized for this study.

CHAPTER IV

RESULTS

Flight Information & Data

Four flights were completed to obtain thermal data of the solar garden. These UAV flights were completed on 2018 October 17, 2018 November 07, 2019 April 24, and 2019 May 10. The images from the flight completed on 2018 November 07 were processed the same as the other flights with Pix4D. However, the November data was deemed unusable due to several anomalies and occurrences where the images did not line up appropriately. This research will therefore focus on the three flights taken in October, April, and May only.

As can be shown in the Figures 26 through 30 in Appendix B, the red lines show the actual flight paths the UAV took on 17 October 2018, 24 April 2019 and 10 May 2019 over the solar garden. The circles in flight path shows the UAV increasing and decreasing altitude. Any uneven flight lines show a bump or direction change in the UAV's flight path, usually due to wind. Overall the drone was able to overcome the challenge of some additional wind and get back to its programmed flight path.

The markers shown on Figures 27 through 30 in Appendix B indicate the location of the drone when the infrared photos were taken. Figure 26 shows the flight path only for the 2018 October 17 flight.

Figure 27 shows the locations of the drone when taking pictures along the flight path. Figure 28 is another perspective of the location of the UAV as it captured infrared images. One can see many images were captured; too many to utilize. For this reason, when the images were brought into Pix4D, the program chose and utilized approximately half of the photos. The processing time for these images, approximately half of the total photos, was over an hour per flight. Figures 29 and 30 show the flight path and drone location when capturing images for the 2019 April 24 and 2019 May 10 flights, respectively.

For each of the flights, the flight times were kept under 20 minutes. For the October, April and May flights, the flight times were approximately 10, 12 and 10 minutes respectively. The resolution parameter for the eBee UAV was set for 14 centimeters per pixel. To obtain this resolution, the eBee flew at approximately 74.1 meters above its takeoff altitude. A single image covered an area of approximately 89.6 meters by 71.6 meters. The eBee took photos about every 7.2 meters. The distance between flight lines was approximately 48.7 and 63.0 meters. These distances give an overlap of 54% and 87% as demonstrated by Figure 12.

Figure 13 is a photo of the computer screen with eMotion running while the eBee UAV was in flight on 2019 May 10. Looking closely, one can see the flight path, time into flight, and the yaw, pitch, and roll of the drone. The angle of the drone icon shown on the screen shows the UAV was adjusting for the wind.

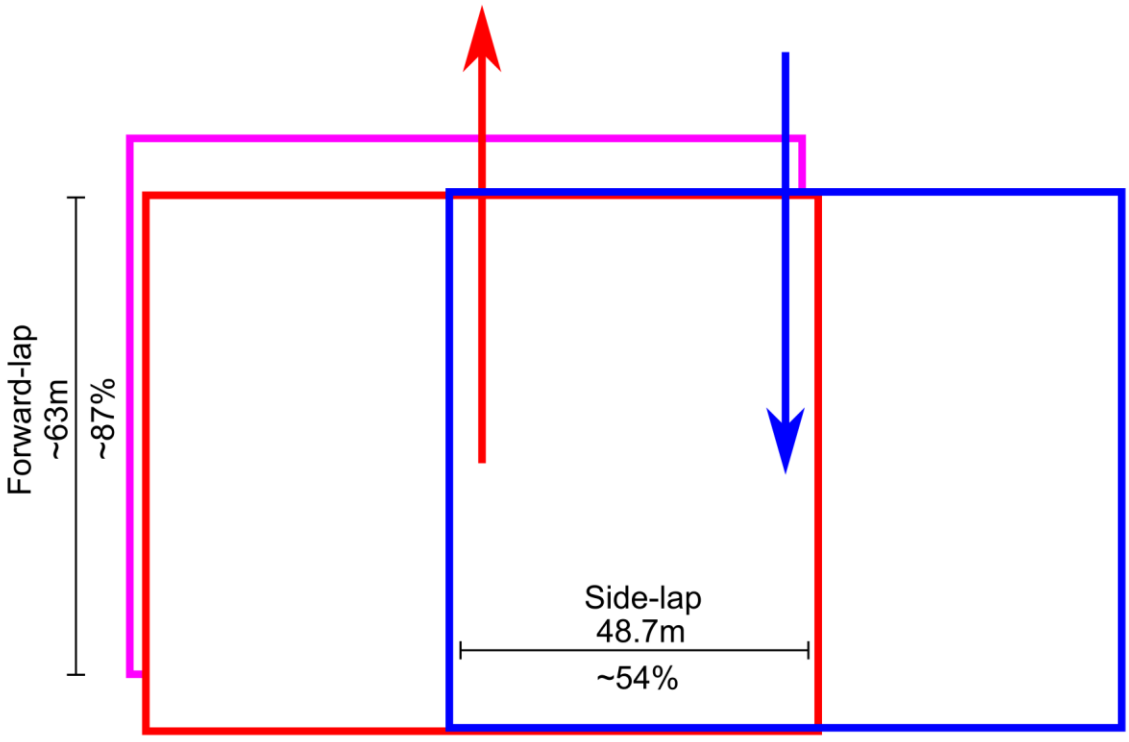

Figure 12. Flight line and photo overlap

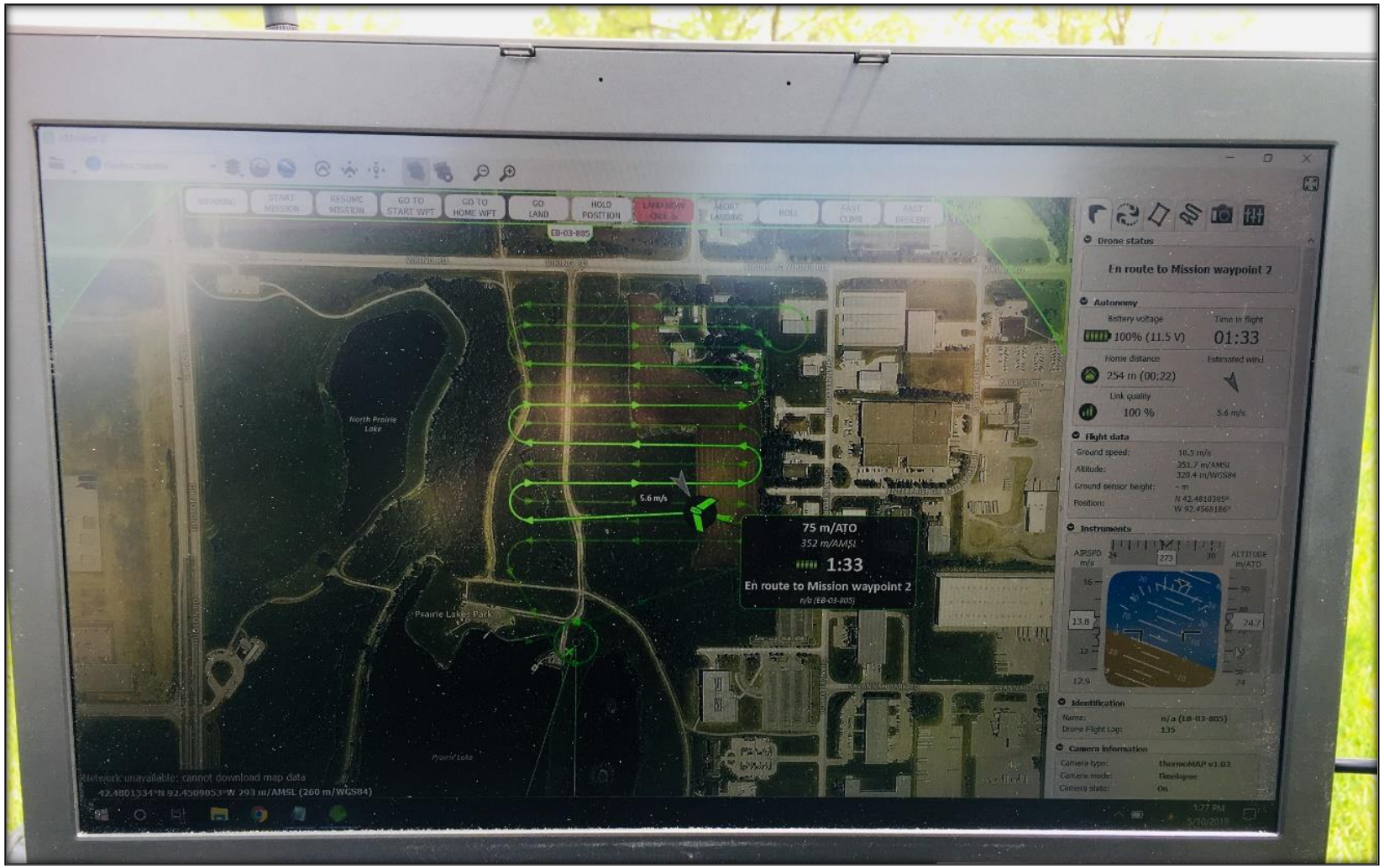

Figure 13. Photo of the computer screen with eMotion during 2019 May 10 flight

Figure 14 shows the camera locations as the UAV passed over the solar garden. Figure 15 demonstrates the numerous images captured in order to obtain the desired highly detailed information such as the thermal images. The screen shot also shows the images overlapping considerably. It is these overlapping images that provide details at an appropriate and detailed resolution.

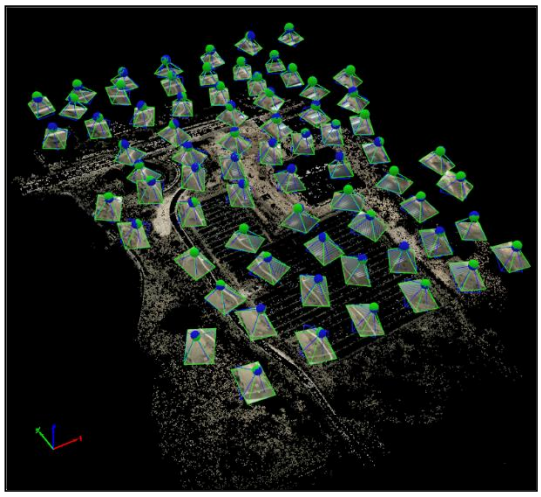

Figure 14. eMotion screen shot of images being processed

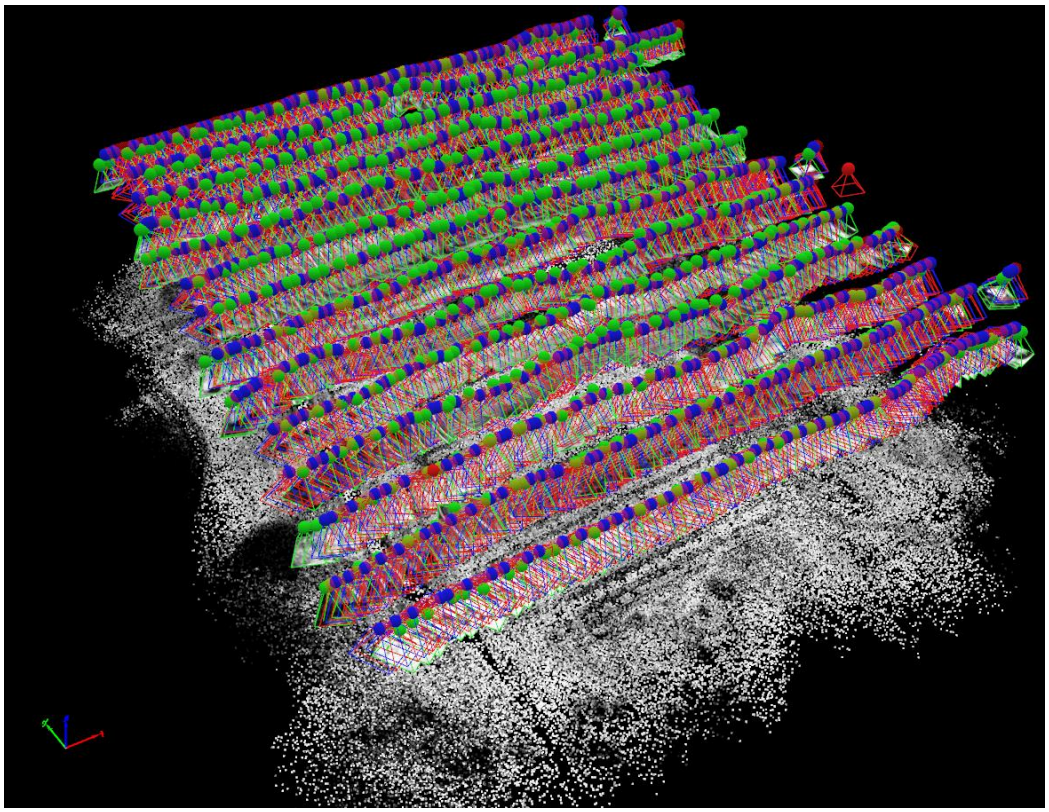

Figure 15. Pix4D image demonstrating independent overlapping images

Ground Temperature Comparison

Fluke 561 Thermometer temperature readings were obtained at nine different locations. These were approximately the same location each day. Without permanent ground markers, these locations, shown on Figure 16, are estimates, but satisfy the need for the readings and comparisons. Notes on these locations are as follows:

Figure 16. Approximate locations of Fluke 561 IR thermometer readings

1. Asphalt, centerline of the road and centerline of the solar garden driveway
2. Rock, edge of rock on centerline of the solar garden driveway
3. Rock, center of solar garden driveway
4. Grass, Shadow of the CFU solar garden sign
5. Grass, near corner of asphalt and south side of solar garden driveway
6. Grass (brown prairie), south solar garden driveway
7. Grass, inside the fence approximately 5th row from the south
8. Asphalt, centerline of the road, directly west of southwest chain-link fence corner of the solar garden
9. Grass, on the road shoulder, directly west of the southwest chain-link fence corner of the solar garden

Table 1 shows the readings obtained for these days by the Fluke IR handheld thermometer. Temperature comparisons were made between those obtained from the SenseFly thermographic images and the Fluke 561 Thermometer. The differences were, on average, within 2.8 degrees Celsius. The two greatest differences were 10.8 and 8.2 degrees. The smallest temperature difference was 0.0 degrees and majority of the differences were 5.6 degrees or less. A complete temperature comparison between the Fluke Thermometer readings and the temperatures ArcMap calculated is found on Table 9 in Appendix D. Figures 36, 37 and 38 in Appendix D are graphic comparisons of these temperatures. With minimal temperature differences, it will be assumed that the temperatures obtained by the SenseFly camera are in agreement with the Fluke thermometer and therefore accurate.

Table 1. Fluke IR thermometer temperature readings

Approximate Location (top row) and Degrees Celsius (rows 2-4)									
Date	1	2	3	4	5	6	7	8	9
2018Oct17	21.2	18	17.2	7.3	17.5	11.1	17.5	22.2	12.9
2019Apr24	28.5	24.4	22.9	20.7	19.9	19	20.6	25.6	23.2
2019May10	36.2	27.5	24.3	16.2	23.5	21.9	27.1	34.8	23

Temperature Analysis of the UAV Obtained Data

CFU personnel have been instrumental to this research by providing power data at the time of the UAV flights both at the transformer as well as each of the 41 inverters. The dates in which an UAV flew over the solar garden are 17 October 2018, 07 November 2018, 24 April 2019 and 10 May 2019.

The photos were altered so that temperature variations could be more easily seen. The grayscale infrared photos give each pixel a temperature value in degree Celsius. A grayscale image demonstrating this can be seen in Figure 39 in Appendix D. These were transformed to 256 RGB (Red, Green Blue) color scale so that the temperature differences could be seen more easily by the human eye. Each color gradient shows the temperature of the solar panels and therefore the heat intensity or surface temperature of the panels. These color gradations can be seen in Figures 40, 41 and 42 in Appendix D for October, April and May flights, respectively.

The colors or temperatures obtained from each of the flights can be averaged utilizing “shapes” created within ArcMap. These shapes are outlines of the solar panels. They were created by hand in ArcMap with the aerial photo as a visual guide. The ArcMap program outputs data in the form of a spreadsheet for each of the shapes created, separately by

flight. The solar garden has 41 inverters therefore 41 average temperatures could be calculated.

As can be seen on Figures 40, 41, and 42 in Appendix D, more than 41 rectangles were created. ArcMap allows the user to group individual shapes so that an average can be taken of the group. The values obtained in an output file, in the form of a Microsoft Excel spreadsheet, were compared with the energy output provided by Cedar Falls Utilities. The flight time and the time of the CFU energy values utilized in this comparison were within 5 to 10 minutes of each other. During this time, significant increases or decreases in output or change in temperatures is unlikely. This comparison can be seen on Figure 43 in Appendix D.

CFU's weather collection site approximately one mile north of the solar garden. The temperature collected is in Fahrenheit, so was converted to Celsius using the equation: $(X\ °F - 32) \times 5/9 = Y\ °C$. The wind information was given in degrees. Figure 17 shows graphically that these values indicate winds are from the North-North West, South and

North-North West in October, April and May respectively. Thermal data is best when collected on sunny and cloudless days. "The intensity of the irradiation should be more than 700 W/m^2 on the PV modules surface," (Aghaei et al., 2015). The solar radiation information was not able to be collected at the solar panels themselves. All available weather data CFU collected is shown in Table 2.

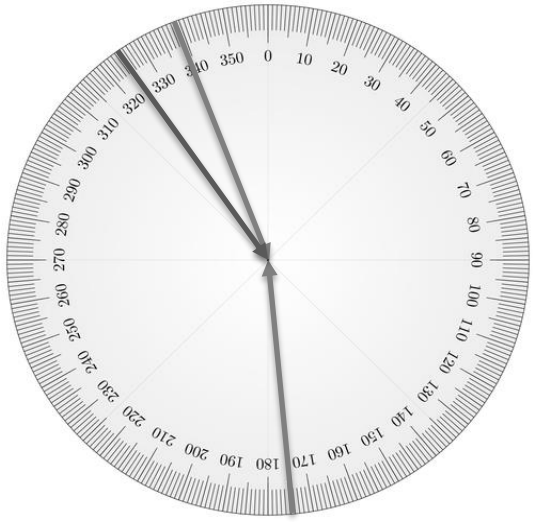

Figure 17. Wind direction

Table 2. Weather data during flights

Date and Time	Outside Temperature (degree C)	Wind Speed (MPH)	Solar Radiation W/m^2	Humidity %	Wind Direction
10/17/2018 13:25	7.95	6	587	50.9	339.1
4/24/2019 13:45	15.09	11	401	74.7	174.6
5/10/2019 13:30	14.70	8	316	44.0	325.3

One of the goals of this research was to determine if there is a correlation between the temperature of the solar panels and the power output. Figures 21, 23 and 25 of Appendix A shows that the power output is similar among the various inverters. The October and May data shows that similar power of about 36 to 38 kW is obtained even though the temperature groups are 18 to 23 degrees Celsius and 24 to 28 degrees Celsius respectively. However, the April data is grouped between 22 and 27 kW and has a temperature grouping between the October and May temperatures with a range of 22 and 24 degrees Celsius.

Abrupt color changes on thermal images, in general, may be indicative of problems of the solar cells. These differences can provide necessary information to those monitoring the efficiency and the well-being of the solar cells. Grayscale thermal images may help determine degradation of the solar cells. Degradation percentage is calculated by area that is white (hot) divided by the whole area of the module. The images can also provide the boundaries of the defects or anomalies.

Thermal images are informative in identifying locations of failures or anomalies, however they do not provide any information regarding the power output of the panels at each solar cell. Power information

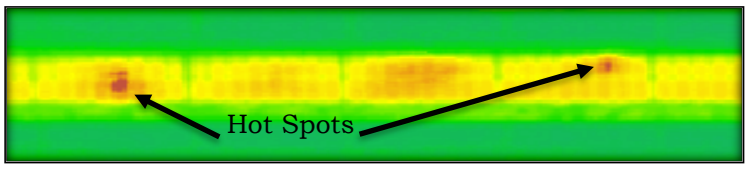

Figure 18. Thermal hot spots on the solar panels

must be obtained by looking at monitoring data at each inverter, in CFU's case, on a spreadsheet. This is because the gradient of colors shown through the thermal images are temperatures relative to each other, not power. After checking the hot spots found on the thermal images taken in October against the data obtained from the inverters, it was determined the power was similar to that of the other inverters. Hot spots are shown in Figure 18. This data shows that the hot spots did not affect the overall power output for these group of panels.

Solar panels have maximum power potential, so even if conditions were right to provide a significant amount of output, only the maximum could run through the inverters at any given time. The excess potential power is lost and unused. There is a maximum temperature the panels can become before heat damages the components of the solar cells. If the cells become too hot, they will shut down to prevent physical damage and restart once the temperature allows energy collection to begin safely. This is a possible reason for the dips in energy shown in Figure 24 in Appendix A during the peak hours, however, further investigation would need to be done to be sure.

Limitations & Recommendations for Future Research

While it seems simple enough to get outside and fly an unmanned aerial vehicle as often as one would like, this is not always the case in Iowa. The weather changes day to day and sometimes hour to hour. There are times in which precipitation and wind make conditions unsafe to fly. Unsafe for the UAV as well as people and objects on the ground. If conditions are not favorable significant damage could incur. A different and stronger platform, such as a quadcopter with a thermal camera, would be something to consider for future research in this area as it may be able to adjust to the wind more easily than the fixed wing eBee.

The flights for this research were conducted in the early afternoon hours. This is the best time for the sun placement as well as scheduling flight time with Dr. Dietrich, a licensed UAV pilot. The thermal images collected at these times provided varying temperatures gradients. However, the solar panels typically exceed their maximum output at this time and so the data collected at the inverters and transformer show a plateau of power output. If money was not a concern, the study could be repeated with solar panels that are connected to inverters which will not limit power production. This would allow peaks in the power data. Along with this repeated study, there may also be other changes to the research methods such as being conducted at varying times of day and

during the cooler months of the year, because cooler temperatures allow for greater conductivity of electricity. As in any research, more data is better because a greater the understanding of the data could be found. A correlation, if there is one, between power and temperature may also be identified.

Future research may include other options for gaining a better understanding of the temperature effects on the solar panels. Researchers could add external monitoring sensors to the panels themselves, continuously measuring the temperature and the energy output of each panel. External sensors could also collect information in relation to the time of day, or the sun's position, and see how it correlates, if at all, to the panel temperatures and electrical outputs. The reflectance of the solar panels is another option for data and finding possible relationships with efficiency and power output.

The thermal camera utilized in this research is an uncooled detector. This means it operates under ambient temperatures. For this reason, the drone must fly in circles not only to increase altitude but also to calibrate the camera so that it is ready when it begins its programed flight and takes photos. Cooled detectors are much more accurate because they are vacuum-sealed and cryogenically cooled. While they are more accurate, cooled detectors are not widely used due to the price of the camera, estimated at ten times higher than an uncooled camera

(Gallardo-Saavedra et al., 2018). As uncooled cameras become more widely utilized, investigating possible “thermal drift” could be a future research topic. Thermal drift is an idea that the temperature of the drone and/or camera heats up in proportion to the flight time. While there may not be a significant influence on the data obtained, especially on short flights, there could be, which is why further research may be warranted.

Some research has shown that the angle in which the camera takes the photos in relation to the photovoltaic cells could alter the data being collected. These angles may pick up hot spots that are not truly present, or the opposite may be true. Further research as to an appropriate height and angle is being conducted and some researchers hope to become standardized as UAV’s are used more and more for this purpose. This would be helpful in being able to better compare research conducted in different regions of the world.

CHAPTER V

CONCLUSION & RECOMMENDATION

The data collected in this quasi-experimental research project has provided information for the research questions and led to more questions about this topic. The questions being answered in this research include inquiring about a relationship between temperature and energy output and the accuracy of the thermal images.

Comparing the data provided by CFU and the information obtained from the UAV flights does not show significant evidence of a correlation between solar panel temperature and power output. A correlation may not be seen because of the design and placement of the solar panels; there are more panels and energy created than the inverters can pass into the electrical system, as they are at their maximum output. Another reason for this lack of correlation is the assumption that the greater the heat of the panel, the greater the amount of energy collected. The exact opposite is true. There is more potential for energy to be created with cooler ambient temperatures as the solar cells and the electrical components are less likely to overheat. When components overheat, they are programmed to shut down to cool and prevent damage. When shut down, no energy is being captured.

It is been recommended and made clear by researchers, as well as the data obtained for this project, that thermal imaging via UAVs is an

accurate method in obtaining information. However, a greater understanding of drones, cameras and thermal images is necessary prior to making any investments in these tools for solar field maintenance. More thoughtful decisions can be made regarding the purchase and use of a UAV, camera, and software with more research. This equipment and technology may work for a large utility company, but it may not be the best choice given the size, design, and information required for a smaller solar garden such as Cedar Falls Utilities'. Battery life is just one of details that needs to be considered. At this time, no standards or baselines are in practice for in the industry related to UAVs and thermal images as maintenance tools. Researchers, drone and software companies and utility operators hope to see standardization processes and values in the future. These standards will assist with weighing the pros and cons of investing in new technologies and processes as is discussed in this research.

Thermal imaging is shown to be an effective and cost-effective method to determine anomalies and defects on solar panels. The data obtained for this research provided data confirming the high accuracy of thermal images. These images may help with maintenance so that solar panels can meet and/or exceed manufacturing estimates of the effective life of the panels. This will also ensure that the customers buying the energy are getting the most economical option. Thermography is not the

only method to evaluate the status of solar panels. Other methods may include, but not limited to, electroluminescence, photoluminescence, and fluorescence (Aghaei et al., 2015).

Further research in the true causes for degradation of the solar panels may also be conducted. Further research may lead to increased quality and effectiveness of newly constructed solar panels and fields. Researchers may also find greater understanding of various solar panel defects and what causes them; manufacturing, installation or daily wear and tear being exposed to natural elements. Operators may be able to utilize research like this to develop observation techniques and programs to identify failures before they become problematic or critical. Identifying the differences between actual exposure degradation and that which is laboratory induced and documenting the level at which the defects and failures effect the output of the panels will be important in future investigations. Do they make a significant difference? Or will these defects lead to significant output reduction if not addressed in a timely manner?

Further research may help establish a baseline to compare current and future solar gardens so that accurate comparisons may be conducted. Standardization for how fields are inspected, measured, and how operators determine the type and severity of each failure would assist operators and utility designers. These are all important concepts

as renewable energy production becomes more necessary and common throughout the world.

REFERENCES

Acciani, G., Simione, G., & Vergura, S. (2010). Thermographic analysis of photovoltaic panels. *International Conference on Renewable Energies and Power Quality.* Granada, Spain.

Aghaei, M., Dolara, A., Leva, S., & Grimaccia, F. (2016). Image resolution and defects detection in PV inspection by unmanned technologies. *IEEE Power and Energy Society General Meetin.* Milano, Italy. doi:10.1109/PESGM.2016.7741605

Aghaei, M., Gandelli, F., Grimaccia, S., Leva, S., & Zich, R. (2015). IR real-time analysis for PV system monitoring by digital image processing techniques. *Event-based Control, Communication, and Signal Processing (EBCCSP).* Krakow, Poland: IEEE. doi:10.1109/EBCCSP.2015.7300708

Aircraft principal axes. (n.d.). Retrieved May 21, 2019, from Wikipedia: https://en.wikipedia.org/wiki/Aircraft_principal_axes

Baker, A. (n.d.). *A history of solar cells: how technology has evolved*. Retrieved March 14, 2019, from Solar Power Authority: https://www.solarpowerauthority.com/a-history-of-solar-cells/

Baschel, S., Koubli, E., Roy, J., & Gottschalg, R. (2018). Impact of component reliability on large scale photovoltaic systems' performance. *Energies, 11*(6), p. 1579.

Certificated remote pilots including commercial operators. (n.d.). Retrieved June 19, 2019, from Federal Aviation Administration: https://www.faa.gov/uas/commercial_operators/

Dixon, C. (2018, September). More than just autopilot. *xyHt*, pp. 21-25.

Donev, J., Afework, B., Campbell, A., Hanania, J., Lloyd, E., Stenhouse, K., & Toor, J. (2018). *Electrical Conductivity*. Retrieved June 27, 2019, from Energy Education at Univeristy of Calgary: https://energyeducation.ca/encyclopedia/Electrical_conductivity

Drones reporting for work. (n.d.). Retrieved March 07, 2019, from Goldman Sachs:

https://www.goldmansachs.com/insights/technology-driving-innovation/drones/

Eisenbeiss, H. (2004). A mini unmanned aerial vehicle (UAV): system overview and image acquisition. *International Workshop on Processing and Visualization Using High-Resolution Imagery*. Pitsanulok, Thailand.

Entrop, A., & Vasenev, A. (2017). Infrared drones in the construction industry: designing a protocol for building thermography procedures. *Energy Procedia of the 11th Nordic Symposium on Building Physics*, (pp. 63-68). Trondheim, Norway. doi:10.1016/j.egypro.2017.09.636

Fox, S. (n.d.). *How does heat affect solar panel efficiencies?* Retrieved March 06, 2019, from Civic Solar: https://www.civicsolar.com/support/installer/articles/how-does-heat-affect-solar-panel-efficienceis

Gallardo-Saavedra, S., Hernandez-Callejo, L., & Duque-Perez, O. (2018, May). Technological review of the instrumentation used in aerial thermographic inspection of photovoltaic plants. *Renewable and Sustainable Energy Reviews, 93*, 566-579. doi:10.1016/j.rser.2018.05.027

Galleguillos, C., Zorrilla, A., Jimenez, A., Diaz, L., Montiano, Á. L., Barroso, M., . . . Lasagni, F. (2015, March 24). Thermographic non-destructive inspection of wind turbine blades using unmanned aerial systems. *Plastics, Rubber and Composites, 44*(3), 98-103. doi:10.1179/1743289815Y.0000000003

Global energy and CO2 status report. (n.d.). Retrieved March 14, 2019, from International Energy Agency: https://www.iea.org/geco/

Grimaccia, F., Aghaei, M., Mussetta, M., Leva, S., & Bellezza Quater, P. (2015). Planning for PV plant performance monitoring by means of unmanned aerial systems (UAS). *International Journal Energy Environmental Engineering, 6*(1), 47-54. doi:https://doi.org/10.1007/s40095-014-0149-6

Grimaccia, F., Leva, S., & Niccolai, A. (2017, August). PV plant digital mapping for modules' defects detection by unmanned aerial vehicles. *IET Renewable Power Generation, 11*(10), 1221-1228.

Grimaccia, F., Leva, S., Niccolai, A., & Cantoro, G. (2018). Assessment of PV plant monitoring system by means of unmanned aerial vehicles. *2018 IEEE International Conference on Environment and Electrical Engineering and 2018 IEEE Industrial and Commercial Power Systems Europe.* EEEIC / I&CPS Europe. doi:10.1109/EEEIC.2018.8494532

Gulkowski, S., & Skomorowska, A. (2018). Autonomous photovoltaic observatory station integrated with UAV - a case study. *E3S Web of Conferences, 49*, 00043. doi:10.1051/e3sconf/20184900043

Hammami, M., Torretti, S., Grimaccia, F., & Grandi, G. (2017, October 25). Thermal and performance analysis of photovoltaic module with an integrated energy storage system. *Applied Sciences, 7*(1107). doi:10.3390/app7111107

Infrared radiation. (n.d.). Retrieved June 18, 2019, from Dictionary: https://www.dictionary.com/browse/infrared-radiation

Kaplani, E. (2012, February 07). Detection of degradation effects in field-aged C-Si solar cells through IR thermography and digial image processing. (P. Rupnowski, Ed.) *International Journal of Photoenergy, 2012*.

Kespry. (2018, July 25). *Kespry announces first drone-based high-resolution thermal inspection capabilities for commercial property and industrial facilities*. Retrieved March 25, 2019, from Kespry.com: https://www.kespry.com/meet-the-press/kespry-thermal/

Lesson: The Temperature Effect. (2009). Retrieved June 27, 2019, from Teach Engineering, STEM Curriculum for k-12: https://www.teachengineering.org/lessons/view/cub_pveff_lesson02

Leva, S., Aghaei, M., & Grimaccia, F. (2015). PV power plant inspection by UAS: correlation between altitude and detection of defects on PV modules. *2015 IEEE 15th International Conference on Environment*

and Electrical Engineering (EEEIC). Rome: IEEE. doi:10.1109/EEEIC.2015.7165466

Li, X., Wagner, F., Peng, W., Yang, J., & Mauzerall, D. L. (2017, November 07). Reduction of solar photovoltaic resources due to air pollution in China. (M. G. Morgan, Ed.) *Proceedings of the National Academy of Sciences of the United States of America, 114*(45), 11867-11872.

Luccio, M. (2018, October). After the storm. *xyHt*, pp. 22-25.

McCabe, S. (2018, Fall). Drones and data: charting the course of disaster recovery. *SWE Magazine of the Society of Women Engineers, 64*(4), pp. 46-50.

Molines, N., & Henriot, C. (2017). Aerial thermography as a diagnostic tool for residential building stock energy assessment, within a local energy policy perspective. *3rd Energy for Sustainability International Conference "Designing Cities & Communities for the Future"*. Funchal, Portugal. Retrieved from https://hal.archives-ouvertes.fr/hal-01870247

Power: what are solar panels? (n.d.). Retrieved June 19, 2019, from Qualitative Reasoning Group, Northwestern University: http://www.qrg.northwestern.edu/projects/vss/docs/power/1-what-are-solar-panels.html

Renewables 2018: global status report. (n.d.). Retrieved March 14, 2019, from REN 21: Renewable Energy Policy Network for the 21st Century: www.ren21.net/gsr-2018

Resolution. (n.d.). Retrieved June 18, 2019, from Merriam-Webster Online Dictionary: https://www.merriam-webster.com/dictionary/resolution

Ristic, A., Bugarinovic, Z., Vrtunski, M., Govedarica, M., & Petrovacki, D. (2017). Integration of modern remote sensing technologies for faster utility mapping and data extraction. *Construction and Building Materials*. doi:http://dx.doi.org/10.1016/j.conbuildmat.2017.07.030

Ritchie, H. (2017, August 08). *How long before we run out of fossil fuels?* Retrieved March 07, 2019, from Our World in Data: https://ourworldindata.org/insights/technology-driving-innovation/drones/

Sharma, V., & Chandel, S. (2013). Performance and degradation analysis for long term reliability of solar photovoltaic systems: a review. *Renewable and Sustainable Energy Reviews, 27*, 753-767.

Si, M., Tang, B., & Li, Z. (2018). Estimation of land surface temperature from unmanned aerial vehicle loaded thermal imager data. *IEEE International Geoscience and Remote Sensing Symposium* (pp. 1210-1213). Valencia, Spain: IEEE. doi:10.1109/IGARSS.2018.8518978

The professional mapping drone - senseFly (.pdf). (n.d.). Retrieved March 14, 2019, from Sensefly: https://www.sensefly.com/app/uploads/2018/05/eBee_EN.pdf

Thermography fundamentals. (n.d.). Retrieved June 19, 2019, from Fluke: https://www.fluke.com/en-us/learn/best-practices/measurement-basics/thermography/what-is-infrared-thermography

Thomas, C. (2018, October). Poised to transform industry. *Magazine of the Society of Women Engineers, 64*(4), pp. 40-44.

Trojak, L. (2018, September). Cooperative effort takes off. *xyHt*, pp. 35-39.

Tsanakas, J., Chrysostomou, D., Botsaris, P., & Gasteratos, A. (2013). Fault diagnosis of photovoltaic modules through image processing and canny edge detection on field thermographic measurements. *International Journal of Sustainable Energy, 34*(6), 351-372. doi:http://dx.doi.org/10.1080/14786451.2013.826223

Tsanakas, J., Ha, L., & Buerhop, C. (2016, September). Faults and infrared thermographic diagnosis in operating c-Si photovoltaic modules: a review of research and future challenges. *Renewable and Sustainable Energy Reviews, 62*, 695-709. doi:10.1016/j.rser.2016.04.079

Tsanakas, J., Vannier, G., Plissonnier, A., Ha, D. L., & Barruel, F. (2015). *Fault diagnosis and classification of large-scale photovoltaic plants through aerial orthophoto thermal mapping.* WIP.

Unmanned aerial vehicle. (n.d.). Retrieved June 19, 2019, from Wikipedia: https://en.wikipedia.org/wiki/Unmanned_aerial_vehicle

Vodermayer, C., Mayer, M., Mayer, M., Muller, T., Niess, M., Wotruba, G., . . . Schumacher, J. (2008, January). First results - correlation between IR images and electrical behavior and energy yield of PV modules. Retrieved from https://www.researchgate.net/publication/229005381

Waco, D. (n.d.). *How long do solar panels last*. Retrieved March 07, 2019, from Civic Solar: https://www.civicsolar.com/support/installer/articles/how-long-do-solar-panels-last

What is the Kyoto protocol? (n.d.). Retrieved April 29, 2019, from United Nations Climate Change: https://unfccc.int/process-and-meetings/the-kyoto-protocol/what-is-the-kyoto-protocol/what-is-the-kyoto-protocol

Yahyanejad, S., Misiorny, J., & Rinner, B. (2011). Lens distortion correction for thermal cameras to improve aerial imaging with small-scale UAVs. *IEEE International Symposium on Robotic and Sensors Environments (ROSE).* Montreal, QC, Canada: IEEE. doi:10.1109/ROSE.2011.6058528

Zaoui, F., Titaouine, A., Becherif, M., Emziane, M., & Aboubou, A. (2015). A combined experimental and simulation study on the effects of irradiance and temperature on photovoltaic modules. *Energy Procedia, 75*, 373-380. doi:10.1016/j.egypro.2015.07.393

Zhang, J., Jung, J., Sohn, G., & Cohen, M. (2015). Thermal infrared inspection of roof insulation using unmanned aerial vehicles. *International Conference on Unmanned Aerial Vehicles in Geomatics, XL-1/W4*. Toronto, Canada.

APPENDIX A: CFU SOLAR GARDEN

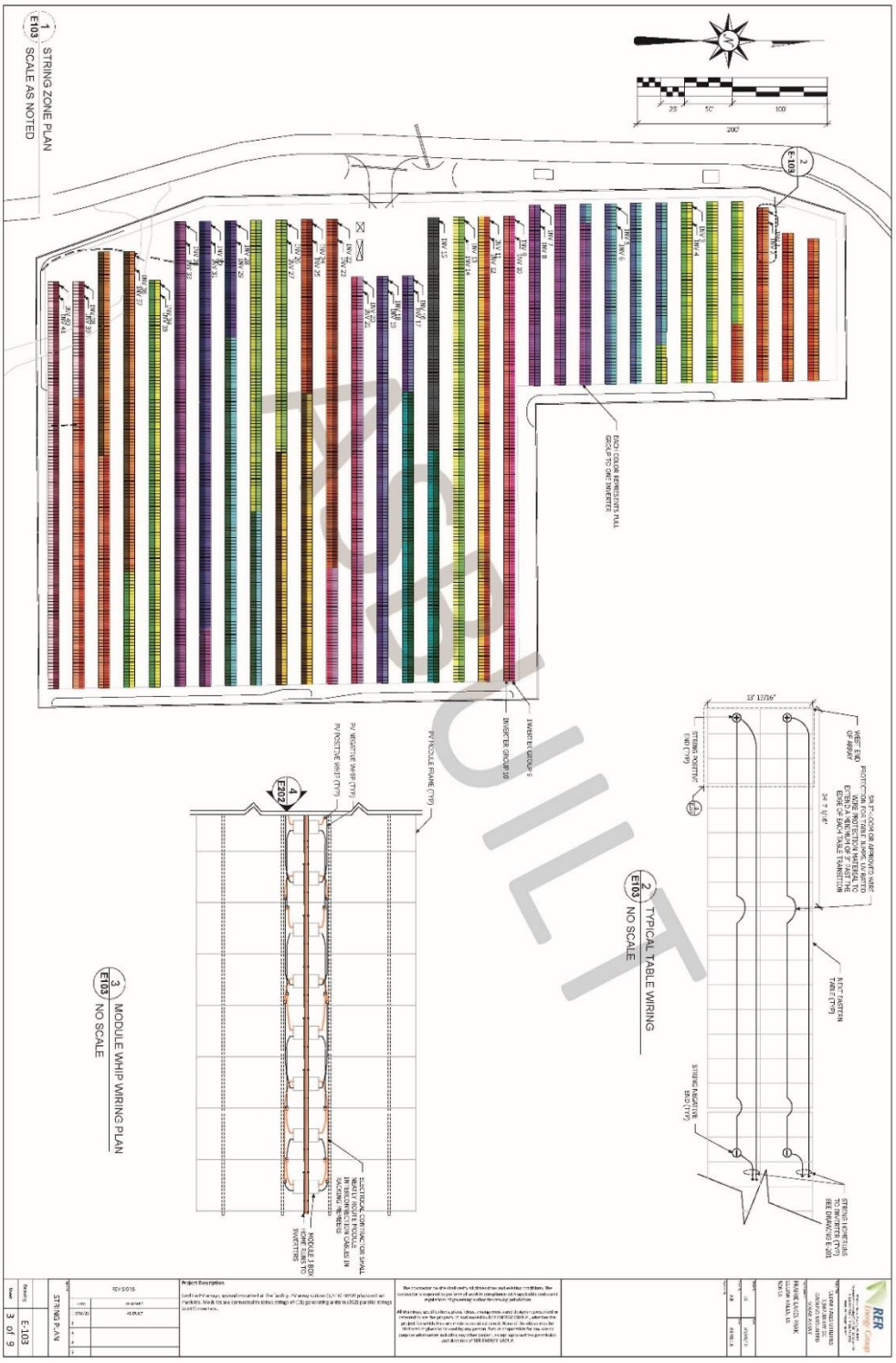

Figure 19. CFU solar garden as-built inverter map

Table 3. 2018 October 17 CFU solar garden & weather data

(Solar Garden Total kWatts) - Average Values	Time	OUTSIDE TEMP DEG F - Average Values	WIND SPEED MPH - Average Values	SOLAR RADIATION W/m^2 - Average Values	OUTSIDE HUMIDITY % - Average Values	WIND DIRECTION - Average Values
1504.56	1:15:00 PM	46.31	3.12	594.00	52.23	256.25
1504.25	1:16:00 PM	46.44	7.23	594.00	53.55	306.67
1503.99	1:17:00 PM	46.61	9.87	594.00	53.00	328.77
1504.64	1:18:00 PM	46.70	6.73	594.00	51.63	298.28
1504.57	1:19:00 PM	46.70	8.27	594.00	50.30	327.73
1504.75	1:20:00 PM	46.63	11.65	592.60	49.97	342.70
1504.18	1:21:00 PM	46.46	8.65	592.00	49.00	322.33
1504.57	1:22:00 PM	46.37	8.93	591.32	49.35	224.85
1504.61	1:23:00 PM	46.30	7.57	591.00	50.00	244.03
1504.21	1:24:00 PM	46.30	4.18	590.43	50.00	320.47
1504.19	1:25:00 PM	46.31	5.50	587.00	50.93	339.08
1504.53	1:26:00 PM	46.45	4.42	585.93	52.10	252.88
1504.75	1:27:00 PM	46.57	7.45	585.60	52.20	330.05
1504.07	1:28:00 PM	46.70	7.83	585.00	51.37	330.23
1504.10	1:29:00 PM	46.70	8.10	585.13	52.00	312.00
1504.47	1:30:00 PM	46.70	9.62	586.23	51.28	244.85
1504.11	1:31:00 PM	46.70	8.60	585.00	51.00	321.80
1504.25	1:32:00 PM	46.70	9.08	584.20	51.00	335.78
1503.62	1:33:00 PM	46.77	8.63	583.93	50.68	331.25
1503.03	1:34:00 PM	46.80	10.23	582.00	49.53	337.38
1502.53	1:35:00 PM	46.80	11.37	582.00	49.68	319.20
1503.01	1:36:00 PM	46.80	12.53	582.00	50.00	237.07
1503.57	1:37:00 PM	46.73	7.20	581.00	49.37	170.85
1503.19	1:38:00 PM	46.70	8.85	578.60	50.00	9.95
1502.55	1:39:00 PM	46.70	7.38	577.35	50.00	228.17
1503.11	1:40:00 PM	46.80	10.33	578.00	50.00	317.37
1503.25	1:41:00 PM	46.80	6.65	577.62	50.00	247.60
1503.96	1:42:00 PM	46.80	9.10	576.30	50.00	340.77
1503.18	1:43:00 PM	46.81	4.10	575.00	50.12	202.20
1503.12	1:44:00 PM	46.91	10.03	575.00	50.92	329.72
1502.93	1:45:00 PM	47.00	9.57	573.60	49.67	323.55

Table 4. 2018 October 17 CFU solar garden raw inverter data

Prairie Lakes Solar Garden 5 minute snap shots of Solectria Inverter Output AC Power (avg) kW for 10/17/2018																																									
		Inverter #																																									
	sum (kW)	1	2	3	4	5	6	7	8	9	10	11	12	13	14	15	16	17	18	19	20	21	22	23	24	25	26	27	28	29	30	31	32	33	34	35	36	37	38	39	40	41
1:15:00 PM	1515.2	37.3	37.2	36.5	37.3	37.2	36.8	37.4	37.1	36.3	37.1	36.7	37	36.6	36.8	37.2	37	36.9	36.8	36.9	36.9	36.9	36.5	36.7	37.3	36.8	37.3	36.7	37	37.1	36.7	36.9	36.8	37.1	36.6	37.1	37.2	36.9	37.2	37	37.2	37.2
1:20:00 PM	1515.5	37.3	37.2	36.6	37.3	37.2	36.9	37.4	37	36.3	37.2	36.7	36.3	36.6	37	37.1	37.1	36.9	36.8	36.8	37	36.9	36.5	36.6	37.2	36.8	37.4	36.8	37	37.1	36.8	36.9	36.9	37.2	36.7	37.1	37.2	36.9	37.3	37.1	37.2	37.2
1:25:00 PM	1515.6	37.3	37.1	36.7	37.3	37.2	36.9	37.4	37	36.1	37	36.6	36.9	36.5	37.1	37	37.1	36.9	36.8	36.9	37	36.8	36.5	36.7	37.3	36.8	37.5	36.8	37.1	37.1	36.8	36.8	36.9	37.2	36.7	37.1	37.2	36.8	37.2	37.1	37.2	37.2
1:30:00 PM	1515.8	37.3	37.1	36.6	37.3	37.2	36.9	37.5	37.1	36.2	37.1	36.6	36.6	36.5	37	37.1	37.1	37	36.8	36.9	36.9	36.9	36.5	36.7	37.3	36.9	37.5	36.9	37	37.1	36.8	36.8	36.9	37.1	36.7	37.1	37.2	36.8	37.3	37	37.3	37.2
1:35:00 PM	1514.7	37.3	37.2	36.6	37.3	37.3	36.8	37.4	37.1	36	36.9	36.4	36.9	36.3	36.9	36.8	37	37	36.8	36.9	36.9	36.9	36.5	36.7	37.3	36.9	37.5	36.7	37	37.1	36.8	36.9	36.9	37.1	36.8	37	37.2	36.8	37.3	37.1	37.2	37.2
1:40:00 PM	1514.3	37.3	37.2	36.7	37.3	37.2	36.9	37.4	37.1	35.9	36.8	36.3	36.8	36.2	36.8	36.8	37	37	36.9	36.9	37	36.9	36.5	36.7	37.3	36.8	37.5	36.9	37	37.1	36.8	36.9	36.9	37.2	36.6	37	37.2	36.8	37.3	37	37.2	37.2
1:45:00 PM	1513.8	37.3	37.2	36.7	37.4	37.2	36.9	37.4	37.1	35.9	36.8	36.3	36.8	36.2	36.8	36.8	37	37	36.8	36.9	37	36.8	36.5	36.7	37.2	36.8	37.5	36.7	37	37	36.8	36.8	36.9	37.1	36.7	37	37.2	36.8	37.3	37	37.3	37.2

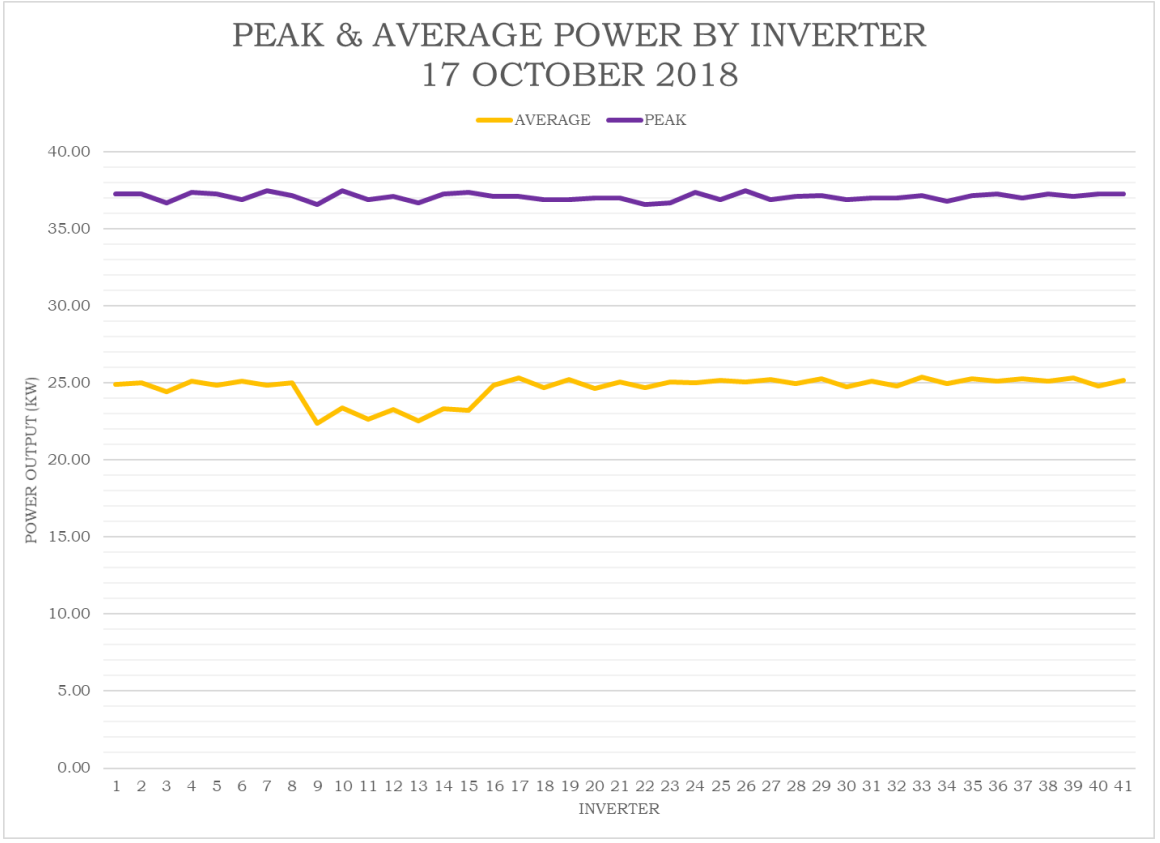

Figure 20. 2018 October 17 peak & average power

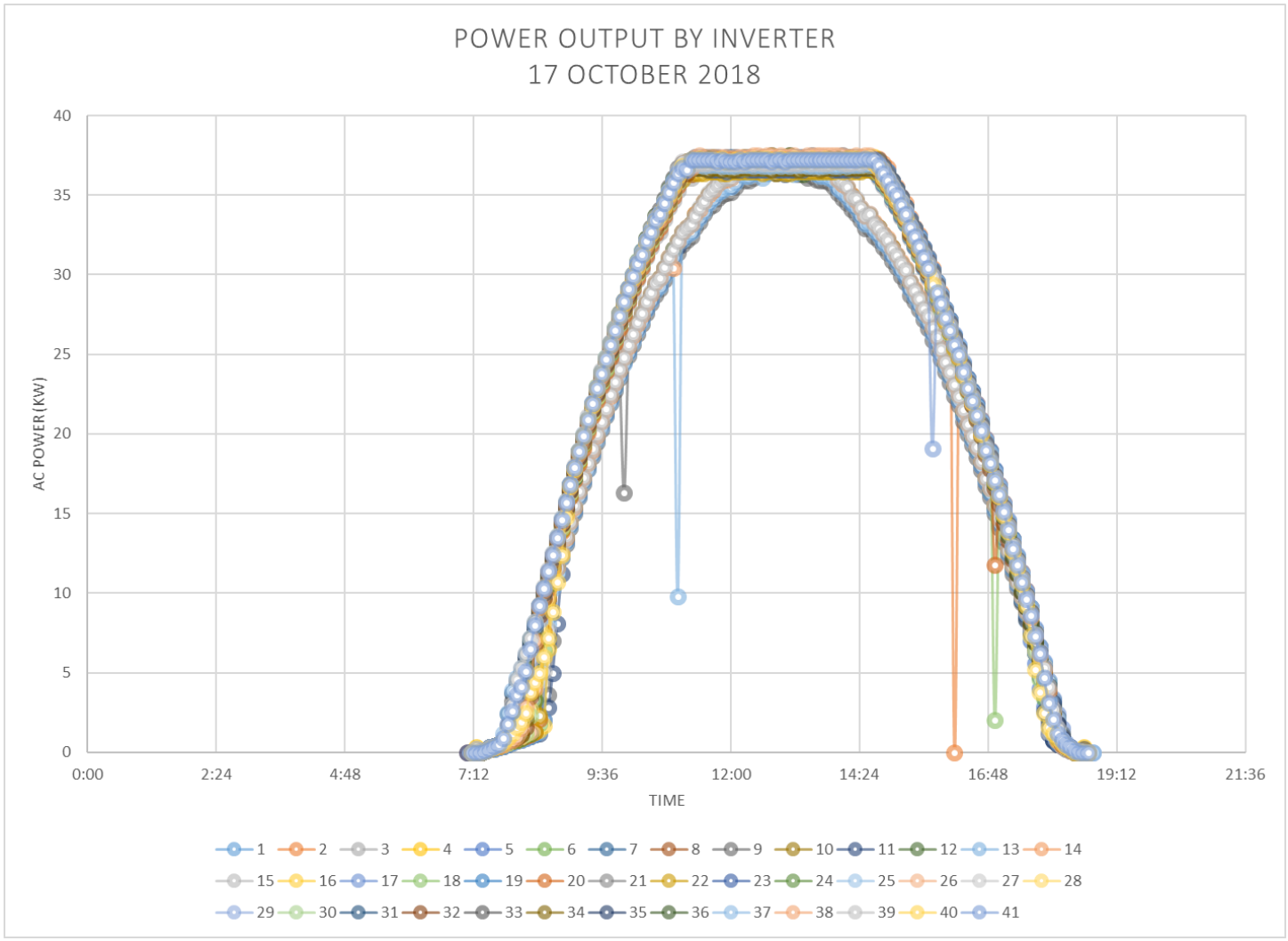

Figure 21. 2018 October 17 power by inverter – full day

Table 5. 2019 April 24 CFU solar garden & weather data

Solar Garden Total kWatts - Average Values	Time	OUTSIDE TEMP DEG F - Average Values	WIND SPEED MPH - Average Values	SOLAR RADIATION W/m^2 - Average Values	OUTSIDE HUMIDITY % - Average Values	WIND DIRECTION - Average Values
755.26	1:40:00 PM	59.10	10.07	436.60	74.73	165.13
696.95	1:41:00 PM	59.15	9.88	450.38	74.00	178.78
678.94	1:42:00 PM	59.12	9.18	434.50	74.00	169.33
728.84	1:43:00 PM	59.10	11.63	444.00	74.00	155.53
579.60	1:44:00 PM	59.10	9.60	447.00	74.00	172.33
682.21	1:45:00 PM	59.17	10.75	400.63	74.70	174.57
1028.70	1:46:00 PM	59.20	7.73	362.00	74.53	185.95
889.05	1:47:00 PM	59.20	6.93	367.70	74.00	173.62
839.00	1:48:00 PM	59.22	7.83	386.17	74.00	180.17
949.53	1:49:00 PM	59.27	10.95	467.67	74.00	190.73
1133.84	1:50:00 PM	59.27	10.55	512.68	73.00	184.97

Table 6. 2019 April 24 CFU solar garden raw inverter data

Prairie Lakes Solar Garden 5 minute snap shots of Solectria Inverter Output AC Power (avg) kW for 4/24/2019																																										
		Inverter #																																									
	sum (kW)	1	2	3	4	5	6	7	8	9	10	11	12	13	14	15	16	17	18	19	20	21	22	23	24	25	26	27	28	29	30	31	32	33	34	35	36	37	38	39	40	41
1:40:00 PM	770.4	20.1	20.5	20.4	21	20.3	20.7	19.5	19.7	16.8	17.5	16.8	17.3	16.6	17.1	17.1	18.9	19.4	18.8	19.3	16.5	19.4	18.9	19.3	18.9	19.3	18.8	19.2	18.9	19.2	18.5	18.9	18.6	19.1	18.6	18.9	18.4	18.7	18.4	18.8	18.6	18.7
1:45:00 PM	1014.7	23.2	23.7	23.1	23.8	23.6	24.1	23.9	24.2	24.2	25	25.1	25.9	24.6	25.3	22.4	26.3	26.8	24.9	25.4	21.7	25.5	25.3	25.8	26.3	26.8	24.7	25.1	25.1	25.5	24.4	24.8	24.6	25.2	24.6	24.8	24.6	24.9	24.5	24.9	25	25.1
1:50:00 PM	1056.3	26	26.4	25.5	26.1	25.3	25.7	24.8	24.9	21.9	22.6	22.1	22.6	22	22.5	22.3	25.8	26.2	25.5	25.9	22.8	26.7	25	25.4	25.8	26.2	25.2	25.4	26.4	26.7	25.4	25.7	26.3	26.8	27.3	27.4	25.8	26.1	32	33.1	30.4	30.3
1:55:00 PM	654.8	16.6	16.9	16.3	16.9	16.4	16.8	16.2	16.5	14.2	14.8	14.3	14.7	14.1	14.6	14.6	16.1	16.6	16.1	16.5	14.1	16.7	16.1	16.5	16.1	16.5	16.1	16.5	16.2	16.5	16	16.3	16.1	16.5	16.1	16.3	16	16.2	16	16.3	16.2	16.3

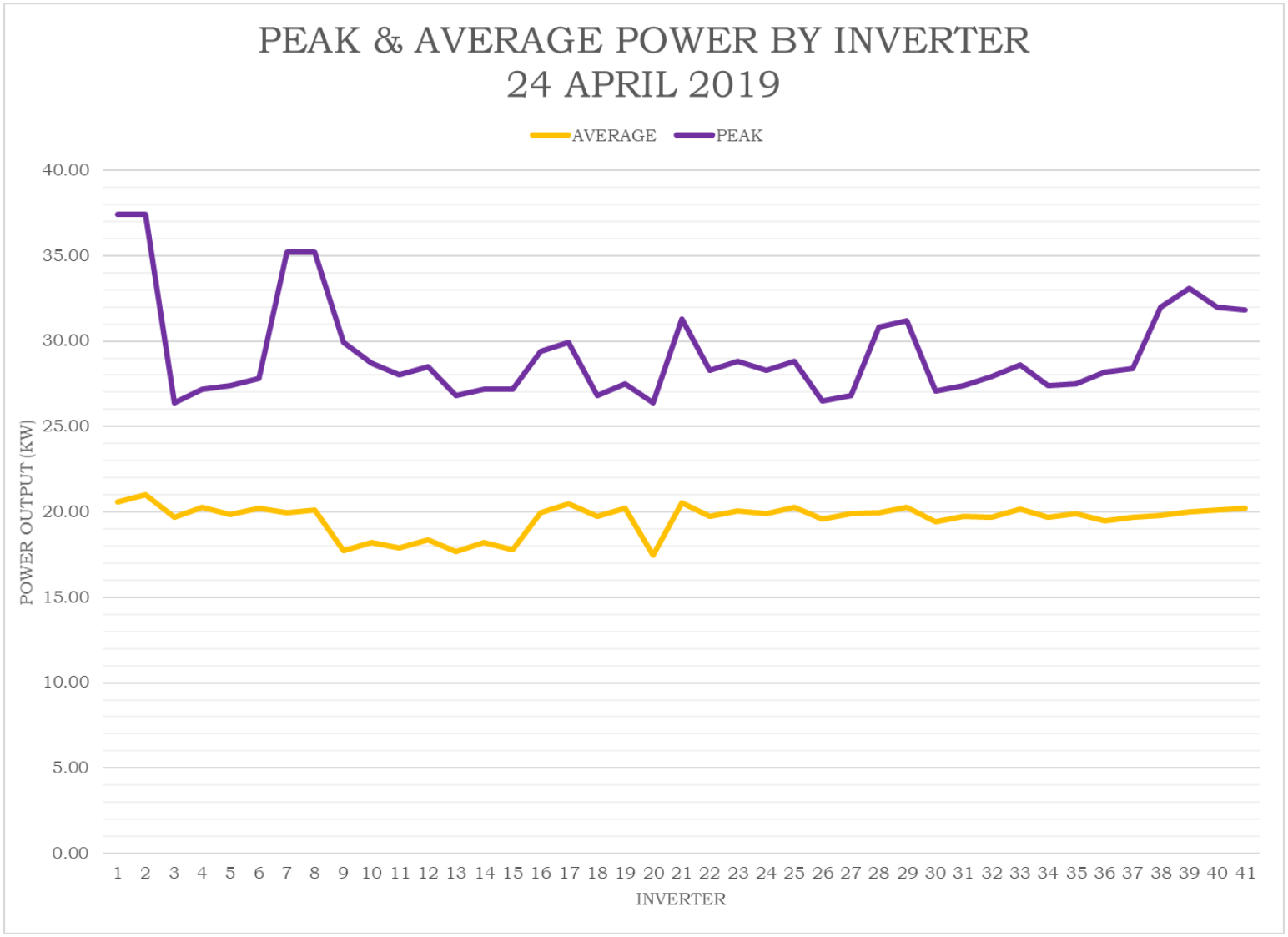

Figure 22. 2019 April 24 peak & average power

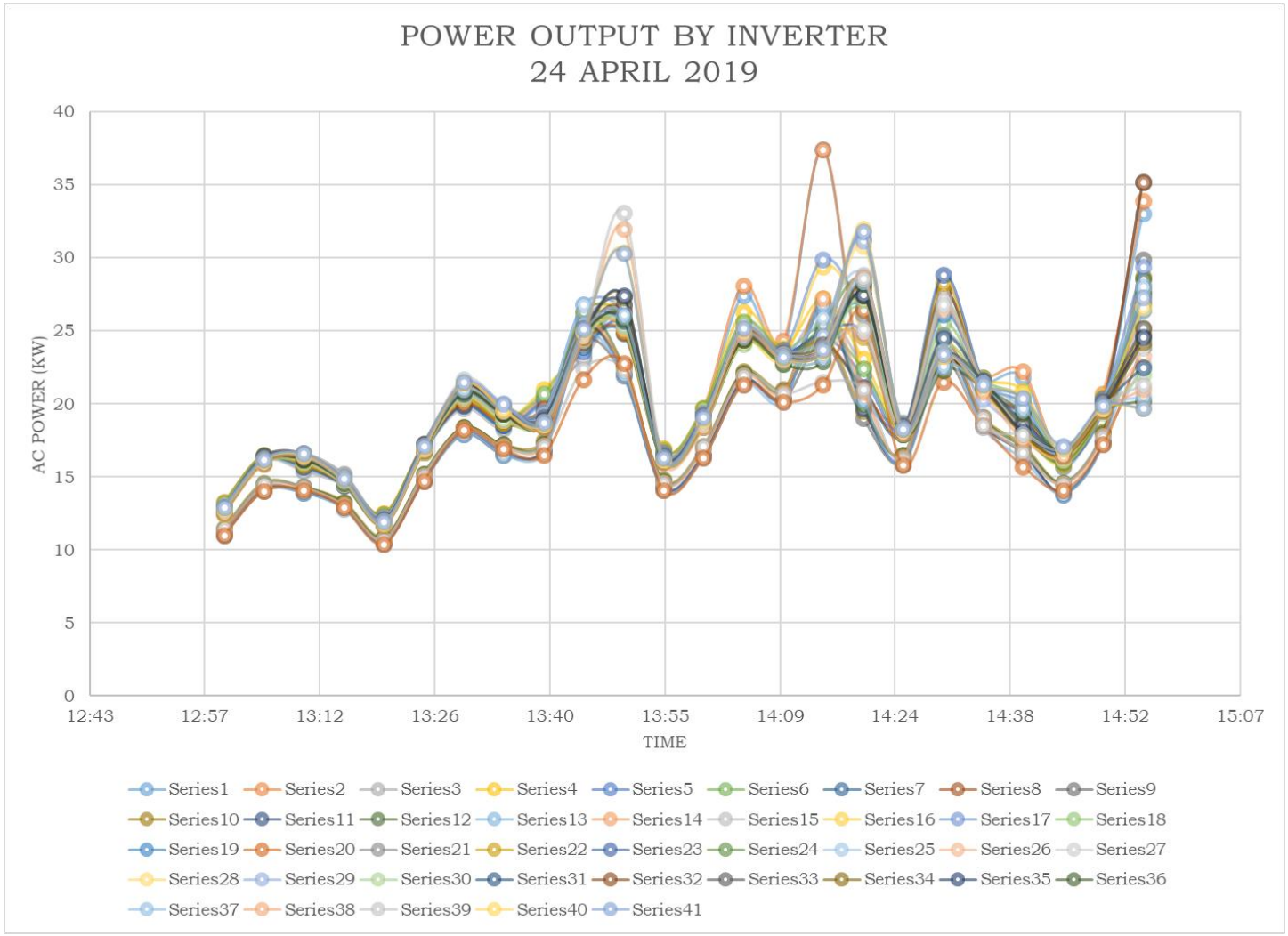

Figure 23. 2019 April 24 power by inverter – partial day

Table 7. 2019 May 10 CFU solar garden & weather data

Solar Garden Total kWatts - Average Values	Time	OUTSIDE TEMP DEG F - Average Values	WIND SPEED MPH - Average Values	SOLAR RADIATION W/m^2 - Average Values	OUTSIDE HUMIDITY % - Average Values	WIND DIRECTION - Average Values
639.07	1:25:00 PM	58.81	5.72	1054.00	44.92	323.60
647.81	1:26:00 PM	58.77	4.95	1048.85	44.95	287.90
1096.90	1:27:00 PM	58.77	8.37	1071.60	43.43	319.33
692.87	1:28:00 PM	58.70	12.73	1109.00	43.73	335.78
1445.47	1:29:00 PM	58.53	9.67	712.50	43.73	340.28
1504.97	1:30:00 PM	58.45	7.57	316.00	44.00	325.33
1324.82	1:31:00 PM	58.31	11.28	618.50	43.07	188.87
1231.10	1:32:00 PM	58.30	10.42	1024.58	43.00	301.75
1404.03	1:33:00 PM	58.30	10.12	1021.30	43.57	322.20
1274.81	1:34:00 PM	58.31	6.80	1033.83	44.30	337.93
1506.67	1:35:00 PM	58.45	2.92	1047.38	46.35	330.90

Table 8. 2019 May 10 CFU solar garden raw inverter data

Prairie Lakes Solar Garden 5 minute snap shots of Solectria Inverter Output AC Power (avg) kW for 5/10/2019

		Inverter #																			
	sum (kW)	1	2	3	4	5	6	7	8	9	10	11	12	13	14	15	16	17	18	19	20
1:20:00 PM	1521.00	37.30	37.30	36.70	37.30	37.30	36.90	37.50	37.20	37.10	37.70	37.10	37.20	36.90	37.30	37.40	36.60	37.00	36.80	36.90	37.00
1:25:00 PM	607.60	16.20	16.90	16.10	17.00	16.00	16.90	15.40	16.00	13.00	13.80	13.10	13.70	13.00	13.70	13.80	14.50	15.20	14.80	15.50	12.90
1:30:00 PM	1517.50	37.30	37.20	36.60	37.20	37.20	36.90	37.30	37.10	37.00	37.50	36.90	37.00	36.80	37.30	37.30	37.00	36.80	36.70	36.80	36.90
1:35:00 PM	1519.80	37.30	37.30	36.60	37.40	37.30	36.80	37.30	37.10	37.00	37.60	37.00	37.10	36.90	37.20	37.40	37.10	37.00	36.80	36.80	37.00
1:40:00 PM	1517.70	37.30	37.30	36.50	37.20	37.20	36.80	37.40	37.10	37.00	37.50	37.00	37.00	36.80	37.30	37.30	37.00	36.80	36.80	36.80	37.00

	21	22	23	24	25	26	27	28	29	30	31	32	33	34	35	36	37	38	39	40	41
1:20:00 PM	37.40	36.60	36.90	37.30	36.90	37.40	36.90	37.10	37.20	36.80	37.00	36.90	37.10	36.70	37.20	37.20	37.00	37.40	37.00	37.30	37.20
1:25:00 PM	15.40	14.50	15.20	14.20	14.90	14.60	15.30	14.30	14.90	14.40	15.10	14.40	15.10	14.40	14.80	14.60	15.10	14.40	14.90	14.60	15.00
1:30:00 PM	37.20	36.50	36.90	37.20	36.80	37.30	36.80	37.00	37.20	36.70	36.90	36.90	37.10	36.60	37.00	37.10	36.80	37.30	37.00	37.20	37.20
1:35:00 PM	37.20	36.50	36.90	37.30	36.80	37.40	36.90	37.10	37.10	36.90	36.90	36.90	37.20	36.70	37.10	37.20	36.90	37.20	37.10	37.30	37.20
1:40:00 PM	37.30	36.40	37.00	37.20	36.80	37.50	36.80	37.00	37.00	36.80	36.80	36.90	37.10	36.60	37.00	37.10	36.90	37.20	36.90	37.20	37.10

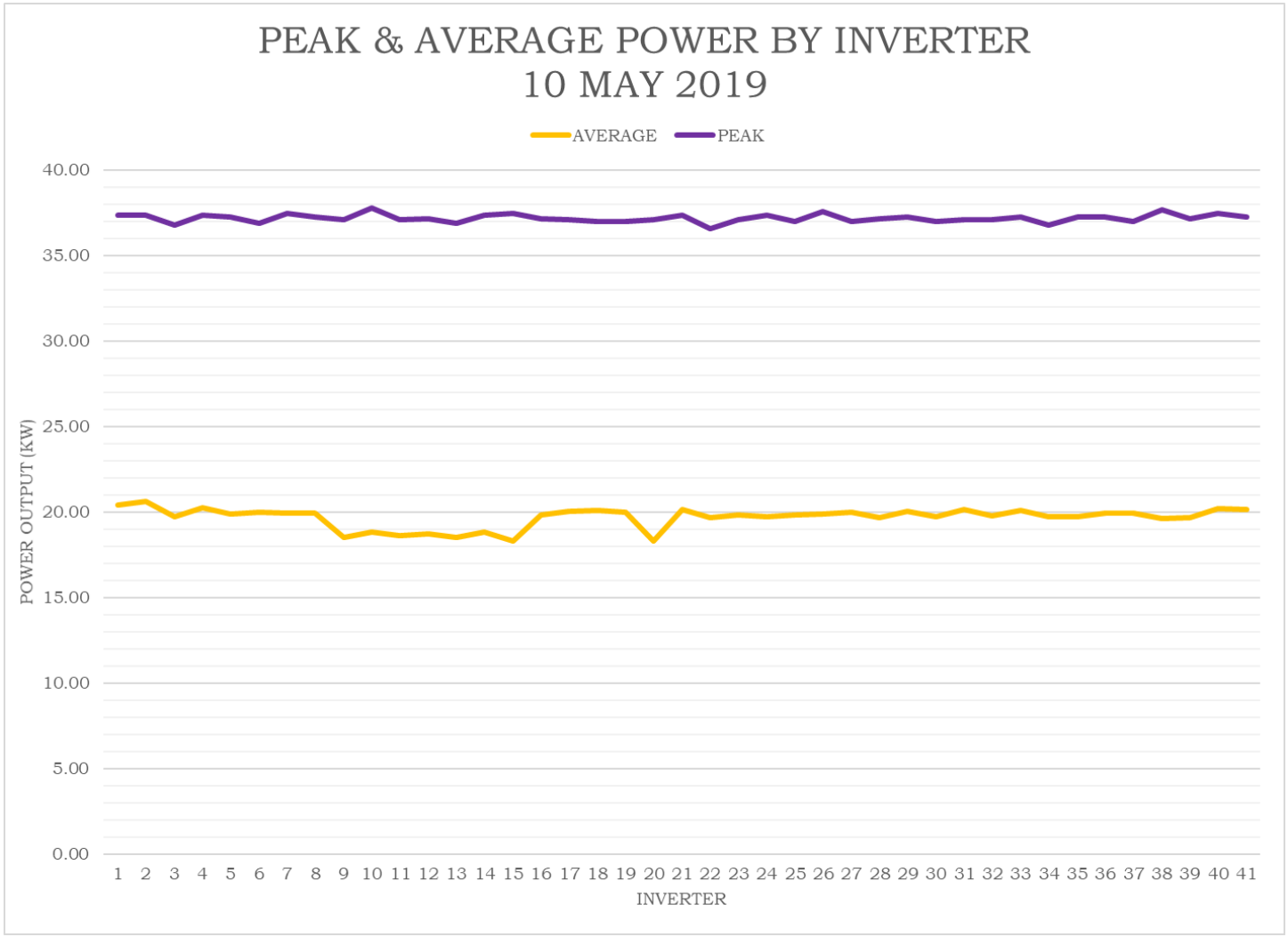

Figure 24. 2019 May 10 peak & average power

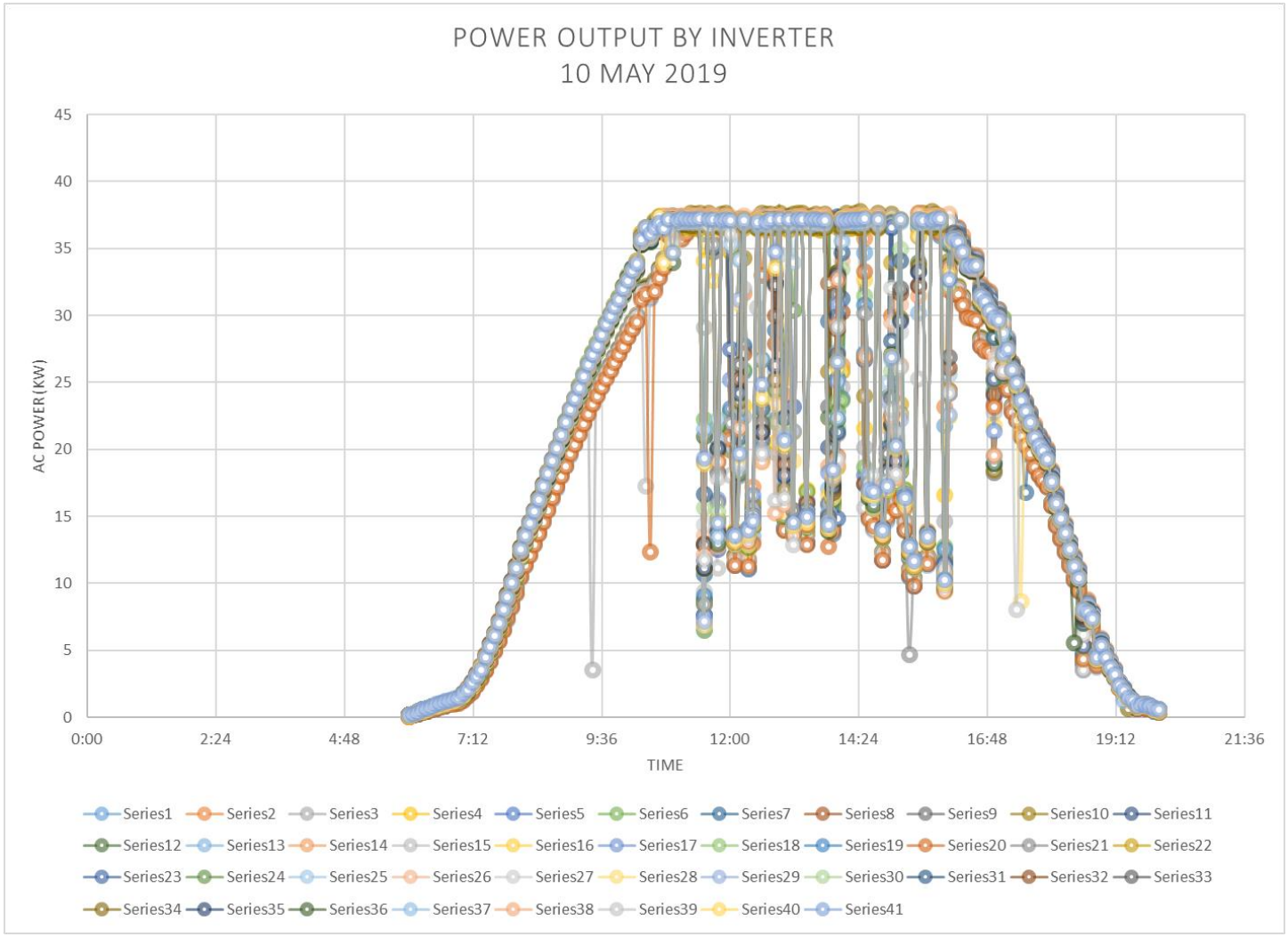

Figure 25. 2019 May 10 power by inverter – full day

APPENDIX B: VISUAL FLIGHT DATA

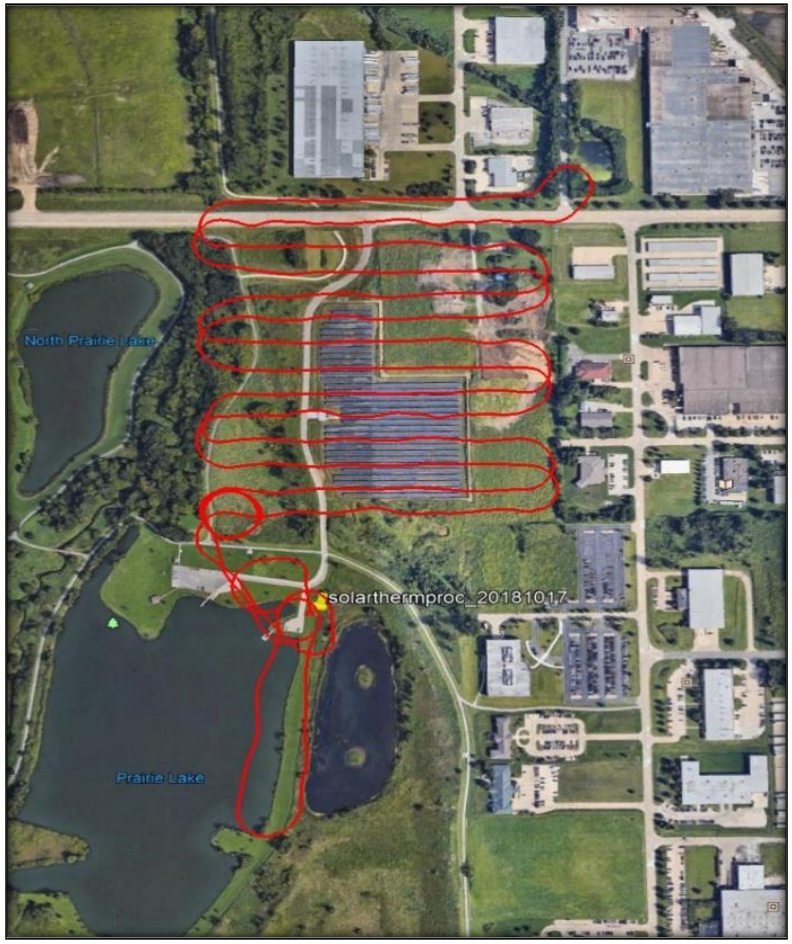

Figure 26. Flight path on 2018 October 17

Figure 27. Flight path photo locations on 2018 October 17

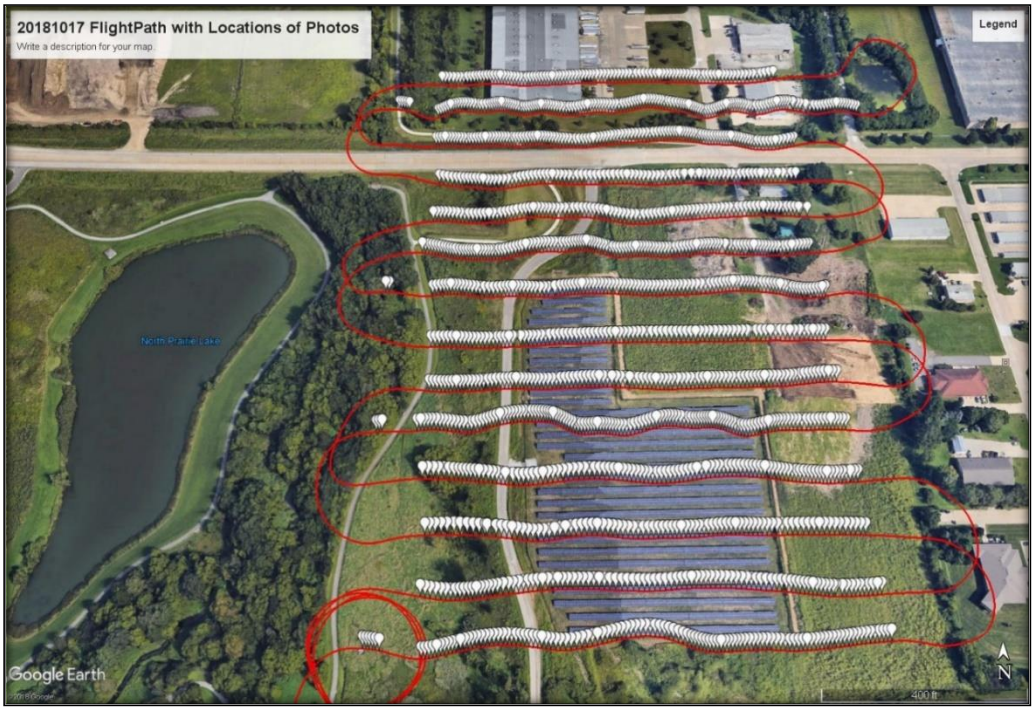

Figure 28. A different perspective of the 2018 Oct 17 flight path with photo locations

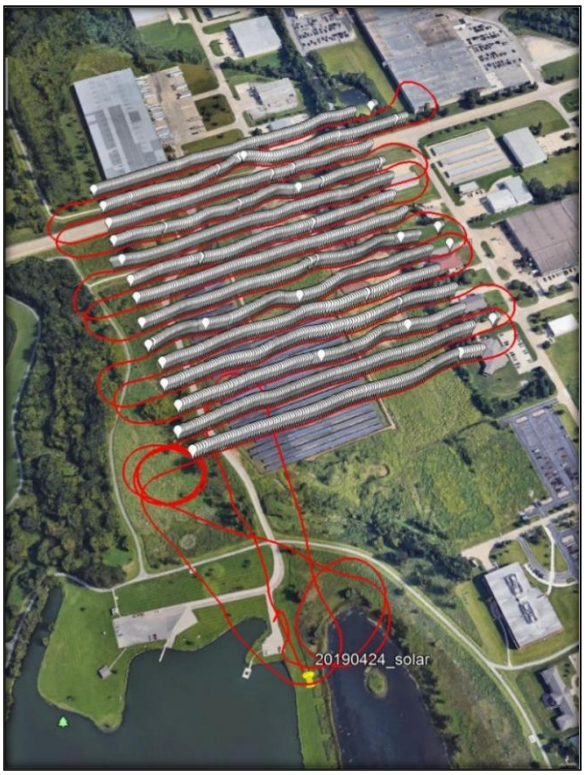

Figure 29. Flight path & photo locations for 2019 April 24

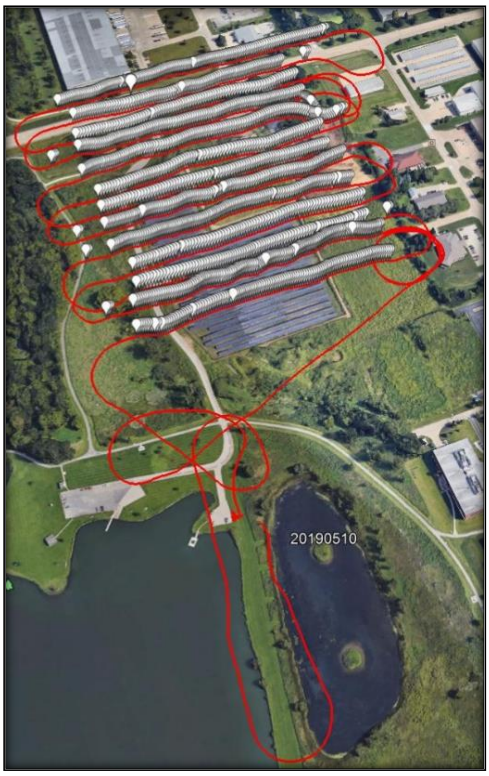

Figure 30. Flight path & photo locations for 2019 May 10

APPENDIX C: Pix4D ANALYSIS & REPORTS

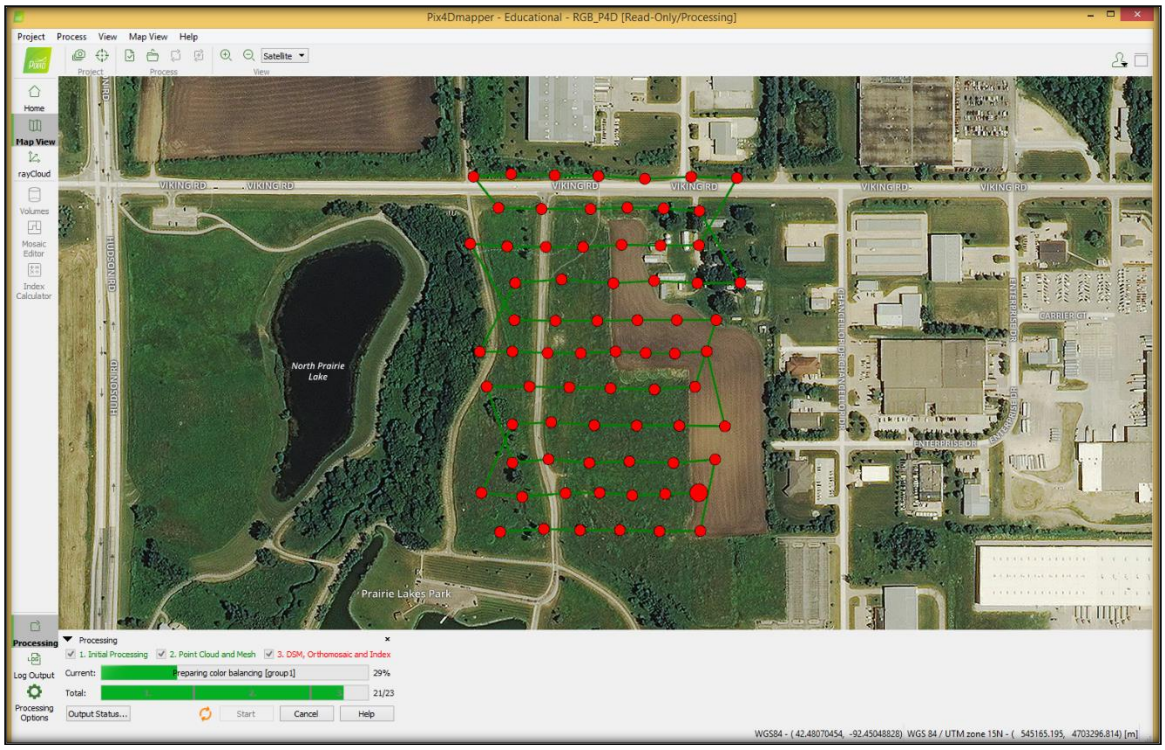

Figure 31. Pix4D screen shot during processing

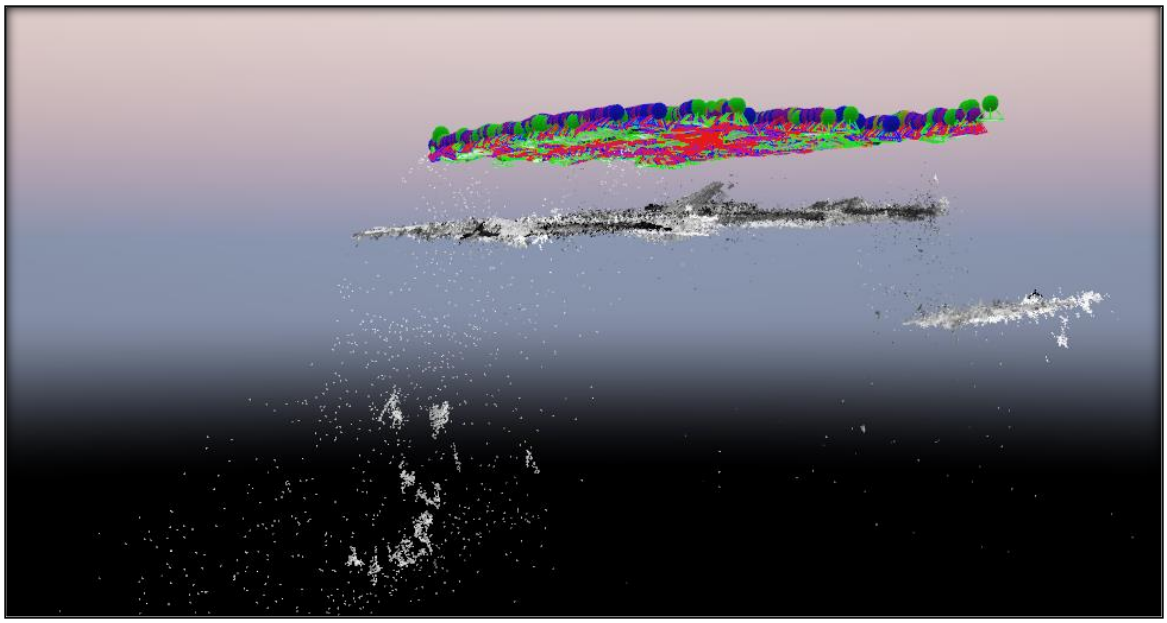

Figure 32. Pix4D outlier images for 2018 November 18

Figure 33. October Pix4D report

Quality Report

Generated with Pix4Dmapper Pro version 4.2.27

Important: Click on the different icons for:

Help to analyze the results in the Quality Report

Additional information about the sections

Click here for additional tips to analyze the Quality Report

Summary

Project	SolarTherm_20181017_P4D
Processed	2018-10-23 13:43:36
Camera Model Name(s)	thermoMAP_9.0_640x512 (Thermal IR)
Average Ground Sampling Distance (GSD)	16.51 cm / 6.50 in
Area Covered	0.183 km^2 / 18.3124 ha / 0.07 sq. mi. / 45.2744 acres
Time for Initial Processing (without report)	38m:19s

Quality Check

Images	median of 7345 keypoints per image	⚠
Dataset	462 out of 463 images calibrated (99%), 1021 images disabled	✓
Camera Optimization	0.24% relative difference between initial and optimized internal camera parameters	✓
Matching	median of 3024.12 matches per calibrated image	✓
Georeferencing	yes, no 3D GCP	⚠

Preview

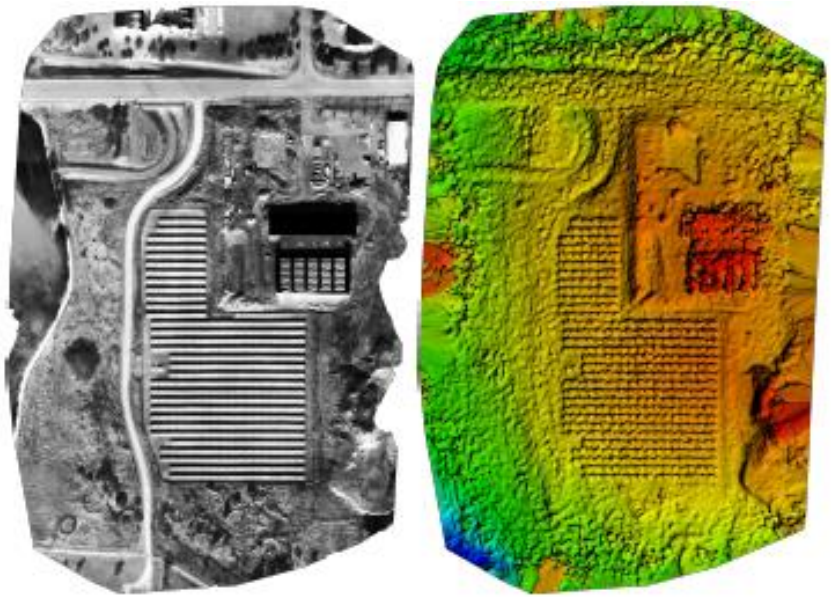

Figure 1: Orthomosaic and the corresponding sparse Digital Surface Model (DSM) before densification.

Calibration Details

Number of Calibrated Images	462 out of 1484
Number of Geolocated Images	1484 out of 1484

Initial Image Positions

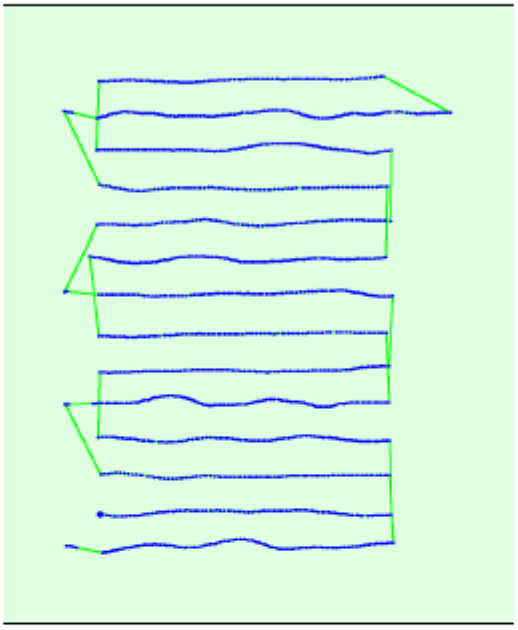

Figure 2: Top view of the initial image position. The green line follows the position of the images in time starting from the large blue dot.

Computed Image/GCPs/Manual Tie Points Positions

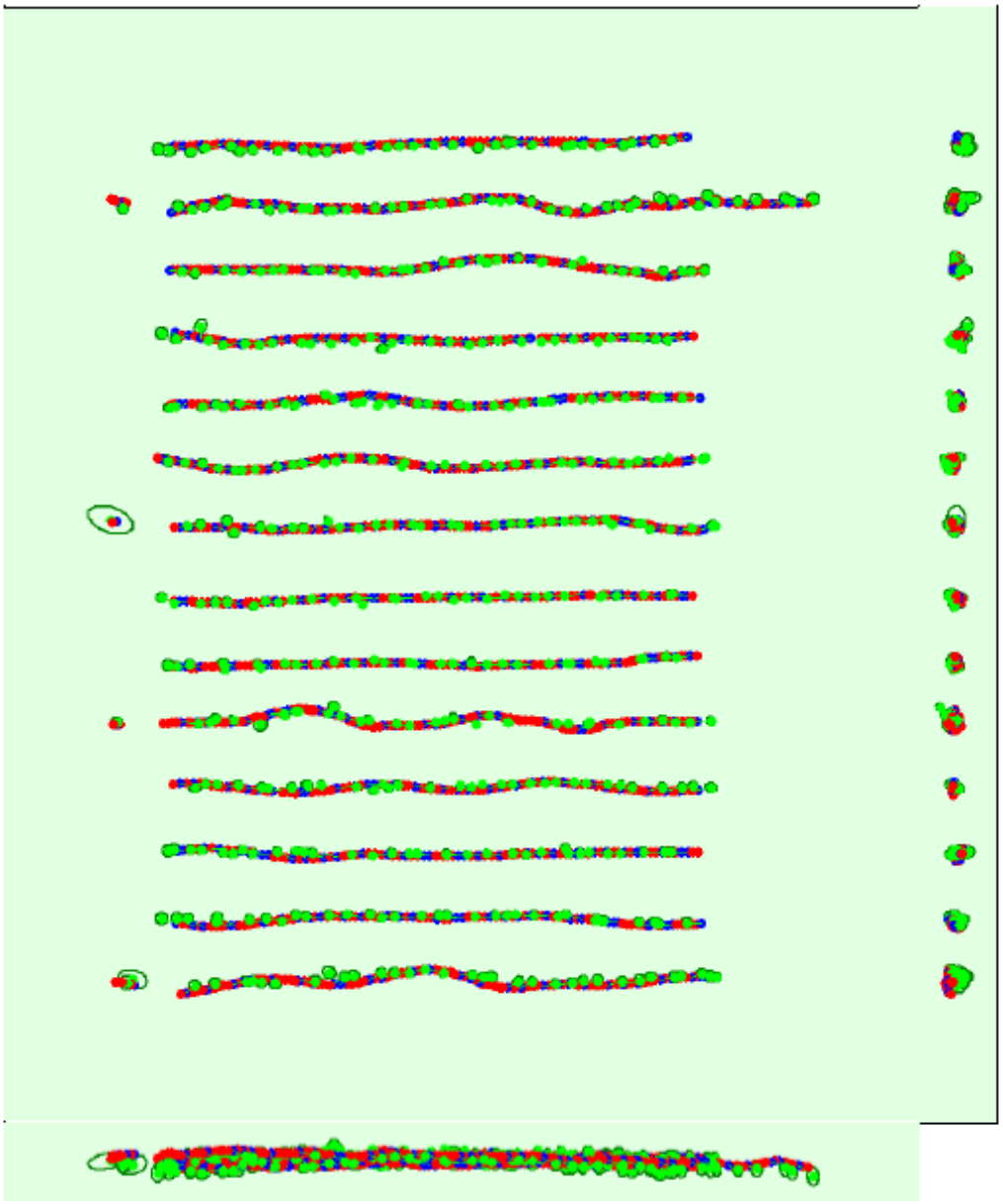

Uncertainty ellipses 10x magnified

Figure 3: Offset between initial (blue dots) and computed (green dots) image positions as well as the offset between the GCPs initial positions (blue crosses) and their computed positions (green crosses) in the top-view (XY plane), front-view (XZ plane), and side-view (YZ plane). Red dots indicate disabled or uncalibrated images. Dark green ellipses indicate the absolute position uncertainty of the bundle block adjustment result.

Absolute camera position and orientation uncertainties

	X [m]	Y [m]	Z [m]	Omega [degree]	Phi [degree]	Kappa [degree]
Mean	0.213	0.202	0.248	0.128	0.135	0.059
Sigma	0.057	0.041	0.055	0.022	0.033	0.011

Overlap

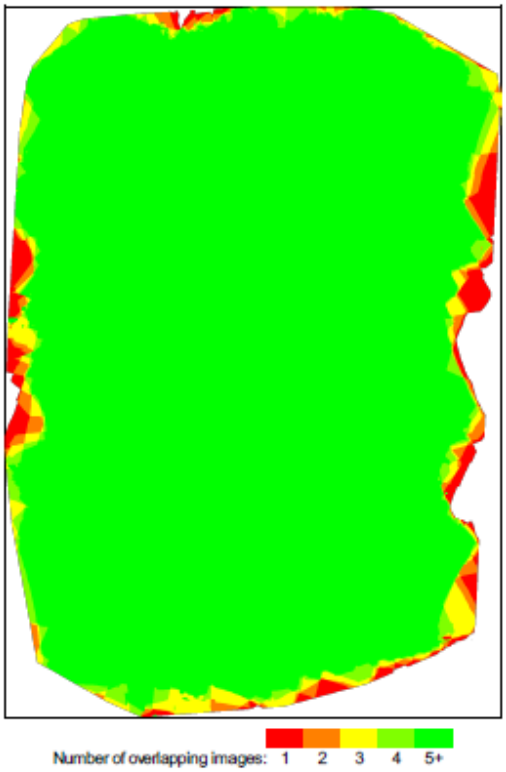

Figure 4: Number of overlapping images computed for each pixel of the orthomosaic.
Red and yellow areas indicate low overlap for which poor results may be generated. Green areas indicate an overlap of over 5 images for every pixel. Good quality results will be generated as long as the number of keypoint matches is also sufficient for these areas (see Figure 5 for keypoint matches).

Bundle Block Adjustment Details

Number of 2D Keypoint Observations for Bundle Block Adjustment	1401884
Number of 3D Points for Bundle Block Adjustment	326000
Mean Reprojection Error [pixels]	0.697

Internal Camera Parameters

thermoMAP_9.0_640x512 (Thermal IR). Sensor Dimensions: 10.880 [mm] x 8.704 [mm]

EXIF ID: thermoMAP_9.0_640x512

	Focal Length	Principal Point x	Principal Point y	R1	R2	R3	T1	T2
Initial Values	558.824 [pixel] 9.500 [mm]	320.000 [pixel] 5.440 [mm]	256.000 [pixel] 4.352 [mm]	-0.294	0.104	-0.019	0.000	0.000
Optimized Values	560.169 [pixel] 9.523 [mm]	318.010 [pixel] 5.406 [mm]	247.383 [pixel] 4.206 [mm]	-0.303	0.099	-0.008	0.003	-0.001
Uncertainties (Sigma)	0.504 [pixel] 0.009 [mm]	0.183 [pixel] 0.003 [mm]	0.218 [pixel] 0.004 [mm]	0.001	0.005	0.005	0.000	0.000

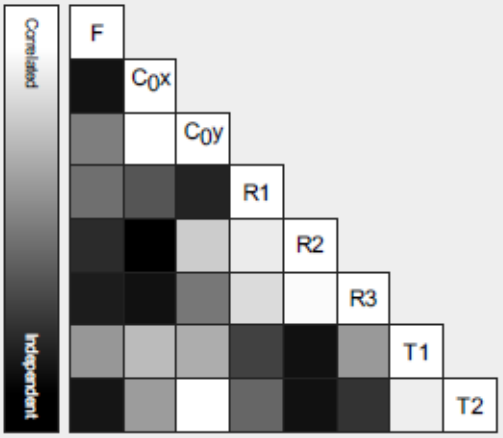

The correlation between camera internal parameters determined by the bundle adjustment. White indicates a full correlation between the parameters, ie. any change in one can be fully compensated by the other. Black indicates that the parameter is completely independent, and is not affected by other parameters.

The number of Automatic Tie Points (ATPs) per pixel, averaged over all images of the camera model, is color coded between black and white. White indicates that, on average, more than 16 ATPs have been extracted at the pixel location. Black indicates that, on average, 0 ATPs have been extracted at the pixel location. Click on the image to the see the average direction and magnitude of the re-projection error for each pixel. Note that the vectors are scaled for better visualization. The scale bar indicates the magnitude of 1 pixel error.

2D Keypoints Table

	Number of 2D Keypoints per Image	Number of Matched 2D Keypoints per Image
Median	7345	3024
Min	2565	201
Max	10120	5536
Mean	7300	3034

3D Points from 2D Keypoint Matches

	Number of 3D Points Observed
In 2 Images	138134
In 3 Images	66996
In 4 Images	36096
In 5 Images	21616
In 6 Images	13824
In 7 Images	9839
In 8 Images	7170
In 9 Images	5591
In 10 Images	4247
In 11 Images	3561
In 12 Images	2865
In 13 Images	2340
In 14 Images	1939
In 15 Images	1694
In 16 Images	1443
In 17 Images	1281
In 18 Images	1074
In 19 Images	969
In 20 Images	747
In 21 Images	703

In 22 Images	632
In 23 Images	525
In 24 Images	476
In 25 Images	426
In 26 Images	323
In 27 Images	316
In 28 Images	245
In 29 Images	213
In 30 Images	167
In 31 Images	139
In 32 Images	114
In 33 Images	79
In 34 Images	69
In 35 Images	48
In 36 Images	26
In 37 Images	26
In 38 Images	22
In 39 Images	9
In 40 Images	7
In 41 Images	6
In 42 Images	1
In 43 Images	1
In 44 Images	1

2D Keypoint Matches

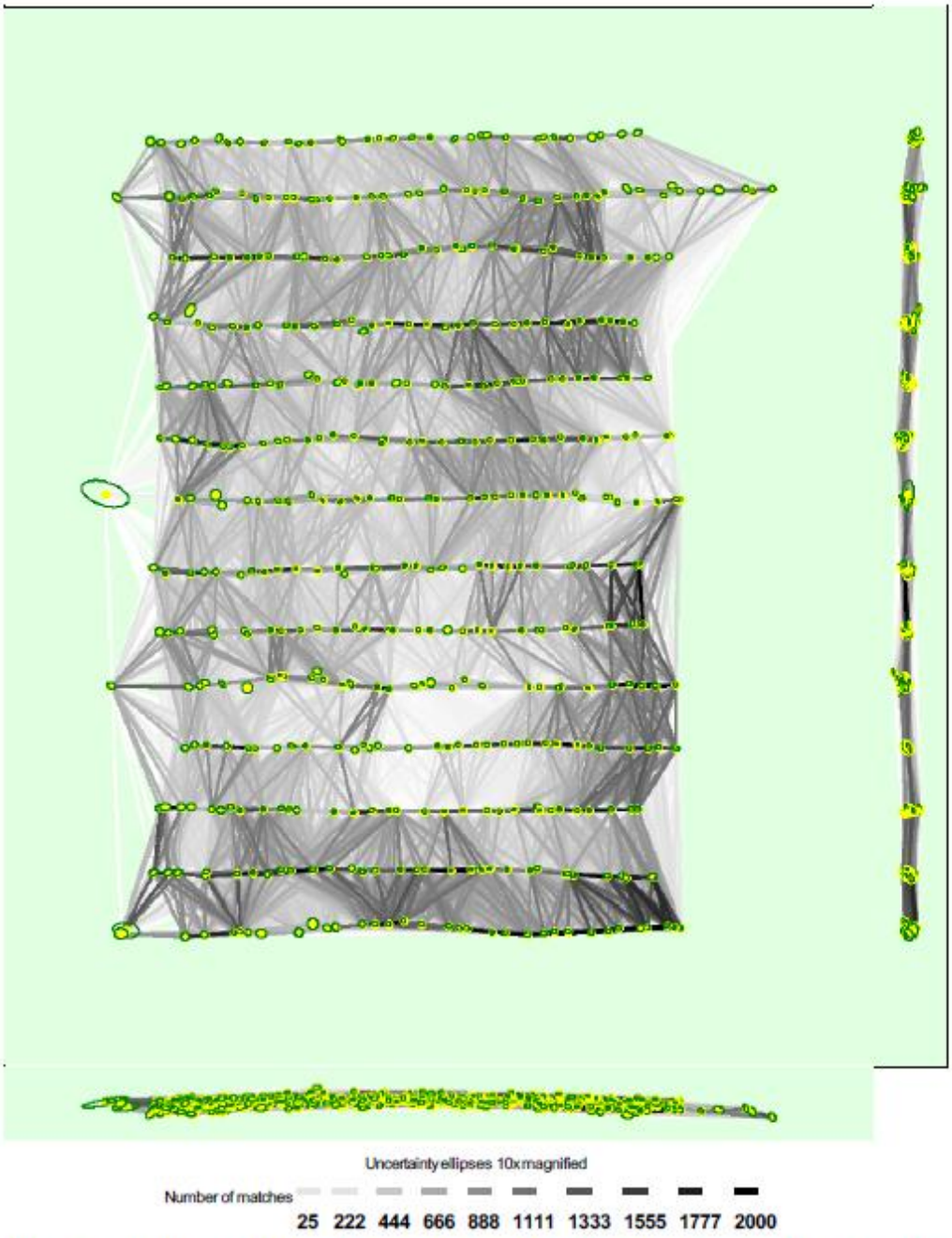

Figure 5: Computed image positions with links between matched images. The darkness of the links indicates the number of matched 2D keypoints between the images. Bright links indicate weak links and require manual tie points or more images. Dark green ellipses indicate the relative camera position uncertainty of the bundle block adjustment result.

Relative camera position and orientation uncertainties

	X [m]	Y [m]	Z [m]	Omega [degree]	Phi [degree]	Kappa [degree]
Mean	0.150	0.134	0.090	0.097	0.107	0.036
Sigma	0.062	0.041	0.031	0.029	0.040	0.013

Geolocation Details

Absolute Geolocation Variance

Min Error [m]	Max Error [m]	Geolocation Error X [%]	Geolocation Error Y [%]	Geolocation Error Z [%]
-	-4.18	47.19	0.43	0.65
-4.18	-3.34	2.16	1.08	0.87
-3.34	-2.51	1.08	3.25	4.76
-2.51	-1.67	0.43	6.28	10.17
-1.67	-0.84	0.22	15.15	17.75
-0.84	0.00	0.43	24.03	18.61
0.00	0.84	0.43	23.38	16.45
0.84	1.67	0.00	15.37	15.15
1.67	2.51	0.22	7.36	5.84
2.51	3.34	0.22	2.81	5.41
3.34	4.18	1.08	0.65	2.60
4.18	-	46.54	0.22	1.73
Mean [m]		0.038199	-0.022450	0.010339
Sigma [m]		6.659985	1.412753	1.774822
RMS Error [m]		6.660094	1.412932	1.774852

Min Error and Max Error represent geolocation error intervals between -1.5 and 1.5 times the maximum accuracy of all the images. Columns X, Y, Z show the percentage of images with geolocation errors within the predefined error intervals. The geolocation error is the difference between the initial and computed image positions. Note that the image geolocation errors do not correspond to the accuracy of the observed 3D points.

Relative Geolocation Variance

Relative Geolocation Error	Images X [%]	Images Y [%]	Images Z [%]
[-1.00, 1.00]	1.30	81.39	80.74
[-2.00, 2.00]	3.46	98.05	98.48
[-3.00, 3.00]	20.35	100.00	100.00
Mean of Geolocation Accuracy [m]	1.806489	1.806489	2.326132
Sigma of Geolocation Accuracy [m]	0.075617	0.075617	0.137884

Images X, Y, Z represent the percentage of images with a relative geolocation error in X, Y, Z.

Geolocation Orientational Variance	RMS [degree]
Omega	8.298
Phi	5.040
Kappa	5.453

Geolocation RMS error of the orientation angles given by the difference between the initial and computed image orientation angles.

Initial Processing Details

System Information

Hardware	CPU: Intel(R) Xeon(R) CPU E3-1240 v5 @3.50GHz RAM: 16GB GPU: NVIDIA Quadro K620 (Driver: 23.21.13.9189), Freedom Scientific Accessibility Display Driver (Driver: unknown)
Operating System	Windows 8.1 Enterprise, 64-bit

Coordinate Systems

Image Coordinate System	WGS84
Output Coordinate System	WGS 84 / UTM zone 15N

Processing Options

Detected Template	ThermoMAP Camera
Keypoints Image Scale	Full, Image Scale: 2
Advanced: Matching Image Pairs	Aerial Grid or Corridor
Advanced: Matching Strategy	Use Geometrically Verified Matching: yes
Advanced: Keypoint Extraction	Targeted Number of Keypoints: Automatic
Advanced: Calibration	Calibration Method: Alternative Internal Parameters Optimization: All External Parameters Optimization: All Rematch: Auto, no

Point Cloud Densification details

Processing Options

Image Scale	multiscale, 1 (Original image size, Slow)
Point Density	Optimal
Minimum Number of Matches	3
3D Textured Mesh Generation	no
LOD	Generated: no
Advanced: Image Groups	Thermal IR
Advanced: Use Processing Area	yes
Advanced: Use Annotations	yes
Time for Point Cloud Densification	20m:02s
Time for Point Cloud Classification	NA
Time for 3D Textured Mesh Generation	NA

Results

Number of Generated Tiles	1
Number of 3D Densified Points	2846760
Average Density (per m^3)	2.77

DSM, Orthomosaic and Index Details

Processing Options

DSM and Orthomosaic Resolution	1 x GSD (16.5 [cm/pixel])
DSM Filters	Noise Filtering: yes Surface Smoothing: yes, Type: Sharp
Index Calculator: Reflectance Map	Generated: yes Resolution: 1 x GSD (16.5 [cm/pixel]) Merge Tiles: no
Index Calculator: Indices	temperature [°C]
Time for DSM Generation	00s
Time for Orthomosaic Generation	00s
Time for DTM Generation	00s
Time for Contour Lines Generation	00s
Time for Reflectance Map Generation	13m:24s
Time for Index Map Generation	55s

Figure 34. April Pix4D report

Quality Report

Generated with Pix4Dmapper version 4.3.31

Important: Click on the different icons for:

Help to analyze the results in the Quality Report

Additional information about the sections

Click here for additional tips to analyze the Quality Report

Summary

Project	20190424
Processed	2019-05-13 12:16:43
Camera Model Name(s)	thermoMAP_9.0_640x512 (Thermal IR)
Average Ground Sampling Distance (GSD)	13.89 cm / 5.47 in
Area Covered	0.178 km^2 / 17.8054 ha / 0.07 sq. mi. / 44.0210 acres
Time for Initial Processing (without report)	28m:32s

Quality Check

Images	median of 7545 keypoints per image	⚠
Dataset	644 out of 646 images calibrated (99%), 1368 images disabled	✓
Camera Optimization	1.08% relative difference between initial and optimized internal camera parameters	✓
Matching	median of 2813 matches per calibrated image	✓
Georeferencing	yes, no 3D GCP	⚠

Preview

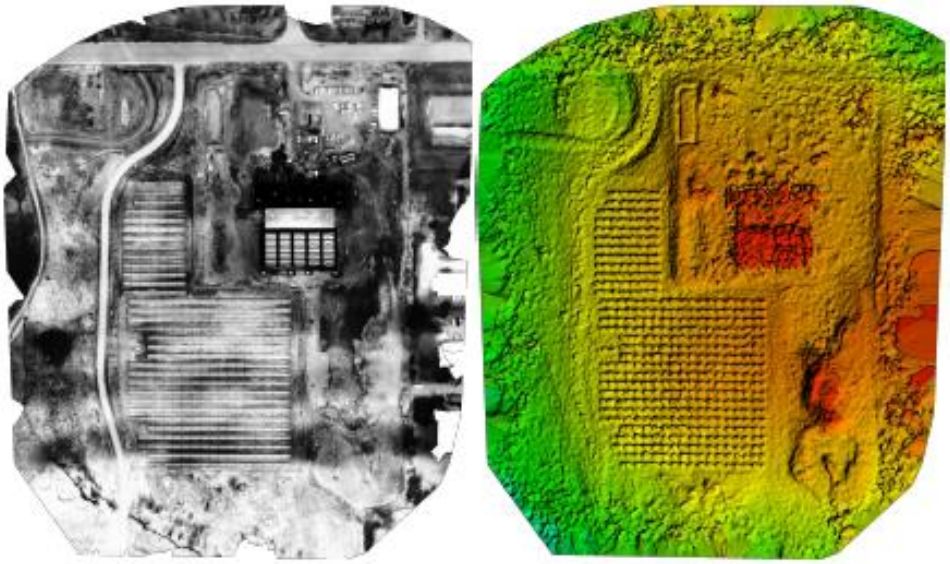

Figure 1: Orthomosaic and the corresponding sparse Digital Surface Model (DSM) before densification.

Calibration Details

Number of Calibrated Images	644 out of 2014
Number of Geolocated Images	2014 out of 2014

Initial Image Positions

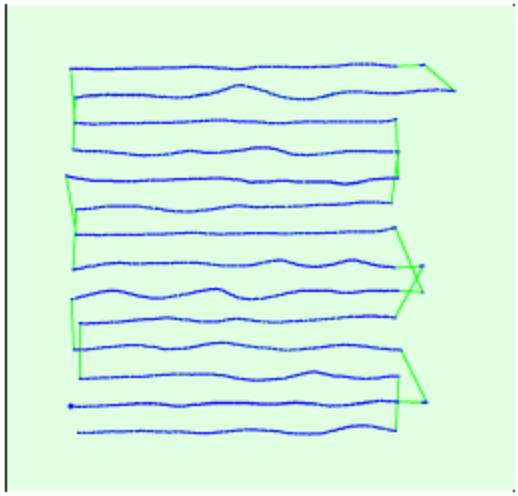

Figure 2: Top view of the initial image position. The green line follows the position of the images in time starting from the large blue dot.

Computed Image/GCPs/Manual Tie Points Positions

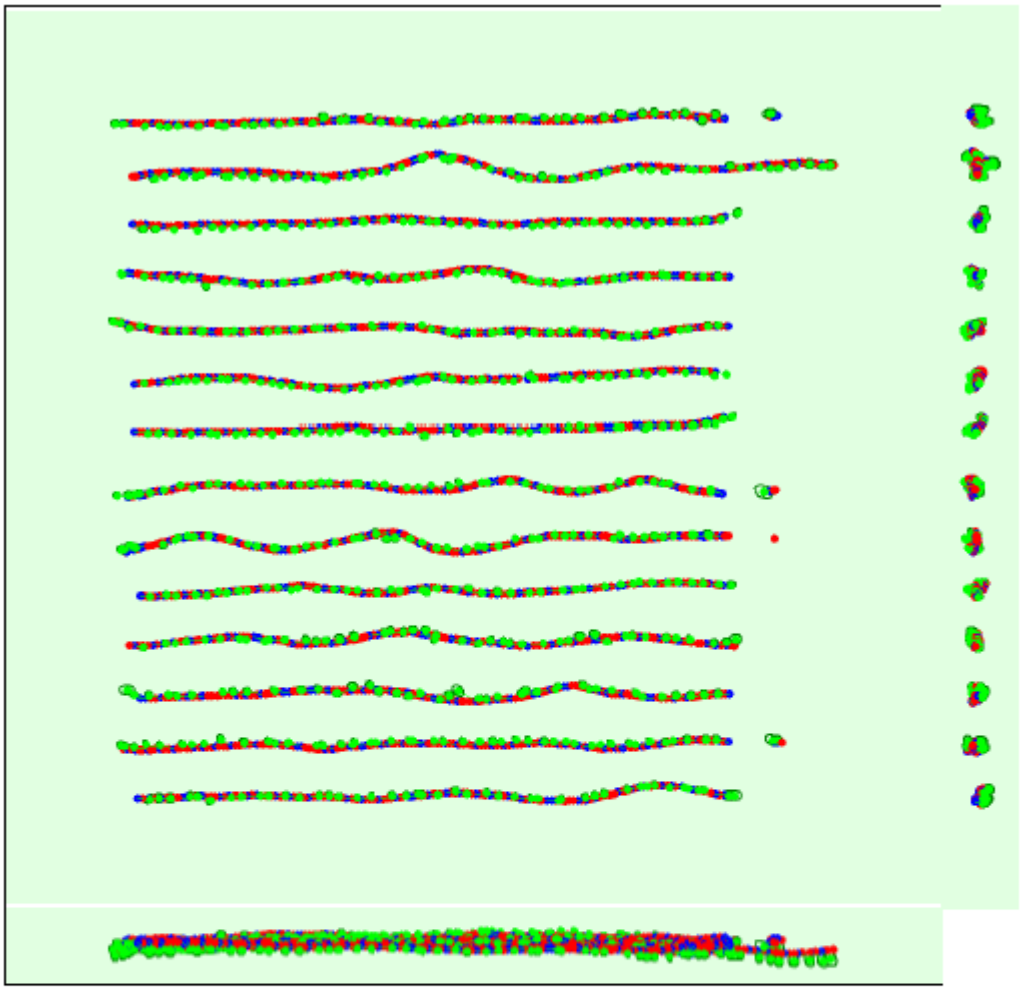

Uncertainty ellipses 10x magnified

Figure 3: Offset between initial (blue dots) and computed (green dots) image positions as well as the offset between the GCPs initial positions (blue crosses) and their computed positions (green crosses) in the top-view (XY plane), front-view (XZ plane), and side-view (YZ plane). Red dots indicate disabled or uncalibrated images. Dark green ellipses indicate the absolute position uncertainty of the bundle block adjustment result.

Absolute camera position and orientation uncertainties

	X[m]	Y[m]	Z[m]	Omega [degree]	Phi [degree]	Kappa [degree]
Mean	0.179	0.170	0.189	0.120	0.129	0.055
Sigma	0.035	0.028	0.039	0.024	0.031	0.015

Overlap

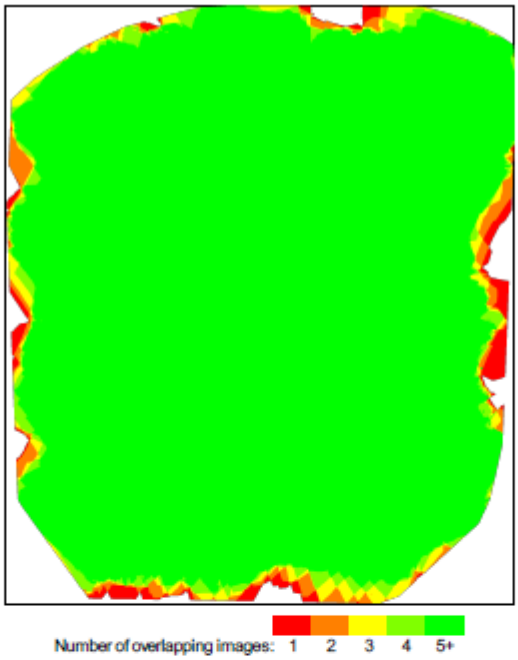

Figure 4: Number of overlapping images computed for each pixel of the orthomosaic.
Red and yellow areas indicate low overlap for which poor results may be generated. Green areas indicate an overlap of over 5 images for every pixel. Good quality results will be generated as long as the number of keypoint matches is also sufficient for these areas (see Figure 5 for keypoint matches).

Bundle Block Adjustment Details

Number of 2D Keypoint Observations for Bundle Block Adjustment	1825632
Number of 3D Points for Bundle Block Adjustment	510636
Mean Reprojection Error [pixels]	0.571

Internal Camera Parameters

thermoMAP_9.0_640x512 (Thermal IR). Sensor Dimensions: 10.880 [mm] x 8.704 [mm]

EXIF ID: thermoMAP_9.0_640x512

	Focal Length	Principal Point x	Principal Point y	R1	R2	R3	T1	T2
Initial Values	558.824 [pixel] 9.500 [mm]	320.000 [pixel] 5.440 [mm]	256.000 [pixel] 4.352 [mm]	-0.294	0.104	-0.019	0.000	0.000
Optimized Values	552.757 [pixel] 9.397 [mm]	313.095 [pixel] 5.323 [mm]	247.412 [pixel] 4.206 [mm]	-0.300	0.111	-0.025	0.002	0.001
Uncertainties (Sigma)	0.495 [pixel] 0.008 [mm]	0.178 [pixel] 0.003 [mm]	0.218 [pixel] 0.004 [mm]	0.001	0.004	0.004	0.000	0.000

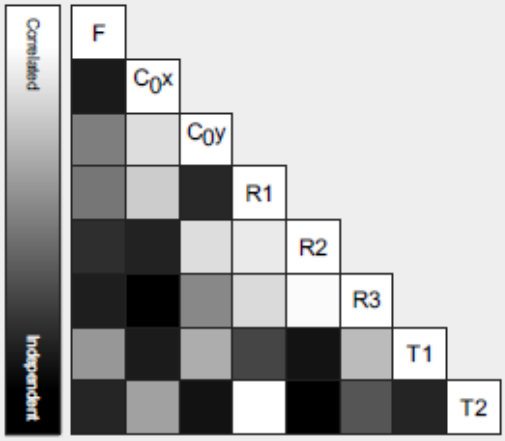

The correlation between camera internal parameters determined by the bundle adjustment. White indicates a full correlation between the parameters, ie. any change in one can be fully compensated by the other. Black indicates that the parameter is completely independent, and is not affected by other parameters.

The number of Automatic Tie Points (ATPs) per pixel, averaged over all images of the camera model, is color coded between black and white. White indicates that, on average, more than 16 ATPs have been extracted at the pixel location. Black indicates that, on average, 0 ATPs have been extracted at the pixel location. Click on the image to the see the average direction and magnitude of the re-projection error for each pixel. Note that the vectors are scaled for better visualization. The scale bar indicates the magnitude of 1 pixel error.

2D Keypoints Table

	Number of 2D Keypoints per Image	Number of Matched 2D Keypoints per Image
Median	7545	2813
Min	4533	251
Max	10665	6013
Mean	7489	2835

3D Points from 2D Keypoint Matches

	Number of 3D Points Observed
In 2 Images	251758
In 3 Images	107565
In 4 Images	52355
In 5 Images	29858
In 6 Images	18889
In 7 Images	12625
In 8 Images	9055
In 9 Images	6729
In 10 Images	5078
In 11 Images	3702
In 12 Images	2796
In 13 Images	1969
In 14 Images	1446
In 15 Images	1132
In 16 Images	936
In 17 Images	718
In 18 Images	619
In 19 Images	531
In 20 Images	512
In 21 Images	386

In 22 Images	358
In 23 Images	275
In 24 Images	238
In 25 Images	213
In 26 Images	182
In 27 Images	152
In 28 Images	122
In 29 Images	100
In 30 Images	92
In 31 Images	58
In 32 Images	49
In 33 Images	39
In 34 Images	35
In 35 Images	22
In 36 Images	7
In 37 Images	12
In 38 Images	7
In 39 Images	7
In 40 Images	3
In 41 Images	4
In 42 Images	1
In 43 Images	1

2D Keypoint Matches

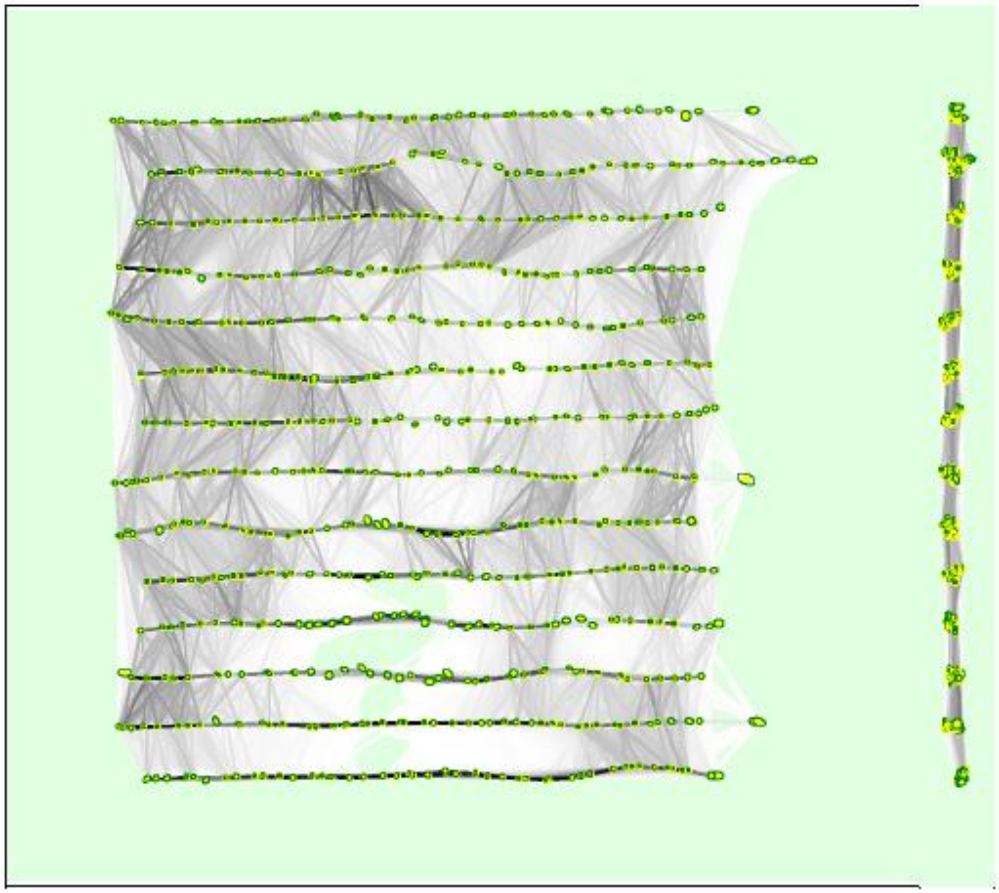

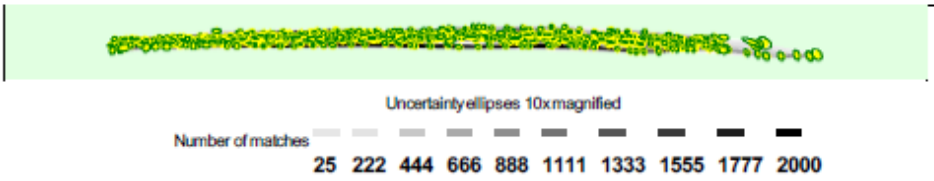

Figure 5: Computed image positions with links between matched images. The darkness of the links indicates the number of matched 2D keypoints between the images. Bright links indicate weak links and require manual tie points or more images. Dark green ellipses indicate the relative camera position uncertainty of the bundle block adjustment result.

Relative camera position and orientation uncertainties

	X[m]	Y[m]	Z[m]	Omega [degree]	Phi [degree]	Kappa [degree]
Mean	0.139	0.126	0.098	0.112	0.124	0.043
Sigma	0.038	0.031	0.036	0.029	0.036	0.017

Geolocation Details

Absolute Geolocation Variance

Min Error [m]	Max Error [m]	Geolocation Error X[%]	Geolocation Error Y[%]	Geolocation Error Z[%]
-	-3.90	47.20	0.31	0.31
-3.90	-3.12	1.40	0.00	2.33
-3.12	-2.34	0.16	2.02	7.61
-2.34	-1.56	0.16	7.45	11.18
-1.56	-0.78	0.00	16.61	14.44
-0.78	0.00	0.16	22.52	16.15
0.00	0.78	0.16	24.22	15.37
0.78	1.56	0.31	18.32	14.44
1.56	2.34	0.16	6.06	7.61
2.34	3.12	0.78	2.02	5.12
3.12	3.90	1.71	0.47	2.48
3.90	-	47.83	0.00	2.95
Mean [m]		0.001595	0.004856	0.003356
Sigma [m]		5.978792	1.197148	1.827976
RMS Error [m]		5.978792	1.197158	1.827979

Min Error and Max Error represent geolocation error intervals between -1.5 and 1.5 times the maximum accuracy of all the images. Columns X, Y, Z show the percentage of images with geolocation errors within the predefined error intervals. The geolocation error is the difference between the initial and computed image positions. Note that the image geolocation errors do not correspond to the accuracy of the observed 3D points.

Relative Geolocation Variance

Relative Geolocation Error	Images X[%]	Images Y[%]	Images Z[%]
[-1.00, 1.00]	0.78	88.20	77.64
[-2.00, 2.00]	2.95	99.69	98.60
[-3.00, 3.00]	33.07	100.00	100.00
Mean of Geolocation Accuracy [m]	1.813460	1.813460	2.317019
Sigma of Geolocation Accuracy [m]	0.093022	0.093022	0.123772

Images X, Y, Z represent the percentage of images with a relative geolocation error in X, Y, Z.

Geolocation Orientational Variance	RMS [degree]
Omega	7.453
Phi	4.574
Kappa	6.001

Geolocation RMS error of the orientation angles given by the difference between the initial and computed image orientation angles.

Initial Processing Details

System Information

Hardware	CPU: Intel(R) Xeon(R) CPU E3-1240 v5 @ 3.50GHz RAM: 16GB GPU: NVIDIA Quadro K620 (Driver: 23.21.13.9189), Freedom Scientific Accessibility Display Driver (Driver: unknown)
Operating System	Windows 8.1 Enterprise, 64-bit

Coordinate Systems

Image Coordinate System	WGS 84
Output Coordinate System	WGS 84 / UTM zone 15N

Processing Options

Detected Template	ThermoMAP Camera
Keypoints Image Scale	Full, Image Scale: 2
Advanced: Matching Image Pairs	Aerial Grid or Corridor
Advanced: Matching Strategy	Use Geometrically Verified Matching: yes
Advanced: Keypoint Extraction	Targeted Number of Keypoints: Automatic
Advanced: Calibration	Calibration Method: Alternative Internal Parameters Optimization: All External Parameters Optimization: All Rematch: Auto, no

Point Cloud Densification details

Processing Options

Image Scale	multiscale, 1 (Original image size, Slow)
Point Density	Optimal
Minimum Number of Matches	3
3D Textured Mesh Generation	no
LOD	Generated: no
Advanced: Image Groups	Thermal IR
Advanced: Use Processing Area	yes
Advanced: Use Annotations	yes
Time for Point Cloud Densification	19m:34s
Time for Point Cloud Classification	NA
Time for 3D Textured Mesh Generation	NA

Results

Number of Generated Tiles	1
Number of 3D Densified Points	3900143
Average Density (per m^3)	5.76

DSM, Orthomosaic and Index Details

Processing Options

DSM and Orthomosaic Resolution	1 x GSD (13.9 [cm/pixel])
DSM Filters	Noise Filtering: yes Surface Smoothing: yes, Type: Sharp
Index Calculator: Reflectance Map	Generated: yes Resolution: 1 x GSD (13.9 [cm/pixel]) Merge Tiles: no
Index Calculator: Indices	temperature [°C]
Time for DSM Generation	00s
Time for Orthomosaic Generation	00s
Time for DTM Generation	00s
Time for Contour Lines Generation	00s
Time for Reflectance Map Generation	05m:37s
Time for Index Map Generation	07s

Figure 35. Pix4D May report

Quality Report

Generated with Pix4Dmapper version 4.3.31

Important: Click on the different icons for:

- Help to analyze the results in the Quality Report
- Additional information about the sections

Click here for additional tips to analyze the Quality Report

Summary

Project	20190510
Processed	2019-05-10 15:20:34
Camera Model Name(s)	thermoMAP_9.0_640x512 (Thermal IR)
Average Ground Sampling Distance (GSD)	14.45 cm / 5.69 in
Area Covered	0.155 km^2 / 15.4684 ha / 0.06 sq. mi. / 38.2431 acres
Time for Initial Processing (without report)	22m:01s

Quality Check

Images	median of 8375 keypoints per image	⚠
Dataset	505 out of 507 images calibrated (99%), 879 images disabled	✓
Camera Optimization	2.65% relative difference between initial and optimized internal camera parameters	✓
Matching	median of 3409.82 matches per calibrated image	✓
Georeferencing	yes, no 3D GCP	⚠

Preview

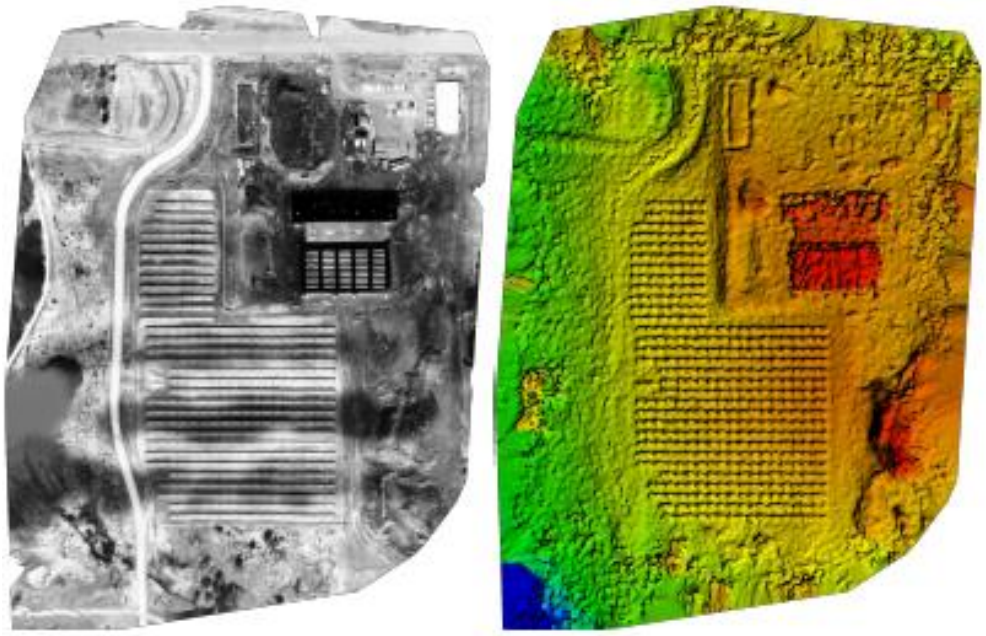

Figure 1: Orthomosaic and the corresponding sparse Digital Surface Model (DSM) before densification.

Calibration Details

Number of Calibrated Images	505 out of 1386
Number of Geolocated Images	1386 out of 1386

Initial Image Positions

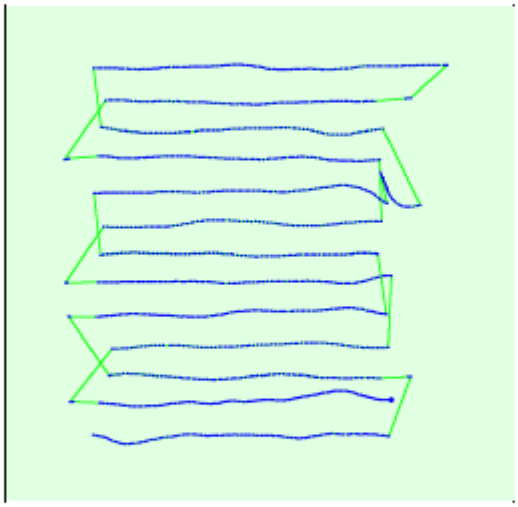

Figure 2: Top view of the initial image position. The green line follows the position of the images in time starting from the large blue dot.

Computed Image/GCPs/Manual Tie Points Positions

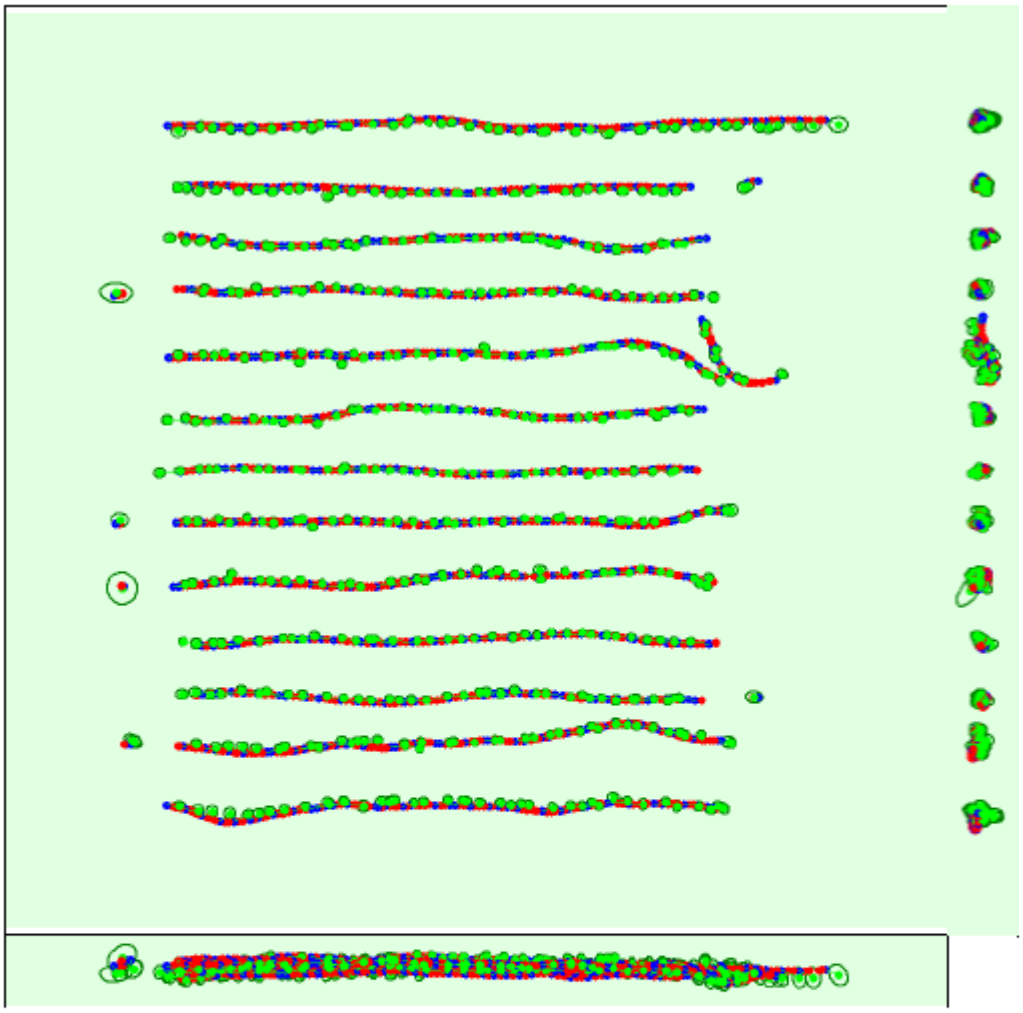

Uncertainty ellipses 10x magnified

Figure 3: Offset between initial (blue dots) and computed (green dots) image positions as well as the offset between the GCPs initial positions (blue crosses) and their computed positions (green crosses) in the top-view (XY plane), front-view (XZ plane), and side-view (YZ plane). Red dots indicate disabled or uncalibrated images. Dark green ellipses indicate the absolute position uncertainty of the bundle block adjustment result.

Absolute camera position and orientation uncertainties

	X[m]	Y[m]	Z[m]	Omega [degree]	Phi [degree]	Kappa [degree]
Mean	0.223	0.209	0.282	0.147	0.161	0.069
Sigma	0.050	0.041	0.058	0.028	0.032	0.013

Overlap

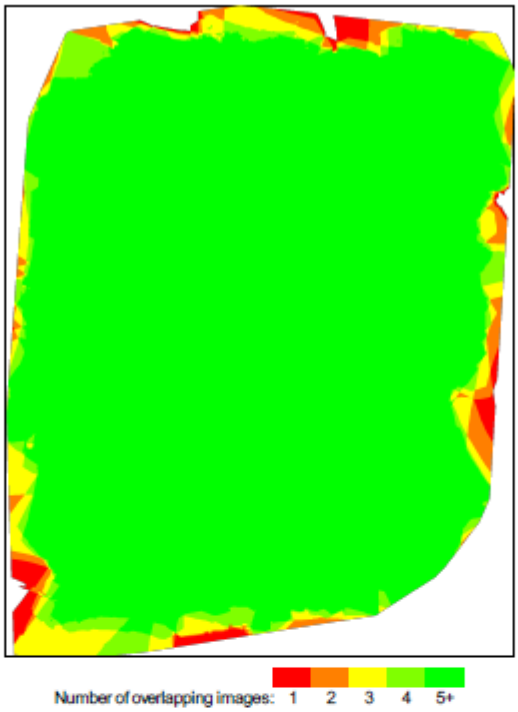

Figure 4: Number of overlapping images computed for each pixel of the orthomosaic.
Red and yellow areas indicate low overlap for which poor results may be generated. Green areas indicate an overlap of over 5 images for every pixel. Good quality results will be generated as long as the number of keypoint matches is also sufficient for these areas (see Figure 5 for keypoint matches).

Bundle Block Adjustment Details

Number of 2D Keypoint Observations for Bundle Block Adjustment	1711259
Number of 3D Points for Bundle Block Adjustment	456440
Mean Reprojection Error [pixels]	0.679

Internal Camera Parameters

thermoMAP_9.0_640x512 (Thermal IR). Sensor Dimensions: 10.880 [mm] x 8.704 [mm]

EXIF ID: thermoMAP_9.0_640x512

	Focal Length	Principal Point x	Principal Point y	R1	R2	R3	T1	T2
Initial Values	558.824 [pixel] 9.500 [mm]	320.000 [pixel] 5.440 [mm]	256.000 [pixel] 4.352 [mm]	-0.294	0.104	-0.019	0.000	0.000
Optimized Values	543.969 [pixel] 9.247 [mm]	318.989 [pixel] 5.423 [mm]	255.117 [pixel] 4.337 [mm]	-0.291	0.090	-0.006	0.000	-0.000
Uncertainties (Sigma)	0.542 [pixel] 0.009 [mm]	0.218 [pixel] 0.004 [mm]	0.241 [pixel] 0.004 [mm]	0.001	0.005	0.005	0.000	0.000

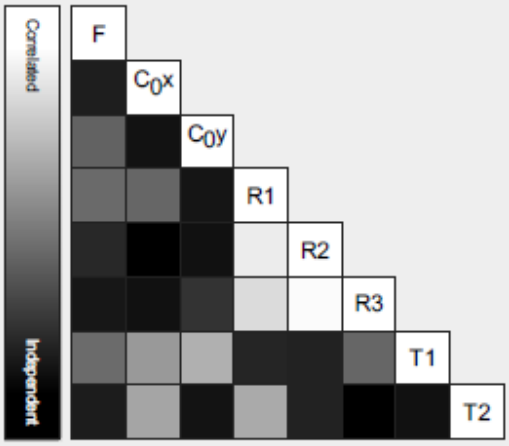

The correlation between camera internal parameters determined by the bundle adjustment. White indicates a full correlation between the parameters, ie. any change in one can be fully compensated by the other. Black indicates that the parameter is completely independent, and is not affected by other parameters.

The number of Automatic Tie Points (ATPs) per pixel, averaged over all images of the camera model, is color coded between black and white. White indicates that, on average, more than 16 ATPs have been extracted at the pixel location. Black indicates that, on average, 0 ATPs have been extracted at the pixel location. Click on the image to the see the average direction and magnitude of the re-projection error for each pixel. Note that the vectors are scaled for better visualization. The scale bar indicates the magnitude of 1 pixel error.

2D Keypoints Table

	Number of 2D Keypoints per Image	Number of Matched 2D Keypoints per Image
Median	8375	3410
Min	4754	202
Max	11740	6692
Mean	8285	3389

3D Points from 2D Keypoint Matches

	Number of 3D Points Observed
In 2 Images	209102
In 3 Images	99330
In 4 Images	50407
In 5 Images	28569
In 6 Images	18373
In 7 Images	12520
In 8 Images	9016
In 9 Images	6831
In 10 Images	5158
In 11 Images	3755
In 12 Images	2606
In 13 Images	1922
In 14 Images	1428
In 15 Images	1166
In 16 Images	949
In 17 Images	802
In 18 Images	657
In 19 Images	584
In 20 Images	471
In 21 Images	426

In 22 Images	413
In 23 Images	331
In 24 Images	285
In 25 Images	242
In 26 Images	191
In 27 Images	198
In 28 Images	150
In 29 Images	101
In 30 Images	92
In 31 Images	80
In 32 Images	51
In 33 Images	54
In 34 Images	27
In 35 Images	39
In 36 Images	24
In 37 Images	25
In 38 Images	16
In 39 Images	14
In 40 Images	10
In 41 Images	9
In 42 Images	5
In 43 Images	4
In 44 Images	3
In 45 Images	1
In 46 Images	3

2D Keypoint Matches

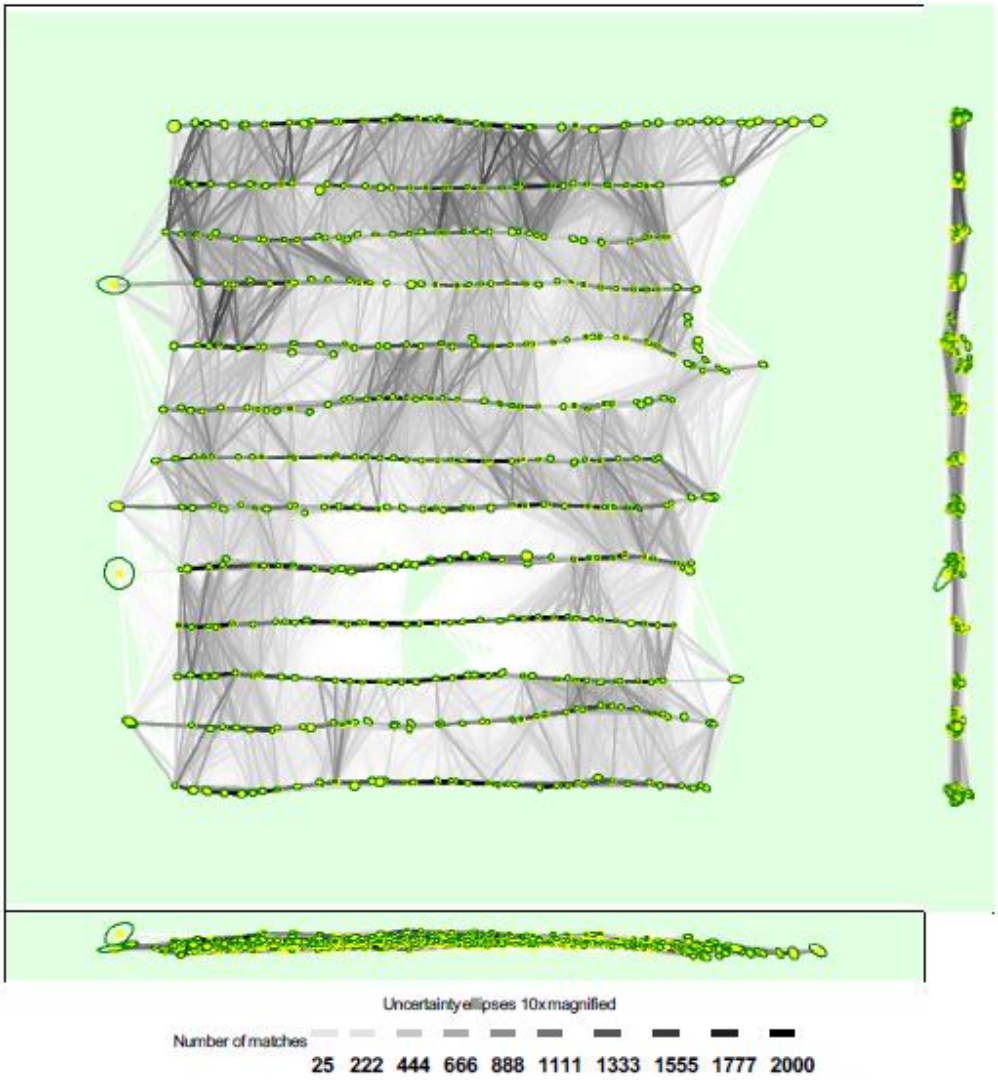

Figure 5: Computed image positions with links between matched images. The darkness of the links indicates the number of matched 2D keypoints between the images. Bright links indicate weak links and require manual tie points or more images. Dark green ellipses indicate the relative camera position uncertainty of the bundle block adjustment result.

Relative camera position and orientation uncertainties

	X[m]	Y[m]	Z[m]	Omega [degree]	Phi [degree]	Kappa [degree]
Mean	0.156	0.135	0.092	0.117	0.126	0.042
Sigma	0.052	0.041	0.039	0.035	0.039	0.016

Geolocation Details

Absolute Geolocation Variance

Min Error [m]	Max Error [m]	Geolocation Error X [%]	Geolocation Error Y [%]	Geolocation Error Z [%]
-	-4.91	47.92	0.00	0.00
-4.91	-3.93	4.36	0.20	0.20
-3.93	-2.94	1.78	0.59	1.98
-2.94	-1.96	0.79	4.36	10.50
-1.96	-0.98	1.19	18.22	15.84
-0.98	0.00	0.20	29.31	23.56
0.00	0.98	0.20	26.73	20.99
0.98	1.96	0.40	11.88	14.85
1.96	2.94	0.00	6.14	7.13
2.94	3.93	0.00	1.19	3.76
3.93	4.91	0.59	0.99	1.19
4.91	-	42.57	0.40	0.00
Mean [m]		-0.127652	0.019066	-0.008912
Sigma [m]		7.096585	1.367172	1.634301
RMS Error [m]		7.099733	1.367304	1.634325

Min Error and Max Error represent geolocation error intervals between -1.5 and 1.5 times the maximum accuracy of all the images. Columns X, Y, Z show the percentage of images with geolocation errors within the predefined error intervals. The geolocation error is the difference between the initial and computed image positions. Note that the image geolocation errors do not correspond to the accuracy of the observed 3D points.

Relative Geolocation Variance

Relative Geolocation Error	Images X [%]	Images Y [%]	Images Z [%]
[-1.00, 1.00]	1.98	84.36	90.89
[-2.00, 2.00]	4.55	98.42	100.00
[-3.00, 3.00]	21.19	100.00	100.00
Mean of Geolocation Accuracy [m]	1.889784	1.889784	2.861968
Sigma of Geolocation Accuracy [m]	0.077976	0.077976	0.141529

Images X, Y, Z represent the percentage of images with a relative geolocation error in X, Y, Z.

Geolocation Orientational Variance	RMS [degree]
Omega	8.241
Phi	5.106
Kappa	8.258

Geolocation RMS error of the orientation angles given by the difference between the initial and computed image orientation angles.

Initial Processing Details

System Information

Hardware	CPU: Intel(R) Xeon(R) CPU E3-1240 v5 @ 3.50GHz RAM: 16GB GPU: NVIDIA Quadro K620 (Driver: 23.21.13.9189), Freedom Scientific Accessibility Display Driver (Driver: unknown)
Operating System	Windows 8.1 Enterprise, 64-bit

Coordinate Systems

Image Coordinate System	WGS 84
Output Coordinate System	WGS 84 / UTM zone 15N

Processing Options

Detected Template	ThermoMAP Camera

Keypoints Image Scale	Full, Image Scale: 2
Advanced: Matching Image Pairs	Aerial Grid or Corridor
Advanced: Matching Strategy	Use Geometrically Verified Matching: yes
Advanced: Keypoint Extraction	Targeted Number of Keypoints: Automatic
Advanced: Calibration	Calibration Method: Alternative Internal Parameters Optimization: All External Parameters Optimization: All Rematch: Auto, no

Point Cloud Densification details

Processing Options

Image Scale	multiscale, 1 (Original image size, Slow)
Point Density	Optimal
Minimum Number of Matches	3
3D Textured Mesh Generation	no
LOD	Generated: no
Advanced: Image Groups	Thermal IR
Advanced: Use Processing Area	yes
Advanced: Use Annotations	yes
Time for Point Cloud Densification	13m:03s
Time for Point Cloud Classification	NA
Time for 3D Textured Mesh Generation	NA

Results

Number of Generated Tiles	1
Number of 3D Densified Points	3131851
Average Density (per m^3)	5.05

DSM, Orthomosaic and Index Details

Processing Options

DSM and Orthomosaic Resolution	1 x GSD (14.4 [cm/pixel])
DSM Filters	Noise Filtering: yes Surface Smoothing: yes, Type: Sharp
Index Calculator: Reflectance Map	Generated: yes Resolution: 1 x GSD (14.4 [cm/pixel]) Merge Tiles: no
Index Calculator: Indices	temperature [°C]
Time for DSM Generation	00s
Time for Orthomosaic Generation	00s
Time for DTM Generation	00s
Time for Contour Lines Generation	00s
Time for Reflectance Map Generation	04m:36s
Time for Index Map Generation	08s

APPENDIX D: THERMAL DATA

Table 9. Ground temperatures vs. ArcMap temperatures

Ground Temperature (degrees C), Fluke 561 Thermometer vs. ArcMap Temperatures									
	1	2	3	4	5	6	7	8	9
OctFlukeTemp	21.2	18	17.2	7.3	17.5	11.1	17.5	22.2	12.9
OctArcMap	21.8	20.3	16.8	18.1	18.8	16.6	17.8	22.3	17.1
OctTempDifference	0.6	2.3	0.4	10.8	1.3	5.5	0.3	0.1	4.2
AprFlukeTemp	28.5	24.4	22.9	20.7	19.9	19	20.6	25.6	23.2
AprArcMap	24.9	24.4	21.2	22.3	22.2	20.9	22.7	26.4	25
AprTempDifference	3.6	0	1.7	1.6	2.3	1.9	2.1	0.8	1.8
MayFlukeTemp	36.2	27.5	24.3	16.2	23.5	21.9	27.1	34.8	23
MayArcMap	30.6	29.2	22	24.4	25.6	24	23.6	30.4	26.5
MayTempDifference	5.6	1.7	2.3	8.2	2.1	2.1	3.5	4.4	3.5

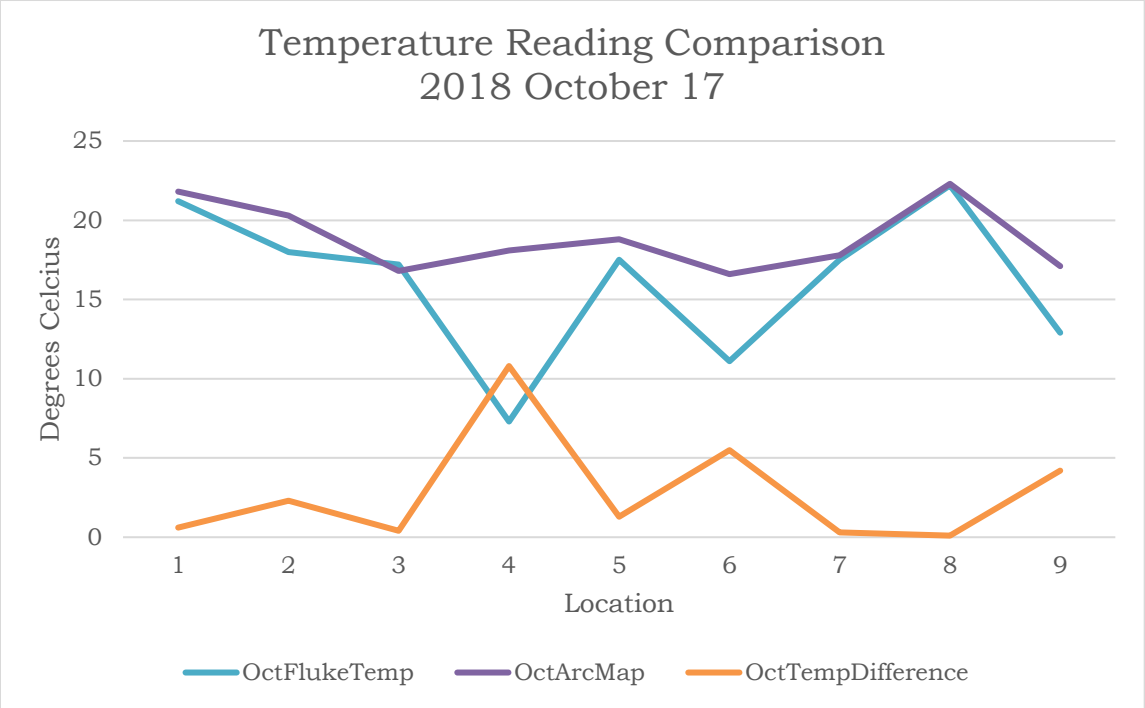

Figure 36. October temperature comparison

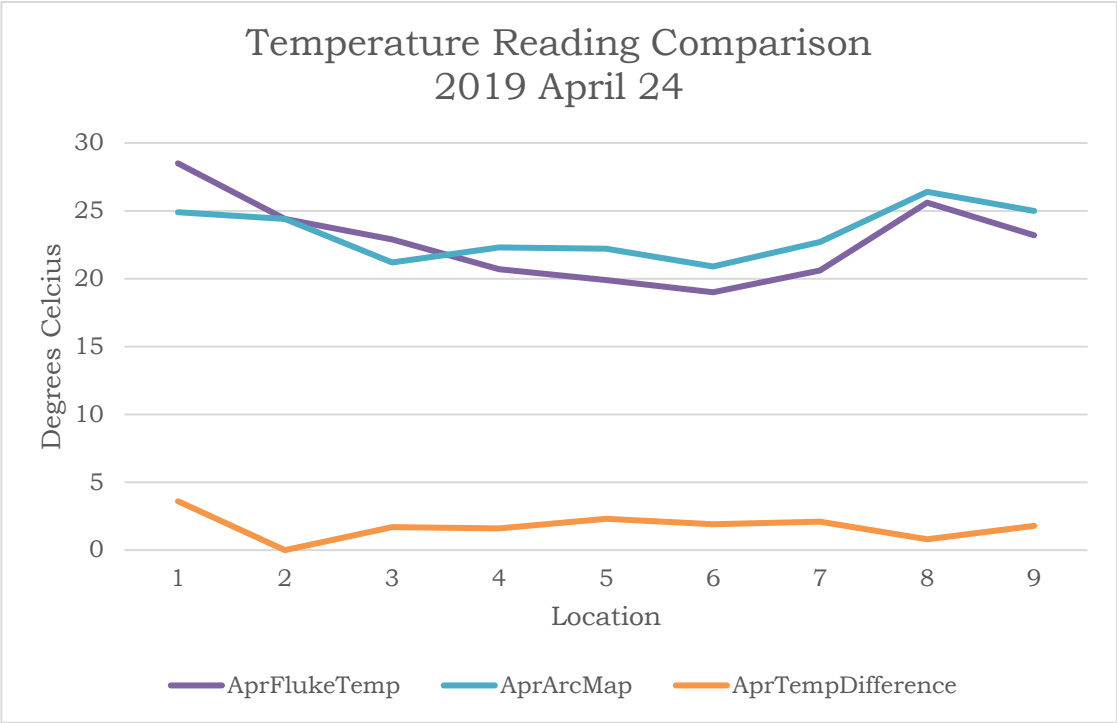

Figure 37 April temperature comparison

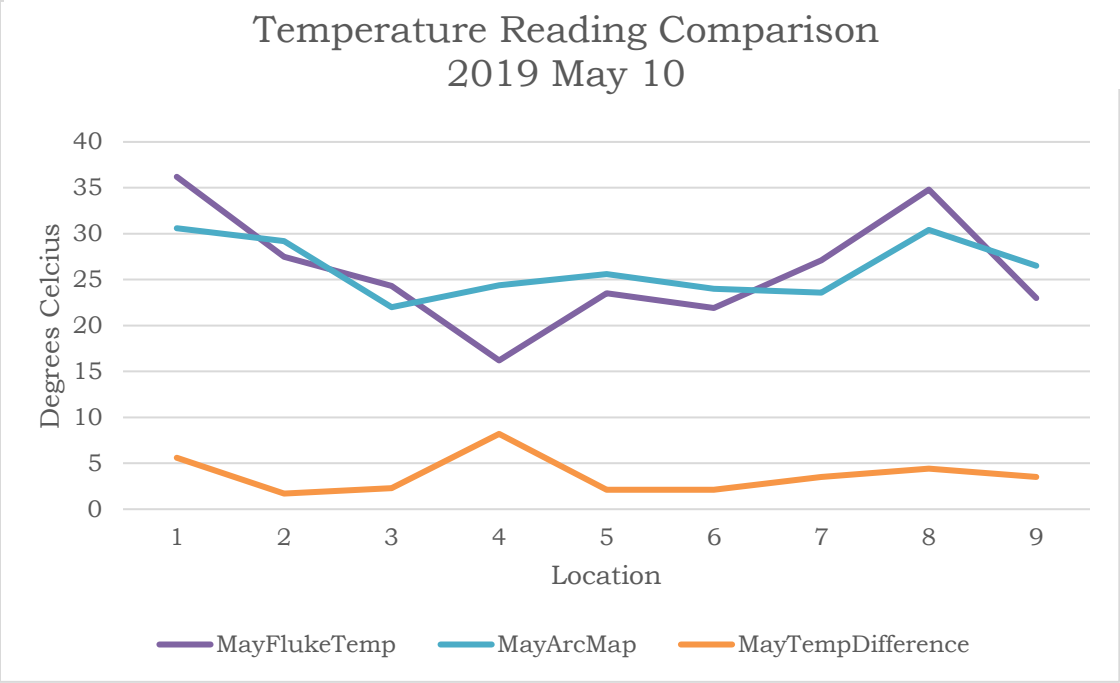

Figure 38. May temperature comparison

Figure 39. Unmatched & broken images taken on 2018 November 18

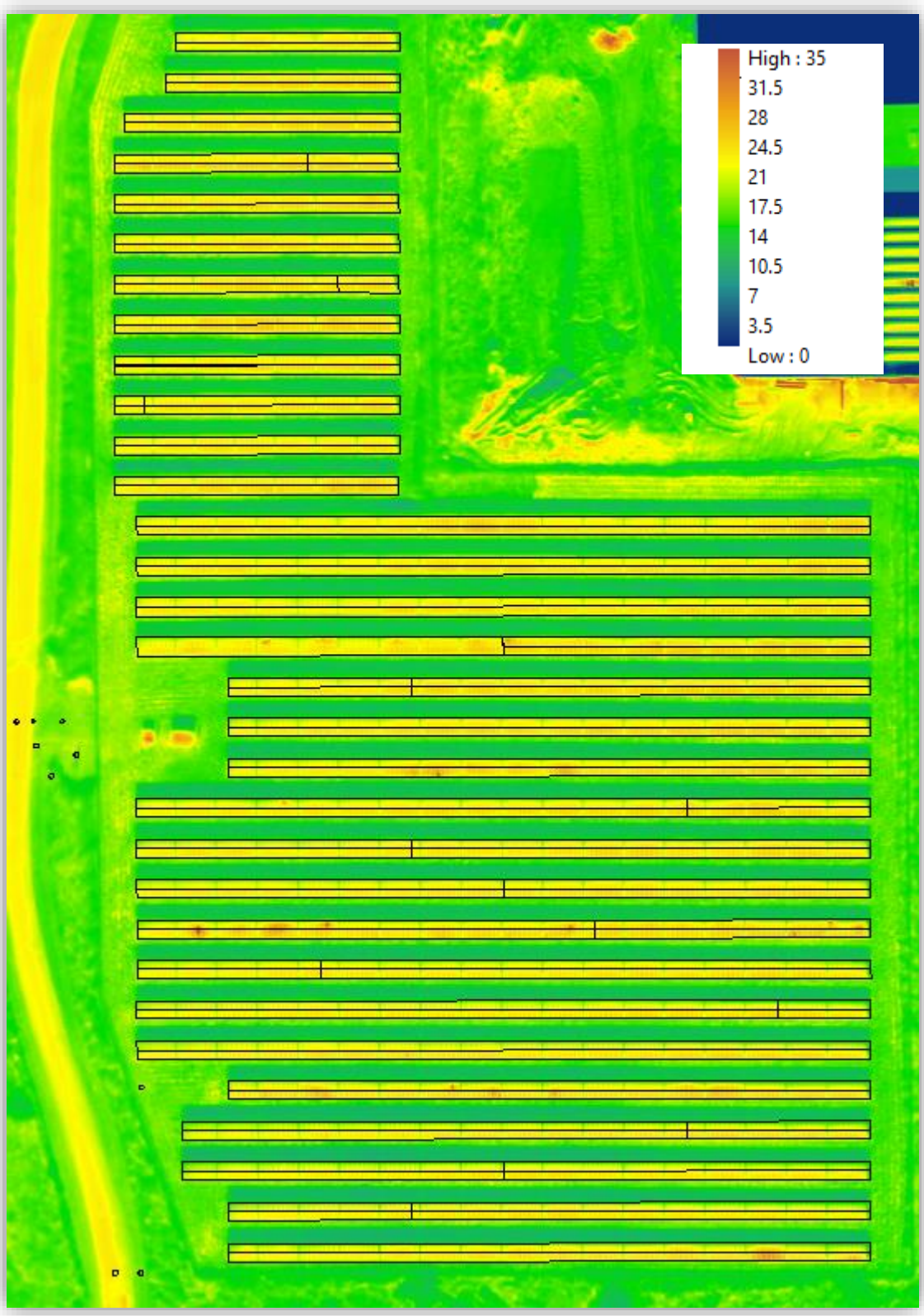

Figure 40. 2018 October 17 thermal image

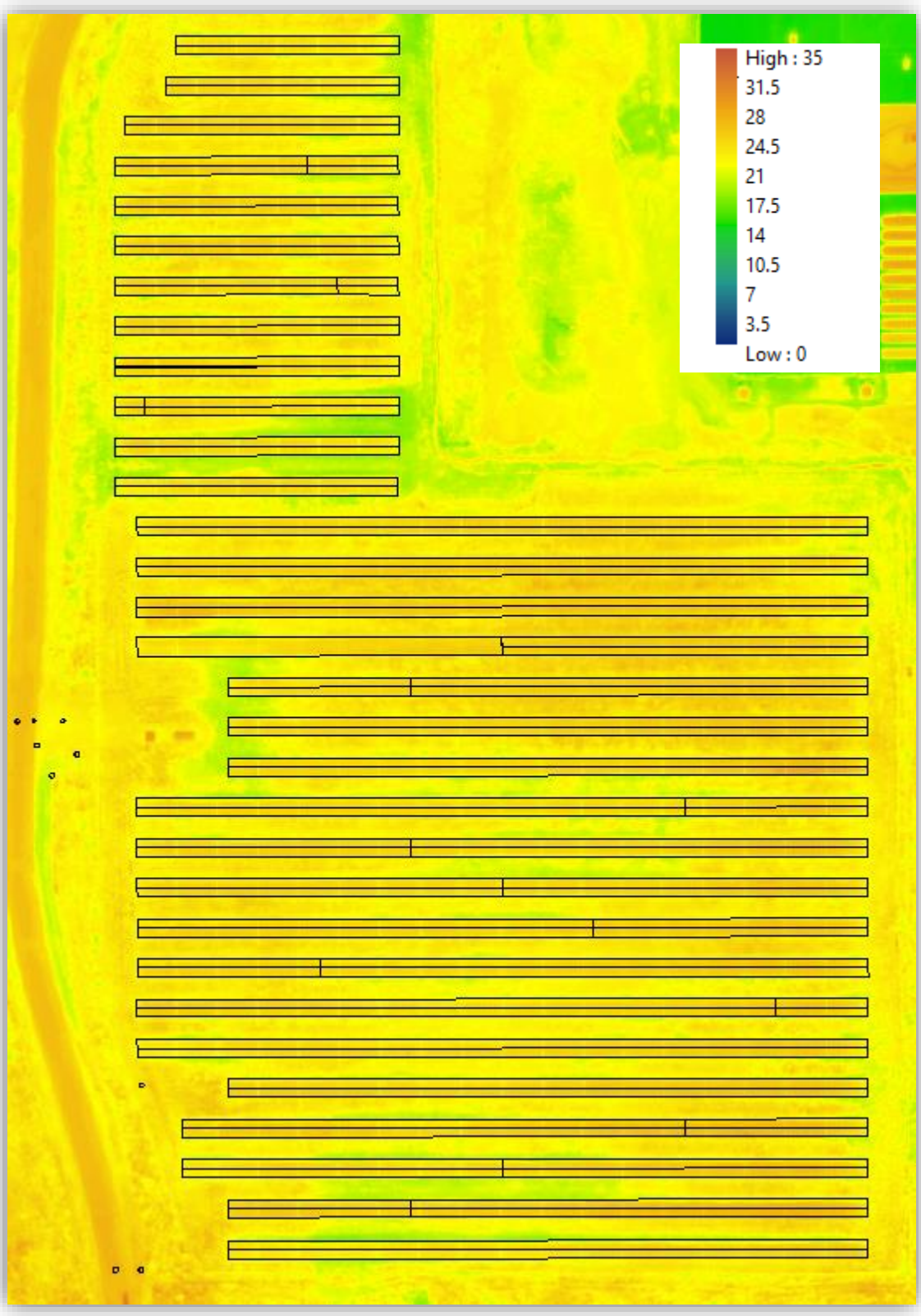

Figure 41. 2019 April 24 thermal image

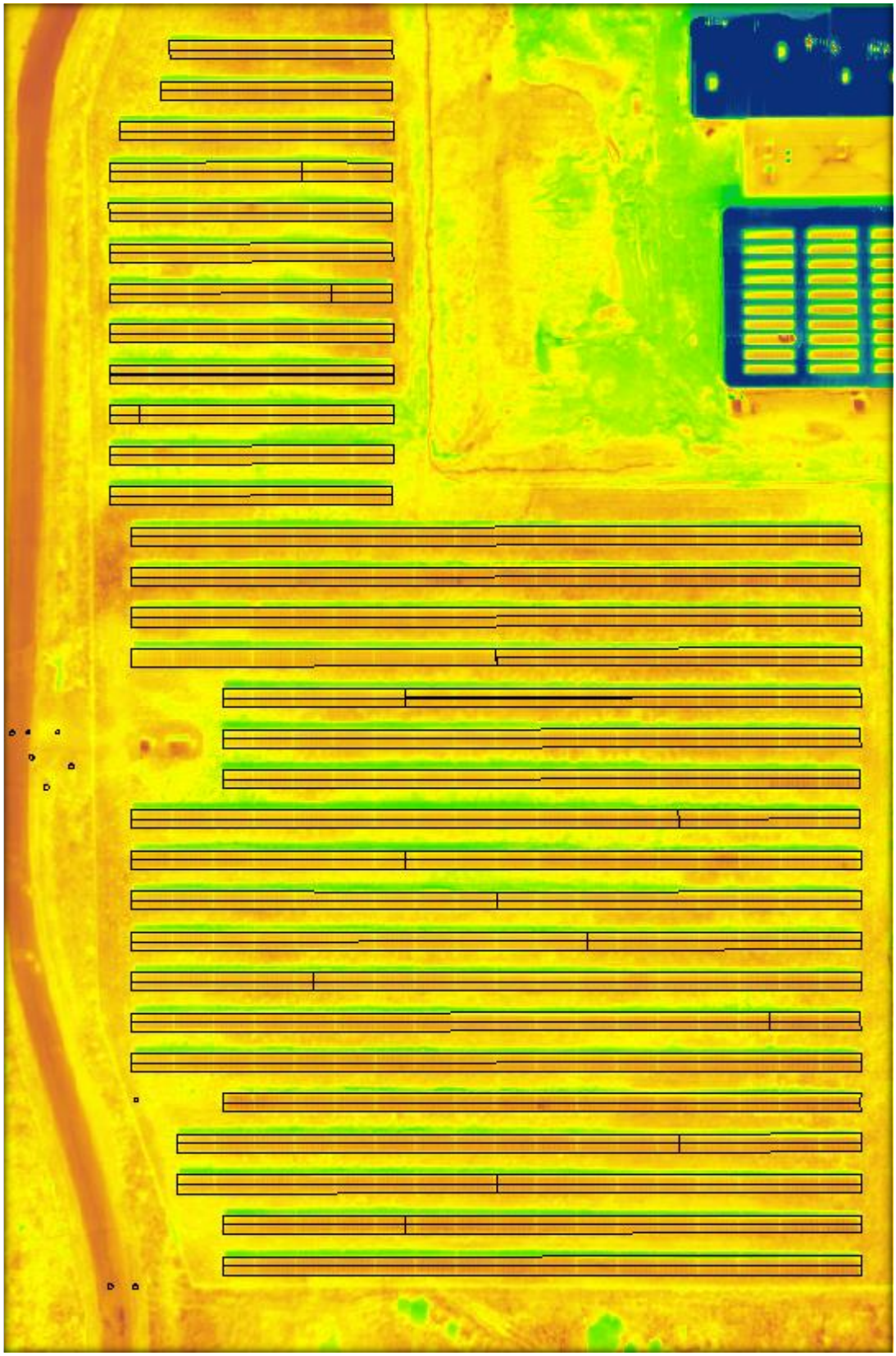

Figure 42. 2019 May 10 thermal image

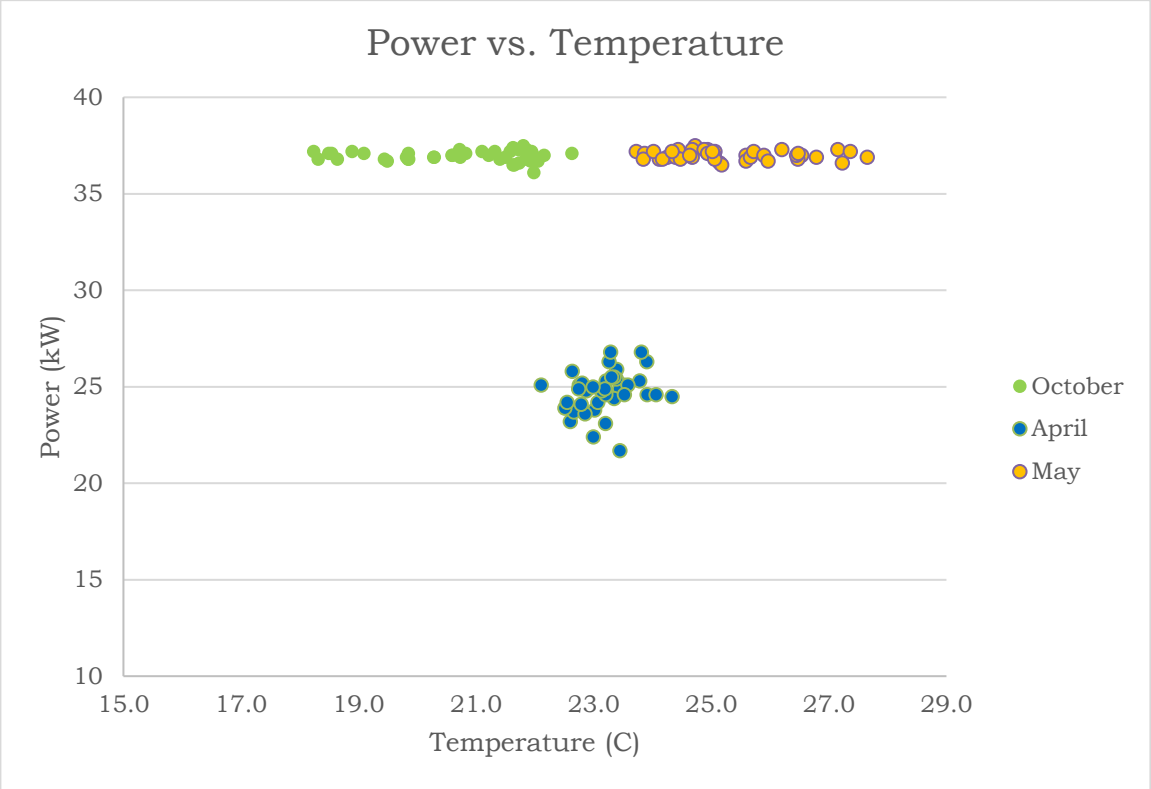

Figure 43. Power-temperature comparison